SET-9 and SET-26 are H3K4me3 readers and play critical roles in germline development and longevity

Wenke Wang[1], Amaresh Chaturbedi[1], Minghui Wang[2], Serim An[1], Satheeja Santhi Velayudhan[1], Siu Sylvia Lee[1]

[1]Department of Molecular Biology and Genetics, Cornell University, Ithaca, New York 14850, USA;

[2]Computational Biology Service Unit, Cornell University, Ithaca, New York 14850, USA;

Correspondence

Siu Sylvia Lee

Address: Department of Molecular Biology and Genetics, Cornell University, Room 341 Biotechnology building, Ithaca NY 14850

Phone: 607-255-8060

Email: sylvia.lee@cornell.edu

Abstract:

C. elegans SET-9 and SET-26 are highly homologous paralogs that share redundant functions in germline development, but SET-26 alone plays a key role in longevity and heat stress response. SET-26 is broadly expressed, but SET-9 is only detectable in the germline, which likely account for their different biological roles. SET-9 and SET-26 bind to H3K4me3 with adjacent acetylation marks *in vitro* and *in vivo*. In the soma, SET-26 acts through DAF-16 to modulate longevity. In the germline, SET-9 and SET-26 restrict H3K4me3 domains around SET-9 and SET-26 binding sites, and regulate the expression of specific target genes, with critical consequence on germline development. SET-9 and SET-26 are highly conserved and our findings provide new insights into the critical role of these H3K4me3 readers in germline function and longevity.

Introduction

Dynamic regulations of histone methylation status have been linked to many biological processes (Santos and Dean 2004). Recent studies have revealed that specific histone methyltransferases and demethylases can play key roles in regulating germline functions and/or modulating longevity (Han and Brunet 2012; Greer and Shi 2012). In *C. elegans*, loss of the COMPASS complex, which is critical for methylating histone H3 lysine 4, results in a global decrease in H3K4 trimethylation (H3K4me3) levels, and a reduced brood size (Li and Kelly 2011; Robert et al. 2014) and extended lifespan (Greer et al. 2010) phenotypes. Interestingly, deletions of *spr-5* or *rbr-2*, both of which encode demethylases that erase methyl marks on H3K4, also result in fertility defects (Alvares et al. 2014; Katz et al. 2009) and altered lifespan (Alvares et al. 2014; Greer et al. 2010).

47 These findings suggest that histone methylations need to be precisely controlled to
48 maintain longevity and germline function. It is important to note that the molecular
49 mechanisms whereby these H3K4 modifying enzymes effect reproduction and longevity
50 functions, including the genomic regions that they act on and how the altered H3K4
51 methylation levels contribute to the biological outcomes in these mutants, are largely
52 unknown.
53 SET (Su(var)3-9, Enhancer of Zeste, Trithorax) domain-containing proteins represent a
54 major group of histone methyltransferases (Dillon et al. 2005). We previously carried out
55 a targeted RNAi screen to identify the SET-domain containing proteins that play a role
56 in longevity in *C. elegans*. We found that RNAi knockdown of *set-9* and *set-26*, two
57 closely related genes, results in significant lifespan extension (Ni et al. 2012). SET-9
58 and SET-26 share 96% sequence identity and both proteins contain highly conserved
59 PHD and SET domains. PHD domains are known to bind to specific histone
60 modifications (Shi et al. 2007, 2006), suggesting that SET-9 and SET-26 could be
61 recruited to chromatin via binding to specific histone marks. Interestingly, the SET
62 domain of SET-9 & SET-26 contains mutations in conserved residues thought to be key
63 for methylating activities (Ni et al. 2012), making it unclear whether SET-9 & SET-26
64 could be active enzymes. Nevertheless, a recent study reported that the SET domain of
65 SET-26 exhibits H3K9me3 activity *in vitro* (Greer et al. 2014).
66
67 In this work, we demonstrated that, despite their high sequence identity, SET-26, but
68 not SET-9, plays a key role in heat stress response and longevity. In addition, we
69 revealed a novel redundant function of SET-9 and SET-26 in germline development. We

also confirmed that SET-26 is broadly expressed, whereas SET-9 is only expressed in the germline, which likely account for their distinct and redundant functions in lifespan and reproduction. Indeed, genetic and transcriptomic analyses supported the notion that SET-26 acts through the FOXO transcription factor DAF-16 in the soma to modulate longevity. Furthermore, we showed that the PHD domain of SET-9 & SET-26 binds to H3K4me3 *in vitro* and that the genome-wide binding patterns of SET-9 and SET-26 are highly concordant with that of H3K4me3 marking in *C. elegans*, indicating that SET-9 and SET-26 are recruited to H3K4me3 marked regions *in vivo*. Although the SET domain of SET-26 was reported to methylate H3K9me3 *in vitro* (Greer et al. 2014), our results indicated that loss of *set-9* & *set-26* does not affect global H3K9me3 levels and the genome-wide binding patterns of SET-9 and SET-26 are highly divergent from that of H3K9me3. Instead, we found that loss of *set-9* & *set-26* results in expansion of H3K4me3 marking surrounding most if not all of the SET-9 and SET-26 binding sites specifically in the germline, and significant RNA expression change of a subset of germline specific genes bound by SET-9 & SET-26. We propose that SET-9 and SET-26 are recruited to the chromatin via binding to H3K4me3, where they function to restrict H3K4me3 spreading and to regulate the expression of specific genes, and together these activities contribute to the proper maintenance of germline development.

Results

set-26, but not *set-9*, single mutant exhibits prolonged lifespan and heightened resistance to heat stress

93 RNAi knockdown of the highly similar paralogs *set-26* and *set-9* were previously shown
94 to significantly extend lifespan in *C. elegans* (Greer et al. 2010; Ni et al. 2012). However,
95 due to their high sequence similarity, RNAi likely knocks down both *set-26* and *set-9* in
96 those experiments. We confirmed the lifespan extension phenotype with multiple
97 available *set-26* single mutants, but a *set-9* single mutant was not available at the time
98 (Ni et al. 2012). To delineate whether *set-9*, like *set-26*, also plays a role in lifespan
99 determination, we used CRISPR-cas9 to generate a *set-9* mutant (Figure 1A). The *set-9*
100 mutant we obtained carries a mutation that causes a premature stop codon and is
101 expected to produce a truncated SET-9 protein lacking the conserved PHD and SET
102 domains (Figure 1A). We tested the lifespan phenotype of this *set-9* single mutant along
103 with the *set-26* single and *set-9 set-26* double mutants. Consistent with previous results,
104 the *set-26* single mutant lived longer than wild-type worms (Figure 1B). Surprisingly,
105 although SET-9 and SET-26 proteins share 97% identity in protein sequence, the *set-*
106 *9(rw5)* mutation did not alter lifespan in either wild-type or the *set-26* mutant background
107 (Figure 1B). Similar to the lifespan phenotype, *set-26*, but not *set-9* single mutant, was
108 more resistant to heat stress compared to wild-type worms (Figure 1C). These results
109 suggested that inactivation of *set-26,* but not *set-9,* extends lifespan and improves heat
110 resistance.
111

112 **_set-9_ and _set-26_ act redundantly to maintain germline function**

113 While propagating the *set-9 set-26* double mutant, we noticed a possible fertility defect.
114 To more thoroughly assess the roles of SET-9 and SET-26 in reproduction, we assayed
115 the brood size of *set-9, set-26* single and double mutants. We found that the progeny

116 number produced by *set-9* and *set-26* single mutants was slightly smaller compared to
117 that of wild-type worms (Figure 2A). Interestingly, the homozygous *set-9 set-26* double
118 mutant derived from heterozygous parents (first generation, i.e. F1) also exhibited a
119 mild brood size defect, and this defect became significantly more severe in the second
120 and later generations (F2 to F6, Figure 2A). Deficiency of several histone modifiers has
121 been previously reported to exhibit a “mortal germline” phenotype. We performed a
122 classical mortal germline assay and found that the *set-9 set-26* double mutant indeed
123 displayed a mortal germline phenotype (Figure 2B). Further detailed analyses indicated
124 that the *set-9 set-26* double mutant exhibited a high sterile rate and a low brood size
125 through the F2-F6 generations that we assayed (Figure 2A and Figure 2-figure
126 supplement 1A).
127 Since we noted a large difference between the brood size of the *set-9 set-26* double
128 mutant in the F1 and F2 generations and suspected a possible maternal influence, we
129 therefore performed a series of crosses to test this possibility. We found that *set-9 set-*
130 *26* double mutants derived from homozygous *set-9 set-26* hermaphrodites crossed with
131 heterozygous fathers exhibited a significantly more severe brood size defect compared
132 to those from heterozygous hermaphrodites crossed with homozygous mutant fathers
133 (Figure 2C). In other words, heterozygous mothers, but not heterozygous fathers,
134 helped to maintain better germline function in the progeny. These data support the
135 notion of a maternal contribution in germline maintenance in the *set-9 set-26* double
136 mutant worms.
137 We next used DAPI staining to monitor the germ cells of the *set-9 set-26* double mutant
138 at the F3 and F4 generations. For the double mutant worms that become sterile, we

139 observed variable germline phenotypes, including a very small mitotic region with no
140 differentiated cells, and a small mitotic region with sperms only or a largely normal
141 mitotic region with oocytes only (Figure 2-figure supplement 1B), suggesting problems
142 with both the germline stem cells and their subsequent differentiation. For the double
143 mutant worms that remained fertile, we observed germlines with a smaller but stable
144 number of mitotic cells (Figure 2D). The results together indicated that SET-9 and SET-
145 26 act redundantly to maintain normal germline function and they may regulate both the
146 proliferation and differentiation of the germline stem cells.
147

148 **SET-26 is broadly expressed but SET-9 is only detectable in the germline**

149 Given the high degree of sequence identity between SET-9 and SET-26, and given their
150 differential roles in lifespan and heat resistance, we wondered whether these two
151 proteins could be expressed in different tissues. In an attempt to resolve the expression
152 patterns of SET-9 and SET-26, we previously used RT-PCR at precise temperatures, as
153 well as an antibody that recognized both SET-9 and SET-26, in wild-type, *set-26* single,
154 and germlineless mutant worms, and deduced that SET-26 is likely broadly expressed
155 and SET-9 is likely expressed in the germline (Ni et al. 2012). To unambiguously
156 determine the expression patterns of the SET-9 and SET-26 proteins, we used
157 CRISPR-cas9 to knock-in a GFP tag at the C-terminus of the endogenous *set-9* and
158 *set-26* loci and monitored their expression patterns. Consistent with our previous report
159 (Ni et al. 2012), we found that GFP-tagged SET-9 was only detected in germline cells of
160 *C. elegans* (Figure 3A). In contrast, the GFP-tagged SET-26 was broadly expressed in
161 both the somatic and germline cells (Figure 3B). As expected, expression of these two

162 proteins was restricted to the nucleus, which is consistent with their possible roles in
163 chromatin regulation. The ubiquitous expression of SET-26, but not SET-9, likely
164 explains why SET-26 alone has a role in lifespan and heat resistance.
165 We note that the knock-in worms expressing GFP-tagged SET-26 lived slightly longer
166 than wild-type (but significantly shorter than the *set-26* mutant) (Figure 3-figure
167 supplement 1A) and had a slight heat resistance phenotype (Figure 3-figure supplement
168 1B), and the knock-in worms expressing both SET-9::GFP and SET-26::GFP had a
169 slightly lower brood size compared to wild-type worms, but a significantly larger brood
170 size than the *set-9 set-26* double mutant worms (Figure 3-figure supplement 1C). The
171 data together suggested that the GFP-tag somewhat compromised the functions of
172 SET-9 and SET-26, but the tagged proteins remain largely functional.
173 We next wondered whether the germline or somatic expression of SET-26 is important
174 for lifespan modulation. We previously showed that RNAi knockdown of *set-9/-26* (RNAi
175 targets the two genes due to high sequence identity) in *glp-1(e2141)* germlineless
176 mutant worms extended lifespan to a similar degree as in wild-type worms (Ni et al.
177 2012), suggesting that somatic *set-26* is important for lifespan modulation. To further
178 test this possibility, we used the *rrf-1* mutant, in which RNAi is efficient in the germline
179 but not somatic cells (Sijen et al. 2001), to assess whether knockdown of *set-26* (& *set-*
180 *9*) in the germline alone can extend lifespan. As a control for tissue-specific RNAi, we
181 monitored SET-26::GFP expression in wild-type or *rrf-1* mutant worms treated with *set-*
182 *9/-26* RNAi. As expected, *set-9/-26* RNAi greatly reduced SET-26::GFP expression in
183 most tissues except neurons in wild-type worms (Figure 3-figure supplement 1D),
184 whereas *set-9/-26* RNAi treatment specifically knocked down SET-26::GFP expression

185 in the germline in *rrf-1* mutant worms (Figure 3-figure supplement 1D). We next
186 assessed the lifespan of wild-type or *rrf-1* mutant worms treated with *set-9/-26* RNAi.
187 We included *wdr-5.1* RNAi as a positive control as *wdr-5.1* is known to act in the
188 germline to modulate lifespan (Greer et al. 2010). As expected, RNAi knockdown of
189 *wdr-5.1* extended lifespan in both wild-type and *rrf-1* mutant worms. In contrast, *set-9/-*
190 *26* RNAi knockdown extended lifespan in wild-type but not in the *rrf-1* mutant
191 background (Figure 3C and 3D), indicating that inactivation of *set-26* (& *set-9*) in the
192 germline is not sufficient for lifespan modulation. These results corroborated with our
193 previous findings, and indicated that SET-26 likely acts in the somatic cells to modulate
194 longevity and heat stress response, but SET-9 and SET-26 act redundantly in the
195 germline to maintain reproductive function.
196
197 **Transcriptional profiling revealed candidate longevity and germline function**
198 **genes regulated by SET-9 and SET-26**
199 To gain insights into the molecular changes that may contribute to the somatic SET-26
200 effect on lifespan, we investigated the transcriptional profiles of the long-lived
201 germlineless *glp-1; set-26* double mutant. We isolated total RNA from *glp-1; set-26*
202 double and *glp-1* single mutant worms, and performed RNA sequencing after removing
203 ribosomal RNAs (ribo-minus RNA-seq). We next used edgeR, an RNA-seq analysis tool
204 in the R package (Robinson et al. 2010), to identify the genes that showed statistically
205 significant expression change in the *glp-1; set-26* double mutant compared to *glp-1*
206 mutant (Figure 4A). We identified 887 up-regulated and 946 down-regulated genes in
207 response to *set-26* loss in the soma (Figure 4A), and gene ontology (GO) analyses

208 indicated that these genes were over-represented in multiple functional groups (Figure
209 4-figure supplement 1A), with “collagen” stood out as the most highly enriched GO term.
210 We noted that collagens, as well as some of the other genes with expression change,
211 have been implicated to be important for lifespan in *C. elegans* (Ewald et al. 2015). It
212 would be interesting to test how altered expression of collagens, and other genes
213 identified in our RNA-seq data, might contribute to the extended lifespan of the *set-26*
214 mutant in the future.
215 Since we previously showed that somatic *set-26* largely acts through *daf-16*, which
216 encodes the Forkhead box O (FOXO) transcription factor, to modulate lifespan (Ni et al.
217 2012), we sought to further identify the transcriptional changes in response to somatic
218 *set-26* loss that are also dependent on *daf-16*. Using similar RNA-seq experiments, we
219 investigated the transcriptional profiles of the germlineless *daf-16; glp-1; set-26* triple
220 and *glp-1; set-26* double mutants (Figure 4A). We identified 164 genes that were up-
221 regulated, and 131 genes that were down-regulated in the *daf-16; glp-1; set-26* triple
222 mutant (Figure 4A). By comparing these gene lists with the gene lists discussed above
223 for the germlineless *glp-1; set-26* double mutant vs. *glp-1*, we deduced the somatic
224 genes whose expression become significantly up-regulated or down-regulated when
225 *set-26* is deleted, but those expression changes were reverted when *daf-16* was
226 simultaneously lost (down-regulated or up-regulated in the *daf-16; glp-1; set-26* triple
227 mutant, respectively) (Figure 4A). We termed these DAF-16-depednent somatic SET-26
228 regulated genes. Interestingly, GO term analyses revealed that the functional group
229 “determination of adult lifespan” was highly enriched in these DAF-16-dependent
230 somatic SET-26 regulated genes (Figure 4B). Therefore, the transcriptomic analysis

231 corroborated the genetic analysis, and supports a model that DAF-16-mediated gene
232 regulation likely contributes to the lifespan phenotype of the *set-26* mutant.
233 We additionally investigated the transcriptional profiles of the long-lived fertile *set-26*
234 single mutant and revealed that 869 genes showed significant expression change in the
235 *set-26* mutant compared with wild-type worms. As expected, there was a significant and
236 substantial overlap between the genes that exhibited expression change in response to
237 whole-body loss of *set-26* and the somatic SET-26 regulated genes discussed above
238 (Figure 4-figure supplement 1B). Interestingly, the analysis using germlineless worms
239 revealed far greater number of genes with expression change compared to that using
240 reproductive worms. This could be due to technical variations between experiments, but
241 might also suggest that some genes exhibit selective expression changes only in
242 somatic cells, and those expression changes could be masked when germ cells were
243 included in the analysis.
244 To gain insights into the molecular changes that may underlie the germline phenotypes,
245 we next compared the transcriptional profiles of the *set-9* single, *set-26* single, and F1
246 *set-9 set-26* double mutants, all of which were fertile. We identified 162, 334, 1888
247 genes that were up-regulated, and 545, 534, 1644 genes that were down-regulated in
248 the *set-9*, *set-26*, and F1 *set-9 set-26* mutants respectively (Figure 5A). Interestingly,
249 although there was significant overlap among the three gene sets, a substantial number
250 of genes appeared to only show expression changes in the F1 *set-9 set-26* double
251 mutant (Figure 5A, 1,430 down-regulated, 1,781 up-regulated), suggesting a redundant
252 role of SET-9 and SET-26 in regulating gene expression. Since the F1 *set-9 set-26*
253 mutant had a mild brood-size phenotype, and gave rise to progeny that exhibited severe

254 defects in germline development (Figure 2), we speculated that many of these SET-9
255 and SET-26 co-regulated genes could be important for germline function. Indeed, GO
256 analyses revealed that the genes that showed expression change in response to the
257 simultaneous loss of *set-9* and *set-26* were over-represented for a number of different
258 functional groups, including genes with annotated functions in sperm development and
259 function (Figure 5B-C). We further compared these SET-9 and SET-26 co-regulated
260 genes with genes previously determined to be germline-, oocyte-, and sperm-specific
261 (Reinke et al. 2004). Interestingly, we found a significant over-representation of
262 germline-specific genes among the genes that exhibited up-regulated expression in the
263 F1 *set-9 set-26* double mutant, but not the genes that exhibited down-regulated
264 expression (Figure 5D). Both sperm- and oocyte-specific genes (383 and 252,
265 respectively) were among these germline-specific genes that were up-regulated in the
266 F1 *set-9 set-26* double mutant. It is possible that up-regulated expression of these
267 germline-specific genes contribute to the reproductive defects of the *set-9 set-26* double
268 mutant (Greer et al. 2014; Katz et al. 2009; Kerr et al. 2014).
269 Considering the maternal effect of SET-9 and SET-26 on fertility (Figure 2C), we also
270 profiled the transcriptome of the F3 *set-9 set-26* double mutant, which exhibited greatly
271 compromised fertility (Fig. 2A), and compared that with the transcriptional profile of the
272 F1 *set-9 set-*26 double mutant discussed above. We noted that the germline of the F3
273 *set-9 set-26* was morphologically quite different from wild-type and the F1 *set-9 set-26*
274 double mutant (Figure 2-figure supplement 1). Interestingly, we found that the genes
275 with significant expression change in the F1 *set-9 set-26* and F3 *set-9 set-26* double
276 mutants not only substantially overlapped, but they were also enriched for similar

277 functional groups based on GO term analyses (Figure 5-figure supplement 1A, 1B and
278 1C). The fold change of gene expression, compared to wild-type, in the F1 *set-9 set-26*
279 and the F3 *set-9 set-26* double mutants also positively correlated (Figure 5-figure
280 supplement 1D and 1E). These results together suggested that the transcriptional
281 profiles of the F1 and the F3 *set-9 set-26* double mutants are highly correlative despite
282 that the F3 *set-9 set-26* double mutant has a more severely defective germline. We note
283 that the GO term "development and reproduction" was unique for the F3 *set-9 set-26*
284 (Figure 5-figure supplement 1B), which may reflect the more severe germline defects in
285 these mutant worms.
286

287 **Loss of SET-9 and SET-26 does not affect the global levels of H3K9me3**

288 We next investigated the possible normal functions of SET-9 and SET-26, which could
289 inform how their inactivations lead to the gene expression changes and biological
290 phenotypes discussed above. The SET domain of SET-26 was recently reported to
291 show H3K9me3 methylation activity *in vitro* (Greer et al. 2014). This was a somewhat
292 surprising result, as the SET domain of SET-26 (and SET-9) contains multiple mutations
293 in the critical residues generally thought to be key for the methylating enzymatic activity
294 of SET domain proteins (Figure 6-figure supplement 1A), and we have previously
295 speculated that SET-9 and SET-26 are likely not active enzymes (Ni et al. 2012).
296 Furthermore, the likely homologs of SET-9 and SET-26 in flies (UpSET) and mammals
297 (MLL5) have been reported to lack methylating activity (Sebastian et al. 2009; Rincon-
298 Arano et al. 2012). Nevertheless, because of the reported *in vitro* results, we sought to
299 monitor the global levels of H3K9me3 in the *set-9* and *set-26* mutants. We reasoned

300 that if SET-9 & SET-26 are major enzymes for depositing H3K9me3 in *C. elegans*, then
301 we would detect reduced H3K9me3 levels in the *set-9 set-26* double mutant strain.
302 Using Western blotting, we showed that the global levels of H3K9me3 were not
303 detectably altered in the *set-9 set-26* double mutants compared to wild-type worms at
304 the L4 stage (Figure 6-figure supplement 1B). We further investigated the genomic
305 distribution of H3K9me3 in wild-type N2 and the F3 *set-9 set-26* double mutant worms
306 using ChIP-seq (chromatin immunoprecipitation coupled with next generation
307 sequencing). Inspection of the genome-wide H3K9me3 distribution between N2 and the
308 F3 *set-9 set-26* double mutant revealed highly similar patterns (Figure 6-figure
309 supplement 1C and 1D). Furthermore, the Diffbind data analysis pipeline (Bardet et al.
310 2011) identified little significant differences between the two data sets (data not shown).
311 Taken together the Western and ChIP-seq results, we concluded that SET-9 & SET-26
312 are likely not the major enzymes required for H3K9me3 deposition in *C. elegans*.
313 However, we could not rule out the possibility that the SET-9 & SET-26 could deposit
314 H3K9me3 in specific cells, or during a specific time. Indeed, we previously reported that
315 in the germlineless mutant *glp-1*, loss of *set-26* resulted in lower levels of H3K9me3 (Ni
316 et al. 2012). Further investigations will be necessary to resolve whether SET-9/SET-26
317 could regulate H3K9me3 levels under some circumstances. We also note that SET-25
318 has been shown to be important for the deposition of the majority of H3K9me3 in *C.*
319 *elegans*, although the effect could be indirect as direct H3K9 methylating activities of
320 SET-25 have yet to be demonstrated (Towbin et al. 2012).
321

322 **The PHD domains of SET-9 and SET-26 bind to H3K4me3 with adjacent**
323 **acetylation marks *in vitro***
324 We next turned our attention to the PHD domains of SET-9 & SET-26, which are 100%
325 identical. PHD domains are known to recognize specific histone modifications, we
326 therefore tested whether the PHD domains of SET-9 & SET-26 also bind to specific
327 histone modifications *in vitro*. We first used GST-tagged PHD domain of SET-9/SET-26
328 to perform an *in vitro* pull-down experiment using histones from calf thymus. We found
329 that the PHD domain of SET-9 & SET-26 pulled down histones, in particular histone H3
330 (Figure 6A). A small amount of histone H4 was also recovered, which may be due to H3
331 and H4 associating as histone octamers in cells. We next screened for the specific
332 histone modifications that are recognized by the PHD domain of SET-9 & SET-26 using
333 a histone peptide array containing 95 unique modifications and 265 synthetic histone
334 peptides. This assay revealed that the PHD domain of SET-9 & SET-26 specifically
335 interacted with H3 peptides containing the K4me3 modification in combination with
336 nearby acetylation (K9ac, K14ac and/or K18ac), but not H3K4me3 alone (Figure 6B).
337
338 **Genome-wide profiles of SET-9 and SET-26 are highly concordant with that of**
339 **H3K4me3**
340 We further examined the genome-wide binding profiles of SET-9 and SET-26 in *C.*
341 *elegans* using ChIP-seq. Because antibodies capable of immunoprecipitating
342 endogenous SET-9 and SET-26 were not available, we utilized the GFP knock-in
343 strains discussed above. We performed anti-GFP ChIP-seq using the *set-9::gfp*, *set-*
344 *26::gfp*, and *set-9::gfp set-26::gfp* strains. The double GFP strain was used in the hope

345 that higher levels of GFP expression would provide more robust ChIP-seq data (Figure
346 6-figure supplement 2). MACS2 was used to identify the genomic regions significantly
347 enriched for SET-9 and SET-26 binding. From the analyses, 602, 3948, and 5903 peaks
348 were identified as bound by SET-9, SET-26, and SET-9 & SET-26 together, respectively.
349 Interestingly, 67% of the SET-9 peaks (Figure 6-figure supplement 2B) overlapped with
350 the SET-26 peaks, and 87% of the SET-26 peaks overlapped with the SET-9 & SET-26
351 peaks (Figure 6-figure supplement 2C). That SET-9 was found to bind many fewer
352 regions than SET-26, and that the SET-9-bound peaks largely overlapped with those
353 bound by SET-26, are consistent with the earlier data indicating SET-9 has a much
354 more restricted expression pattern and a more limited function in the germline that is
355 redundant with SET-26. Interestingly, ChIP-seq analysis from the double GFP strain
356 nevertheless revealed many more peaks compared to SET-26::GFP alone. We
357 interpreted these results to suggest that the double GFP strain simply represented a
358 better reagent for capturing the SET-9 and SET-26 binding profiles than either of the
359 single GFP strain, because the ChIP assay worked more effectively with higher levels of
360 GFP expression. For further analyses, we used the peak regions identified in the double
361 GFP strain as representation of the binding sites of SET-9 & SET-26.
362 Given the *in vitro* binding of the PHD domain of SET-9 & SET-26 to H3K4me3, we
363 wondered whether SET-9 and SET-26 also bind to H3K4me3 *in vivo*. To test this, we
364 examined the genome-wide pattern of H3K4me3 in wild-type worms using ChIP-seq. A
365 representative genome browser view revealed that the SET-9 & SET-26 binding profile
366 generally correlated well with the H3K4me3 profile (Figure 6C). In contrast, the SET-9 &
367 SET-26 binding profile was largely different from that of H3K9me3 (Figure 6C), again

368 consistent with our earlier conclusion that SET-9 & SET-26 likely do not modify
369 H3K9me3.
370 To more rigorously assess whether the SET-9 & SET-26 profile is concordant with the
371 H3K4me3 profile, we tested whether SET-9 & SET-26, and H3K4me3 were enriched in
372 overlapping genomic regions. To this end, we used MACS2 to identify 5996 genomic
373 regions enriched for H3K4me3 marking (peaks), and then compared the degree of
374 overlap between the SET-9 & SET-26 peaks with those of H3K4me3. In this comparison,
375 we found that 75% of the SET-9 & SET-26 binding regions overlapped with the
376 H3K4me3 peaks (Figure 6D). The reciprocal comparison revealed that 49% of the
377 H3K4me3 peaks overlapped with the SET-9 & SET-26 binding regions (Figure 6E). We
378 sought to further characterize the overlapping profiles between SET-9 & SET-26 and
379 H3K4me3 using meta-analysis. We separated the H3K4me3 peaks into the group that
380 bound by SET-9 & SET-26 and the group that did not, and we plotted the average
381 normalized H3K4me3 levels centered around the summits of the H3K4me3 peaks and
382 oriented at a 5' to 3' direction according the nearest genes associated with the peaks.
383 We found that, on average, the H3K4me3 peaks bound by SET-9 & SET-26 had higher
384 levels of H3K4me3 marking and their H3K4me3 marking was somewhat higher 5' to the
385 summit (Figure 6-figure supplement 3A). This asymmetrical marking of H3K4me3 might
386 relate to that these peaks generally localized around annotated
387 transcriptional/translational start sites (TSSs) and H3K4me3 levels tend to be higher 5'
388 to the start sites of the genes. In contrast, the average plot of the H3K4me3 peaks that
389 were not bound by SET-9 & SET-26 was more symmetrical, and this correlated with
390 these H3K4me3 peaks generally localized to gene body regions (data not shown).

391 We next used a similar meta-analysis approach but plotted the normalized SET-9 &
392 SET-26 ChIP signals for the two groups of H3K4me3 peaks, still oriented at the
393 summits of the H3K4me3 peaks (Figure 6-figure supplement 3B). This analysis allowed
394 us to determine how far the average summit of the SET-9 & SET-26 peaks was relative
395 to that of the H3K4me3 peaks. The results indicated that the average summit of the
396 SET-9 & SET-26 peaks was ~100-200bp upstream of the H3K4me3 summit (Figure 6-
397 figure supplement 3B). Interestingly, for the group of H3K4me3 peaks that were not
398 identified to share SET-9 & SET-26 enrichment based on MACS2, we nevertheless
399 detected a small amount of SET-9 & SET-26 binding exactly at the summits of the
400 H3K4me3 peaks (Figure 6-figure supplement 3B). We interpreted these results to
401 suggest that SET-9 & SET-26 likely bind to most if not all of the H3K4me3 enriched
402 regions, but some of the binding was too weak (or strong binding only in a subset of the
403 *C. elegans* cells) to be called by a statistical program like MACS2. Lastly, we used
404 scatter plot analysis to compare the H3K4me3 enriched signal vs. the SET-9 & SET-26
405 binding signal for each of the H3K4me3 peak region (Figure 6-figure supplement 3C).
406 The results showed that the H3K4me3 signal intensity is positively correlated with that
407 of SET-9 & SET-26 (Figure 6-figure supplement 3C). The data thus far support a model
408 that SET-9 & SET-26 bind to regions marked by H3K4me3 in *C. elegans*, and that the
409 detectable SET-9 & SET-26 binding sites are generally marked by higher levels of
410 H3K4me3.
411 Since the *in vitro* histone peptide array results suggested that histone acetylations are
412 also important for the binding, we next compared the degree of overlap between the
413 SET-9 & SET-26 peaks with those of H3K9ac using data from modENCODE. In this

414 comparison, we found that 28% of the SET-9 & SET-26 binding regions overlapped with
415 the H3K9ac peaks (***p<0.001) (Figure 6-figure supplement 3D), and 98% of these
416 shared peak regions were also marked by H3K4me3 (data not shown). The significant
417 but lower percentage of overlap between SET-9 & SET-26 binding with the H3K9ac
418 enriched regions (relative to the overlap with H3K4me3 enriched regions) is consistent
419 with the *in vitro* observation that SET-9 & SET-26 bind to H3K4me3 with adjacent
420 acetylation, but the exact acetylated residues could vary (Figure 6B), but is also likely
421 partly due to technical differences, e.g. the different ChIP-seq data were generated
422 using worms at different stages and acetyl specific antibodies generally have lower
423 specificity. We additionally compared the overall correlation between H3K4me3 and
424 H3K9ac enriched regions and whether SET-9 & SET-26 may affect their co-occurrence.
425 As expected, we found that the genome-wide distribution of H3K4me3 correlated well
426 with that of H3K9ac (Figure 6-figure supplement 3E). Interestingly, the correlation
427 between H3K4me3 and H3K9ac was higher for the peaks that were bound by SET-9 &
428 SET-26 compared to those that were not (Figure 6-figure supplement 3F and Figure 6-
429 figure supplement 3G). These genomic data are consistent with the model that SET-9 &
430 SET-26 bind to genomic regions marked by H3K4me3 with nearby acetylations in *C.*
431 *elegans*.
432

433 **SET-9 & SET-26 regulate the RNA expression of some of their target genes**

434 We next asked whether SET-9 & SET-26 binding could influence gene expression. To
435 test this, we assigned the 5903 regions bound by SET-9 & SET-26 (based on ChIP-seq
436 results, Figure 6) with their closest genes, and then filtered them for genes that were

437 detectably expressed in our RNA-seq data sets, which yielded 4427 potential targets of
438 SET-9 & SET-26 that were also actively expressed in our experimental conditions. We
439 then compared the list of SET-9 & SET-26 target genes with the lists of genes that
440 exhibited significant gene expression change in the *set-9* single, *set-26* single, and the
441 F1 *set-9 set-26* double mutants compared to wild-type worms based on our RNA-seq
442 data (Figure 7A and Figure 7-figure supplement 1A and 1D). Through this comparison,
443 we identified the putative SET-9 & SET-26 target genes that changed expression when
444 *set-9* and/or *set-26* were inactivated (Figure 7A and Figure 7-figure supplement 1A and
445 1D). Out of the 735, 876, 3532 differentially expressed genes in the *set-9*, *set-26*, and
446 F1 *set-9 set-26* double mutant strains, SET-9 & SET-26 bound to 153, 217, 641 of them
447 respectively (Figure 7A and Figure 7-figure supplement 1A and 1D). GO analyses
448 revealed some interesting over-represented functional groups among these, especially
449 for the SET-9 & SET-26 targets that exhibited expression change in the F1 double
450 mutant (Figures 7B-C and Figure 7-figure supplement 1).
451 In an attempt to identify the somatic SET-26 target genes with a role in longevity, we
452 compared the genes bound by SET-9 & SET-26 to the genes that showed expression
453 change in the germlineless *glp-1; set-26* double mutant (Figure 7D). GO analysis did not
454 reveal functional groups that are directly linked to longevity (Figure 7E and 7F), but
455 “collagen” was again overrepresented. Moreover, for the DAF-16-dependent somatic
456 SET-26 regulated genes that were highly enriched for the functional group
457 “determination of lifespan” (Figure 4), only 3 out of the 134 genes were bound by SET-9
458 & SET-26, a representation that is lower than expected based on random chance.

459 Together, these data suggested that SET-26 indirectly impact DAF-16 activity and DAF-
460 16-mediated longevity change.
461
462 **Loss of SET-9 and SET-26 results in expansion of H3K4me3 marked regions**
463 We next tested whether SET-9 & SET-26, in addition to binding to H3K4me3, can
464 influence the marking of H3K4me3 in anyway. We first examined the global H3K4me3
465 levels in the *set-9* single, *set-26* single and F3 *set-9 set-26* double mutants. We
466 observed a subtle but significant increase in H3K4me3 levels in the F3 *set-9 set-26*
467 double mutant but not in the *set-9* or *set-26* single mutants using Western blotting
468 (Figure 8A and Figure 8-figure supplement 1A). This increase in H3K4me3 levels was
469 more prominent in dissected gonads of the *set-9 set-26* double mutant (Figure 8B).
470 Given our earlier data indicating that SET-9 & SET-26 bind to H3K4me3, the elevated
471 H3K4me3 levels in the *set-9 set-26* double mutant strain could be a result of the lost
472 recruitment of SET-9 and SET-26 at H3K4me3 sites.
473 To test this hypothesis, we examined the genome-wide patterns of H3K4me3 in wild-
474 type, the F1 and F3 *set-9 set-26* double mutant worms. Inspection of the genome-wide
475 H3K4me3 distribution in the three genotypes revealed a “spreading” of H3K4me3
476 enriched regions around SET-9 & SET-26 binding sites in worms lacking *set-9* & *set-26*
477 (Figure 8-figure supplement 1C and 1D). To quantify this “spreading” globally, we
478 separated the H3K4me3 enriched regions into those bound by SET-9 & SET-26 *vs.*
479 those that were not, and compared their average profiles using meta analysis (Figures
480 8C and 8D). The meta analysis plots were centered around the summits of the
481 H3K4me3 peaks and orientated in the 5’ to 3’ direction according to the closest gene

482 associated with each of the peak (Figure 8C and 8D). For the H3K4me3 peaks bound
483 by SET-9 & SET-26, we again observed a “spreading” of H3K4me3 marking, especially
484 towards the 3’ direction. Statistically significant elevated levels of H3K4me3 were
485 detected starting at around +500bp and -1000bp beyond the summit in the F1 and F3
486 *set-9 set-26* double mutant compared to wild-type worms, where the 95% confidence
487 intervals of H3K4me3 marking in the F1 and F3 *set-9 set-26* mutants did not overlap
488 with that in the wild-type worms (Figure 8C). Interestingly, for the H3K4me3 peaks that
489 showed no detectable SET-9 & SET-26 binding, the average plot showed no significant
490 “spreading” of the H3K4me3 marking (Figure 8D). Nevertheless, the genome-wide
491 heatmaps revealed some slight “spreading” of H3K4me3 signals in the *set-9 set-26*
492 double mutant even in regions not determined to be bound by SET-9 & SET-26 (Figure
493 8-figure supplement 1D). This could be due to residual binding of SET-9 & SET-26 that
494 was statistically unable to be detected by the MACS2 pipeline (Figure 6-figure
495 supplement 3B). We further examined the observed “spreading” of H3K4me3 marking
496 by producing meta plot of the H3K4me3 peaks that overlapped with SET-9 & SET-26
497 binding that centered around the summits of SET-9 & SET-26 binding peaks. We again
498 observed an insignificant increase at the center of the plot, where SET-9 & SET-26
499 binding peaked, but a detectable increase of H3K4me3 levels in regions flanking the
500 summit of SET-9 & SET-26 binding sites in the F1 and F3 *set-9 set-26* double mutant
501 compared to wild-type worms (Figure 8-figure supplement 1E).
502 It is interesting to note that the F3 *set-9 set-26* double mutant showed a more obvious
503 expansion of H3K4me3 compared to the F1 *set-9 set-26* double mutant, even though
504 this difference was not statistically significant, as their 95% confidence intervals

505 overlapped (Figure 8C, 8D and Figure 8-figure supplement 1E). Since the F3 *set-9 set-*
506 *26* double mutant had a more severe fertility defect (Figure 2), this observation hinted at
507 a possible correlation between H3K4me3 expansion and germline defects. We
508 previously reported that the levels of H3K4me3 as detected by Western blotting was not
509 impacted by the loss of *set-26* in the germlineless *glp-1* mutant (Ni et al. 2012),
510 suggesting that inactivation of SET-26 does not impact the global levels of H3K4me3 in
511 the soma. To further investigate this possibility, we performed similar H3K4me3 ChIP-
512 seq analysis in the germlineless *glp-1; set-26* and *glp-1* mutants. Interestingly, we
513 observed no significant difference in the genome-wide patterns of H3K4me3 in
514 germlineless worms with or without SET-26, even in regions bound by SET-9 & SET-26
515 (Figure 8-figure supplement 1F). The ChIP-seq results therefore corroborated with our
516 previous Western blotting results, and together they supported the notion that SET-9 &
517 SET-26 binding does not detectably impact H3K4me3 marking in somatic cells. Rather,
518 SET-9 &SET-26 binding likely normally help to restrict H3K4me3 marking specifically in
519 the germline.
520

521 **A subset of germline-specific genes showed correlated changes in H3K4me3 and**
522 **RNA expression levels in the F1 and F3 *set-9 set-26* double mutants**

523 H3K4me3 has been generally associated with active gene expression (Sims et al. 2007).
524 We wondered whether the regions with expanded H3K4me3 marking could be
525 associated with gene expression changes in the F1 and F3 *set-9 set-26* double mutants.
526 To assess this, we used csaw, an R package for differential binding analysis of ChIP-
527 seq data using sliding windows, to identify 3438 and 5456 regions that exhibited

528 statistically significant different H3K4me3 marking in F1 and F3 *set-9 set-26* double
529 mutants compared with wild-type worms (data not shown). Consistent with a slight
530 global increase in H3K4me3 levels in the F1 and F3 *set-9 set-26* double mutant, 92%
531 and 99% of the differential H3K4me3 regions revealed by csaw showed elevated
532 H3K4me3 levels in the F1 and F3 *set-9 set-26* double mutants. We next assigned these
533 differential H3K4me3 peaks to their closest genes and identified 3017 and 4517genes
534 that are associated with altered H3K4me3 markings. We then compared these gene
535 lists with the list of genes that exhibited significant expression change between the F1
536 and F3 *set-9 set-26* double mutants compared to wild-type worms based on our earlier
537 RNA-seq data. In this comparison, only 479 and 310 genes with elevated H3K4me3
538 markings showed expression change in the F1 and F3 *set-9 set-26* double mutants
539 (Figure 8-figure supplement 1G and 1H), an overlap that was significantly lower than
540 what would be expected based on random chance. These results suggested that the
541 expanded H3K4me3 regions were not generally accompanied with detectable gene
542 expression changes based on comparison with RNA-seq analyses from whole worms.
543 Since our data suggested that the "spreading" of H3K4me3 surrounding SET-9 & SET-
544 26 binding sites likely occur specifically in the germline, we wondered whether the SET-
545 9 & SET-26 target genes in the germline would show a correlation between H3K4me3
546 "spreading" and gene expression increase. To investigate this possibility, we compared
547 the H3K4me3 profiles for the genes that were bound by SET-9 & SET-26 and showed
548 expression increase in F1 *set-9 set-26* double mutant compared with wild-type worms
549 (Figure 7), and were determined to be "germline-specific" based on previous reports
550 (Reinke et al. 2004) (Figure 5 & Figure 8- figure supplement 2A). We found that their

551 average H3K4me3 markings were highly upregulated in the F1 and F3 *set-9 set-26*
552 double mutants compared with wild-type worms, and the elevation was noticeable at
553 both the TSS and the TES and throughout the gene body (Figure 8- figure supplement
554 2B). A comparison of this list of germline-specific SET-9 & SET-26 target genes also
555 indicated that their H3K4me3 elevation (based on csaw) was significantly correlated
556 with gene expression increase (based on RNA-seq) (Figure 8- figure supplement 2C).
557 Therefore, it appeared that for the germline-specific genes, H3K4me3 expansion indeed
558 correlates well with RNA expression increase. We concluded that SET-9 & SET-26
559 have a unique function in the germline, where they likely restrict H3K4me3 domains and
560 maintain the expression of a subset of genes.
561
562 **RNAi screens revealed that SET-2, the H3K4me3 methyltransferase, functions**
563 **cooperatively with SET-9 & SET-26 to regulate germline function**
564 Since many histone methyltransferases and demethylases are known to play important
565 roles in germline function in *C. elegans* (Katz et al. 2009; Li and Kelly 2011; Nottke et al.
566 2011; Xiao et al. 2011; Robert et al. 2014; Kerr et al. 2014; Greer et al. 2014), we
567 performed an RNAi screen targeting putative histone methyltransferases and
568 demethylases to uncover genes that potentially work with SET-9 & SET-26 to regulate
569 germline function. We treated F1 *set-9 set-26* double mutant worms, which showed a
570 mild reproductive defect (Figure 2), with each of the RNAi and assayed their
571 consequent brood size. Whereas most of the RNAi treatment did not substantially affect
572 the brood size of the F1 *set-9 set-26* double mutant, we found that three components of
573 the MLL complex, which is well-established to deposit H3K4me3, including *set-2*, *set-16*

574 and *wdr-5.1*, significantly reduced the brood size of the F1 *set-9 set-26* double mutant
575 when knocked down (Figure 9A). To rule out off-target effects, we crossed the partial
576 loss-of-function *set-2(ok952)* mutant with the *set-9 set-26* double mutant and assayed
577 their brood size at the F1 generation. We again observed a synergistic effect, where the
578 *set-2(ok952)* single mutant had a normal brood size as previously reported, but the F1
579 *set-2; set-9 set-26* triple mutant had a drastically reduced brood size compared with the
580 F1 *set-9 set-26* double mutant (Figure 9B). This result is consistent with the model that
581 SET-2 and SET-9 & SET-26 regulate H3K4me3 marking in different ways and their
582 simultaneous loss results in synergistic detrimental effect. Our data above indicated that
583 SET-9 & SET-26 bind to H3K4me3 and restrict H3K4me3 domain, likely specifically in
584 the germline. The results with the weak loss-of-function *set-2* mutation suggested that
585 suboptimal deposition of H3K4me3 together with broadening of H3K4me3 marking
586 could cause substantial defects in germline function.
587

588 **Discussion**

589 In this study, we revealed that the highly homologous paralogs SET-9 and SET-26 have
590 unique as well as redundant functions. We found that SET-9 and SET-26 share
591 redundant function in germline development, but only SET-26, not SET-9, plays a role in
592 modulating lifespan and resistance to heat stress. We confirmed that SET-9 is only
593 detectable in the germline whereas SET-26 is broadly expressed, and we concluded
594 that their differential expression patterns likely account for the different phenotypes
595 associated with the loss of each gene. Our transcriptomic analyses corroborated
596 previous genetic studies and implicated SET-26 to act through DAF-16 in somatic cells

597 to modulate longevity. We further demonstrated that SET-9 and SET-26 bind to
598 H3K4me3 *in vitro* and *in vivo*, and that the loss of *set-9* & *set-26* results in the
599 broadening of H3K4me3 domains surrounding most SET-9 & SET-26 binding regions,
600 likely specifically in the germline. The expanded H3K4me3 domains were associated
601 with increased expression of germline-specific genes bound by SET-9 & SET-26. We
602 propose that in the soma, SET-9 and SET-26 somehow impact DAF-16 activity to
603 modulate longevity, whereas in the germline, they are critical for restricting H3K4me3
604 domains and regulating the expression of specific target genes with important
605 consequence on germline development (Figure 10).
606

607 ***set-9* and *set-26* are duplicated genes**

608 *set-9* and *set-26* share high sequence identity both within the coding regions and in the
609 non-coding sequences flanking the coding regions (near 90% identity in the +/− 500bp
610 regions), and even in the genes 3' of *set-9* and *set-26* (Y24D9B.1 and Y51H4A.13
611 respectively). Although *set-9 & set-26* are highly conserved from worms to yeast to
612 mammals, only one homolog in each of the other diverse species has been detected
613 based on sequence and domain structure alignment (Rincon-Arano et al. 2012; Zhang
614 et al. 2017). Even the closely related *Caenorhabditis* species, such as *C. briggsae*, *C.*
615 *remanei*, *C. brenneri* and *C. japonica*, only harbor one gene that is highly homologous
616 to *set-9 & set-26*. These results suggested that *set-9* and *set-26* have arisen from gene
617 duplication specifically in *C. elegans*. In the future, it will be interesting to explore how
618 this duplication event allowed *set-9* and *set-26* to adopt unique functions.
619

620 **SET-9 and SET-26 in chromatin regulation**

621 Based on the similarity in sequence and domain structure, *Drosophila* UpSET and
622 mammalian SETD5 and MLL5 represent the likely homologs of SET-9 & SET-26. SET-9
623 & SET-26, UpSET, SETD5 and MLL5 all harbor centrally localized SET and PHD
624 domains, and they share ~30-40% sequence identity in their PHD and SET domains.
625 The SET domains of SET-9, SET-26, UpSET, SETD5 and MLL5 proteins are highly
626 conserved and all share similar mutations that suggest they should lack enzymatic
627 activities (Figure 6-figure supplement 1A). Indeed, UpSET, SETD5 and MLL5 have not
628 been found to harbor methylating activities (Osipovich et al. 2016; Rincon-Arano et al.
629 2012; Madan et al. 2009). Whereas the SET domain of SET-26 has been suggested to
630 methylate H3K9me3 *in vitro* (Greer et al. 2014), our data indicated that SET-9 and SET-
631 26 do not have major roles in H3K9me3 deposition in *C. elegans*. The exact function(s)
632 of the SET domain in these proteins remain to be elucidated.
633 The PHD domains of SET-9, SET-26, UpSET and MLL5 proteins are also highly
634 conserved. The PHD domain of MLL5 was found to bind to H3K4me3 *in vitro* (Ali et al.
635 2013), and both MLL5 and UpSET have been shown to localize at promoter regions in
636 cultured cells (Rincon-Arano et al. 2012; Ali et al. 2013). Our results demonstrated that
637 SET-9 & SET-26 also bind to H3K4me3 *in vitro* and *in vivo*. We further revealed that the
638 PHD domains of SET-9 & SET-26 bind to H3K4me3 with adjacent acetylation (e.g. K9,
639 K14, K18) with much greater affinity (Figure 6B). This is an important finding and
640 potentially links SET-9 & SET-26 to the regulation of both H3K4me3 and histone
641 acetylation. Indeed, we showed that loss of *set-9* & *set-26* results in a slight elevation of
642 global H3K4me3 and H3K9Ac levels (Figure 8A and Figure 8- figure supplement 1B).

643 We additionally uncovered expansion of H3K4me3 domains surrounding SET-9 & SET-
644 26 bound regions, and we predict that similar expansion of H3K9Ac likely occurs in the
645 *set-9 set-26* double mutant. Interestingly, loss of *set-26* in somatic tissues does not
646 result in similar H3K4me3 elevation (Figure 8-figure supplement 1F) and we concluded
647 that SET-9 & SET-26 are particularly important for restricting H3K4me3 domains in the
648 germline. These data are reminiscent to those reported for MLL5 and UpSET (Rincon-
649 Arano et al. 2012; Gallo et al. 2015). In human glioblastoma cells with self-renewing
650 potential, it was found that knockdown of MLL5 leads to increased global levels of
651 H3K4me3 and a more open chromatin environment (Gallo et al. 2015). Importantly, this
652 anti-correlation between MLL5 and H3K4me3 was only detected in primary glioblastoma
653 cells with self-renewing potential, but not in bulk glioblastoma samples, nor in non-
654 neoplastic brain samples or colon cancer cells (Gallo et al. 2015), indicating a regulatory
655 process that is highly cell type specific. A possible parallel in *C. elegans* is that the anti-
656 correlation between SET-9 & SET-26 status and H3K4me3 levels is particularly obvious
657 in the germline of adult worms (Figure 8B), which harbor proliferative germline stem
658 cells. In *Drosophila* Kc cells, UpSET knockdown has been shown to increase the levels
659 and spreading of H3K9Ac, H3K16Ac, and H3K4me2/3 around some TSSs, which
660 results in a generally more accessible chromatin environment (Rincon-Arano et al.
661 2012). UpSET achieves this partly through recruitment of specific histone deacetylases.
662 Although the role of SETD5 PHD domain has not been studied, SETD5 also has been
663 found to interact with histone deacetylase complex (Osipovich et al. 2016). Loss of
664 SETD5 causes elevation in histone acetylation at transcriptional start sites and near
665 downstream regions (Osipovich et al. 2016), suggesting that it acts in a similar manner

666 to *Drosophila* UpSET. Taking together the *C. elegans*, *Drosophila*, and mammalian data,
667 it appears that the SET-9, SET-26, UpSET, SETD5, MLL5 family of factors play an
668 important role in binding to H3K4me3, possibly with flanking acetylation sites, and
669 regulating local chromatin accessibility, partly through restricting the spread of histone
670 modifications such as H3K4 methylation and H3K9 acetylation. Extending from the
671 findings with UpSET in *Drosophila* and SETD5 in mammals, SET-9 and SET-26 likely
672 also recruit demethylating and deacetylating enzymes to confine local methylation and
673 acetylation domains.
674
675 **Biological functions of SET-9 and SET-26**
676 In this study, we uncovered a novel redundant function of SET-9 and SET-26 in
677 germline function. It is interesting to note that an earlier report suggested that loss of
678 *set-26*, but not *set-9*, accelerated the progressive sterility of the *spr-5* mutant (Greer et
679 al. 2014). However, our analyses indicated that the *set-9(n4949)* mutant used in the
680 study (Greer et al. 2014) represents a deletion/duplication allele, as we can PCR
681 amplify the *set-9* gene from the mutant (data not shown). Our data using the newly
682 generated *set-9(rw5)* deletion/frame-shift mutant supported a role of SET-9 in
683 collaboration with SET-26 to regulate germline development.
684 In considering the possible homologs of SET-9 and SET-26 in other species, MLL5 has
685 been implicated in male fertility (Heuser et al. 2009; Madan et al. 2009), whereas
686 UpSET is important for female fertility (Rincon-Arano et al. 2012). Our data indicated
687 that SET-9 & SET-26 have a more pleiotropic role in the germline, affecting both
688 germline stem cell proliferation, and the subsequent differentiation into oocytes and

689 sperms. This difference could be due to that *C. elegans* are hermaphrodites and SET-9
690 & SET-26 have adopted broader functions in the germline. In addition, MLL5 has been
691 implicated in regulating cell cycle progression (Deng et al. 2004) and stem cell
692 pluripotency (Zhang et al. 2009), which may parallel the redundant roles of SET-9 &
693 SET-26 in germline stem cells proliferation. Considering the highly conserved functions
694 of SET-9, SET-26, UpSET, SETD5 and MLL5 at the molecular and phenotypic levels,
695 an intriguing possibility is that UpSET, SETD5 and MLL5 have a yet-to-be characterized
696 role in stress response and longevity.
697
698 A key important question is how SET-9 & SET-26 can mediate their effects on stress
699 response, longevity and germline development. Our data clearly supported that SET-26
700 acts in the soma and through DAF-16 to modulate longevity. The exact functional
701 relationship between SET-26 and DAF-16 remains unclear. It was striking that the
702 comparison of the SET-9 & SET-26 bound targets from whole worms and the DAF-16-
703 mediated transcriptomic changes in germlineless mutant not only did not show a
704 significant overlap, it in fact showed an overlap that was much lower than expected by
705 random chance. Although it is difficult to cross-compare results from different
706 experimental set-ups, it seems likely that SET-9 and SET-26 do not bind to candidate
707 DAF-16 regulated genes. Therefore, SET-9 and SET-26 likely mediate their effect on
708 DAF-16 indirectly.
709 We also note that while we were able to identify SET-9 & SET-26 targets whose
710 expression show significant change in response to the loss of *set-9* & *set-26*, the SET-9
711 & SET-26 binding targets were not enriched for genes that showed expression change

712 in the *set-9 set-26* double mutant. In other words, genes bound by SET-9 & SET-26
713 were not more likely to show expression change when *set-9* & *set-26* were deleted.
714 Since our ChIP-seq data were from whole worms and could not distinguish the SET-9
715 and SET-26 binding targets in the soma vs the germline, our current results cannot
716 resolve whether SET-9- & SET-26-binding has a direct consequence on gene
717 expression regulation.
718
719 We detected significant broadening of H3K4me3 marking surrounding the SET-9 &
720 SET-26 bound regions. Although this change was observed in whole worms, it was not
721 detectable in worms lacking germline (Figure 8-figure supplement 1F). We interpreted
722 this to mean that the expansion of H3K4me3 domains likely happen either specifically in
723 the germline, or most noticeable in the germline. Somewhat surprisingly, such
724 broadening of H3K4me3 domains did not appear to correlate with gene expression
725 using whole worm analyses. This finding could partly be due to technical caveats, as the
726 ChIP-seq and RNA-seq data were generated using whole worms, which could mask
727 correlated changes in specific cells. Consistent with this speculation, we detected a
728 significant and positive correlation between H3K4me3 expansion with RNA expression
729 change of germline-specific genes. In the future, ChIP-seq and RNA-seq analyses using
730 dissected gonads *vs* somatic tissues will help to further establish this prediction.
731 In addition to gene regulation, the expanded H3K4me3 regions likely represent
732 perturbed chromatin environment that could interfere with processes other than gene
733 regulation, such as genome maintenance. In fact, in *C. elegans*, altered H3K4
734 methylations have been shown to predispose mutant worms to DNA damage and

735 genome instabilities, which result in germline defects (Nottke et al. 2011). Interestingly,
736 inactivating UpSET in *Drosophila* and MLL5 in mammals also lead to increased genome
737 instability and DNA damage (Tasdogan et al. 2016; Rincon-Arano et al. 2012). In *C.*
738 *elegans*, we observed an increased number of germ cell apoptosis in the *set-9 set-26*
739 double mutant (data not shown). Moreover, RNAi knockdown of *mre-11*, a double-
740 strand break repair protein, synergistically aggravated the fertility defects of the *set-9*
741 *set-26* double mutant (data not shown). These data together suggested that DNA
742 damage and genome instability could be increased in the *set-9 set-26* double mutant,
743 which may contribute to their germline defects.
744
745 In summary, our findings provided new mechanistic insights into the functions of SET-9
746 & SET-26 with important implications for their roles in longevity and germline
747 development. We revealed that SET-9 & SET-26 are recruited to H3K4me3 marked
748 regions and participate in confining H3K4me3 domains, particularly in the germline.
749 Loss of *set-9* & *set-26* in these regions likely leads to a more open and accessible
750 chromatin environment and RNA expression change in a subset of genes. In addition,
751 SET-26 acts in the soma to modulate longevity and it achieves this by regulating DAF-
752 16-mediated transcription indirectly. Our findings are consistent with the possibility that
753 human MLL5 and SETD5 represent functional homologs of SET-9 & SET-26, and the
754 results discussed here provide new insights into how MLL5 and SETD5 may act and
755 also implicate them in stress response and longevity.
756
757 **Materials and Methods**

758 **Worm strains**

759 The N2 strain was used as the wild-type (WT). The mutants used in the study are: *set-*
760 *2(ok952), set-9(rw5)*, *set-26(tm2467)*, *rrf-1(pk1417)*, *daf-16(mgDf47), glp-1(e2141);* the
761 *set-9(rw5) set-26(tm2467)* double mutant was maintain as balanced heterozygote *set-*
762 *9(rw5) set-26(tm2467)* /nT1. The GFP knock-in strains constructed in this study are: *set-*
763 *9::gfp(rw24)*, *set-26::gfp(rw25)*.

764

765 **Antibodies**

766 The antibodies used were anti-H3K4me3(Millipore, Billerica, MA 17-614), anti-
767 H3K9me3(abcam, Cambridge, United Kingdom ab8898), anti-GFP(abcam, Cambridge,
768 United Kingdom ab290), anti-H3(abcam, Cambridge, United Kingdom ab1791), anti-
769 H3K9ac(Wako, Richmond, VA 309-32379).

770

771 **Brood size assay**

772 Brood size assay was performed as described (Li et al. 2008). Each single L4 worm
773 was picked onto individual plate and was transferred to a new plate every 24 hours until
774 the end of its reproductive phase. Dead eggs and alive progenies were counted as its
775 total brood size. All experiments were repeated two to three times. Student's t-test was
776 used to calculate the p-values.

777

778 **Lifespan assay**

779 Lifespan assay was performed as described (Li et al. 2008). All experiments were
780 performed at 20°C. For RNAi plates, the *set-9/26* RNAi construct was taken from the

781 Ahringer RNAi library. RNAi bacteria were grown in LB with 100ug/ml Carbenicillin
782 (Carb) and 15ug/ml Tetracycline (Tet) at 37°C to OD600 around 0.8. The culture was
783 concentrated 5-fold, and seeded onto plates with Carb and Tet. Sufficient IPTG stock
784 was added to plates so that final IPTG concentration is 4mM. Let plates dry and induce
785 for ~4 hrs before use. For lifespan assays using NGM plates seeded with OP50 bacteria,
786 the OP50 bacteria were grown in LB overnight at 37°C and the culture was
787 concentrated 3-fold and seeded onto plates. For all lifespan assays, Worms were
788 picked onto RNAi plates to lay ~40 eggs per plate and the progeny were grown on the
789 plate until they reached adulthood. The worms were transferred to a new plate every
790 day during their reproductive phase and then transferred to a new plate every 4 days.
791 Worms were scored every other day, and those that failed to respond to a gentle
792 prodding with a platinum wire were scored as dead. Animals that bagged, exploded, or
793 crawled off the plate were considered as censored. We defined the day when we
794 transferred the young adult worms as day 0 of adult lifespan. All the lifespan
795 experiments were repeated at least two independent times. Standard survival analysis
796 was performed using SPSS and OASIS software (Yang et al. 2011). The survival
797 function was estimated using the Kaplan-Meier method, and the p-values were
798 calculated using a log-rank test.
799
800 **Heat stress assay**
801 Heat stress assay was performed as described (Li et al. 2008). Synchronous D0 adult
802 worms grown on OP50-NGM plates at 20°C were shifted to 35°C. Worms were scored
803 every 3-4 hours. All the heat stress experiments were repeated at least two independent

804 times. All experiments were repeated two to three times. Standard analysis was
805 performed using OASIS software. The survival function was estimated using the
806 Kaplan-Meier method, and the p-values were calculated using a log-rank test.
807

808 **Analysis of germline mortality**

809 Mortal Germline assays were performed by transferring 6 L1 larvae per plate to fresh
810 NGM plates every generation, as previously described (Ahmed and Hodgkin 2000).
811 Percentage fertile lines were calculated as the number of fertile plates divided by the
812 number of total plates.
813

814 **Immunofluorescence Staining**

815 The gonads from 100-150 worms were dissected out using syringe needle on a poly-
816 lysin coated slide. Gonads were permeabilized by the standard freeze-crack method
817 and were fixed in 4% formaldehyde fixative (PBS / 4 % formaldehyde) for 30 minutes
818 followed by 5-minute incubation in chilled methanol at -20°C in a Coplin jar. Slide was
819 washed twice with PBST for 5 minutes each and finally incubated with blocking buffer
820 (PBS + 5% BSA + 0.1% tween-20 + 0.1% triton-100) for 1 hour. Blocking buffer was
821 removed and gonads were incubated with 25 µl of 1:50 dilution of H3K4me3 antibodies
822 for overnight at 4°C in a humidity chamber. Next day, gonads were washed twice with
823 PBST for 10 minutes each and incubated with 25 µl of 1:50 dilution of secondary
824 antibody for 1-2 hours at RT. DAPI (final concentration 25 ng/ µl) was also added with
825 secondary antibody. Gonads were further washed three times with PBST for 10 minutes
826 each and mounted in 10 µl vectashield mounting medium (Vecta Laboratories).

827 Experiments were repeated twice. 4 worms and 5-7 germline nuclei for each worm were
828 used for quantification of H3K4me3 and DAPI. Student's t-test was used to calculate the
829 p-values.
830
831 **DAPI staining and measuring the number of germ cells within the mitotic region**
832 The gonads from 100-150 worms were dissected out using syringe needle. Gonads
833 were fixed in 4% formaldehyde fixative (PBS / 4 % formaldehyde) for 1 hour. After the
834 removal of fixative, gonads were washed twice with 1 ml PBST (PBS buffer + 0.1 %
835 Tween 20) each. Fixed worms were incubated with DAPI (25 ng/ µl in PBS) for 30
836 minutes. Gonads were further washed three times with 1 ml PBST for 5 minutes each
837 and mounted on agarose pads in 10 µl vectashield mounting medium (Vecta
838 Laboratories). DAPI-stained gonad images were taken using the Z-stacking function of
839 the microscope. To count mitotic germ cell numbers, we marked the boundary between
840 mitotic zone and transition zone by observing the transition zone-specific nuclear
841 morphology (crescent shape) and counted the number of nuclei in each focal plane
842 within the mitotic region. Experiments were repeated three times. 6-9 worms were used
843 for quantification. Student's t-test was used to calculate the p-values.
844
845 **GST protein pull-down assay**
846 pGEX-2TK was used for generating bacteria expression construct. SET-9/26$_{PHD}$ cDNA
847 was amplified from wildtype cDNA by PCR using the primers: SET-9/26$_{PHD}$-F:
848 CTCAGGATCCGATTCCGAATCCGAGGGAA; SET-9/26$_{PHD}$-R:
849 GCGTGAATTCCCGCTCGAAGTCGATTCAAAA; and subcloned into pGEX-2TK.

850 The expression construct was transformed into BL21 bacteria. Bacteria containing
851 cDNA of SET-9/26$_{PHD}$ was culture to OD600 equal to around 0.6 and the SET-9/26$_{PHD}$
852 expression was induced by adding IPTG to final concentration equals to 0.5mM.
853 Bacteria were lysed by sonication and protein was purified by Glutathione Sepharose
854 (Sigma).
855 GST protein pull-down assay was performed as described (Tsai et al. 2010). 25 µg
856 GST-PHD protein were incubated with 10, 100, 1000 µg of calf thymus total histones
857 (Sigma) in 500 µl NTP overnight at 4 °C. 90 µl of a 50% slurry of GST-beads were
858 added and incubated for 2 h at 4 °C, recovered by centrifugation and washed 6 times
859 (10 min at 4 °C) with NTP buffer (50 mM Tris-HCl 7.4, 300mM NaCl, 0.1% NP-40). The
860 protein bound beads were analyzed by SDS-PAGE and detected by Coomassie stain.
861

862 **Array binding assay**

863 The array binding assay was performed by EpiCypher. Briefly, GST-PHD were applied
864 on an EpiTitan™ array that was separated by a gasket such that two chambers were
865 delineated. After the protein incubation, a series of the anti-GST (primary) and the
866 fluorescent AlexaFluor 647 (secondary) antibody incubation steps were carried out to
867 detect the bound protein. Two independent experiments were performed.
868

869 **Immunoblotting and Quantification**

870 Immunoblotting was performed as described (Ni et al. 2012). Synchronized embryos
871 were put onto NGM-OP50 plates and grown at 20°C until reaching mid-L4. Worms were
872 harvested and washed 3 times using ice-cold M9 buffer. Worm pellets were lysed with

873 boiling SDS sample and equal amount of lysates were used for SDS-PAGE(18%) and
874 transferred to nitrocellulose membranes. The membranes were incubated with primary
875 antibodies overnight (H3K4me3/H3K9me3/H3K9ac, 1:1,000; H3, 1:2,000). IRDye
876 secondary antibody was used and the result was quantified using Odyssey imaging
877 system. All experiments were repeated 3-4 times. Modified histone levels were
878 normalized to H3 levels. Student's t-test was used to calculate the p-values.
879

880 **Plasmid and homologous DNA repair template construction**

881 pU6::set-9 sgRNA was generated using pU6::unc-119 sgRNA as described (Friedland
882 et al. 2013). The pU6::unc-119 sgRNA was used as template to amplify two overlapping
883 PCR fragments using the primers U6prom EcoRI F and set-9 gRNA R or set-9 gRNA F
884 and U6prom HindIII R. These PCR products were gel-purified and then mixed together
885 in a second PCR with primers U6prom EcoRI F and U6prom HindIII R. This final PCR
886 product was digested with EcoRI and HindIII and ligated into a pU6::unc-119 sgRNA
887 plasmid that had been digested with EcoRI and HindIII, creating the vector pU6::set-9
888 sgRNA. The pU6::set-9/set26 sgRNAs (1 and 2) that used for generating *set-9::gfp* and
889 *set-26::gfp* strains were constructed using the same strategy. The homologous DNA
890 repair templates that used for generating *set-9::gfp* and *set-26::gfp* strains were
891 designed and synthesized as described (Paix et al. 2014). Homologous arms flanking
892 gfp DNA sequence were generated using the pPD90 plasmid that contains gfp
893 sequence as template and the primers: armF12-GFP:
894 CGAGACGAAGCCGaTCtACgCGaTGGAAcagtaaaggagaagaacttttcactggagttg; armR12-
895 GFP: caagtttttcgcagattccttgCTAtttgtatagttcAtccatgccatgtgtaatccc; The DNA repair

896 template with ~30bp homologous arms was generated using the primer: armF1-
897 complete: ccctcaattttttttcagCTGAAACAAACTCGAGACGAAGCCG; and armR1-
898 complete: gggacaattttattcttcaagtttttcgcagattcc. The DNA repair template with ~60bp
899 homologous arms was generated using the primer: armF2-complete:
900 ccaaaaaatctccttaaaaaccctcaattttttttcagCTGAAACAAACTCGAGACGAAGC; and armR2-
901 complete: cgagatagaaagagatgatatgggacaattttattcttcaagtttttcgcagattcc.
902

903 **CRISPR-mediated genome editing**

904 CRISPR-mediated genome editing was performed as described (Paix et al. 2014;
905 Friedland et al. 2013). For generating *set-9* mutant, day1 adult animals were injected
906 with pDD162 (Peft-3::Cas9::tbb-2 3'UTR), pCFJ90 (pmyo-2::mCherry) and pU6::set-9
907 sgRNA and grown overnight at 16°C. The survived worms were separated, transferred
908 to 20°C and their F2 mCherry-positive animals were genotyped for *set-9* mutation. For
909 generating *set-9::gfp* and *set-26::gfp* strains, day1 adult animals were injected with
910 pDD162 (Peft-3::Cas9::tbb-2 3'UTR), pCFJ90 (pmyo-2::mCherry), pU6::set-9/set26
911 sgRNAs (1 and 2) and homologous DNA repair templates and grown overnight at 16°C.
912 The survived worms were separated, transferred to 20°C and their F2 mCherry-positive
913 animals were genotyped for GFP knock-in strains. sgRNAs that target two loci and two
914 DNA repair templates with different length of homologous arms (one ~30bp and the
915 other ~60bp) were co-injected to increase efficiency. The *set-9::gfp* and *set-26::gfp*
916 strains were mounted on a microscope slide and visualized using a Zeiss 710 confocal
917 system.
918

919 **Chromatin immunoprecipitation following sequencing (ChIP-seq)**

920 ChIP experiments for SET-9::GFP and SET-26::GFP were performed as described
921 (Zhong et al. 2010) with the following modifications. Approximately 70,000-100,000 L4s
922 were harvested and crosslinked in 2% formaldehyde-M9 solution for 25 minutes at room
923 temperature with rotation. The worms were then washed with 100 mM Tris pH 7.5 to
924 quench formaldehyde solution, washed two times with M9, and once with FA buffer (50
925 mM HEPES/KOH pH 7.5, 1 mM EDTA, 1% Triton X-100, 0.1% sodium deoxycholate;
926 150 mM NaCl) supplemented with 2X protease inhibitors (Roche Cat#11697498001,
927 cOmplete Protease Inhibitor Cocktail Tablets). Worms were then collected in a 15 ml
928 conical tube, snap-freezed in liquid N2 and stored at -80°C. The pellet was resuspended
929 in 1 ml FA buffer plus protease inhibitors. Using a Bioruptor sonicator, the sample was
930 sonicated on ice/salt water 30 times with the following settings: 30 sec on, 60 sec off.
931 The chromatin was then further sheared by the covaris s2 40 times with the following
932 settings: 20% duty factor, intensity 8, 200 cycles per burst, 60 sec on, 45 sec off. The
933 tube spun containing worm extract was then spun at 13,000g for 30 minutes at 4°C. The
934 supernatant was then transferred to a new tube and the protein concentration of the
935 supernatant was then determined by Bradford assay. Extract containing approximately
936 2 mg of protein was incubated in a microfuge tube with 6-12ul anti-GFP antibodies
937 overnight at 4°C with gentle rotation. 10% of the material was removed and used as
938 input DNA. Then 30 ul of protein A conjugated to sepharose beads (EMD Millipore)
939 were added to each ChIP sample and rotated at 4°C for 4 hours. The beads were then
940 spun at 2000rpm for 1 min to collect and washed twice for 5 mins each at 4°C in 1 ml of
941 FA buffer, once in FA with 500 mM NaCl and once in FA with 1M NaCl with gentle

942 rotation. The beads were then washed in TEL buffer (0.25 M LiCl, 1% NP-40, 1%
943 sodium deoxycholate, 1 mM EDTA, 10 mM Tris-HCl, pH 8.0) for 5 min and twice in TE
944 for 5 min. To elute the immunocomplexes, 50 ul Elution Buffer (1% SDS in TE with 250
945 mM NaCl) was added and the tube incubated at 65°C for 15 min, with brief vortexing
946 every 5 min. The beads were spun down at 2000rpm for 1 min and the supernatant
947 transferred to a new tube. The elution was repeated and supernatants combined. To
948 each sample, RNAseA was added and incubated at 37°C for 15 min, and proteinase K
949 was added and incubated for 1 hour at 55°C, then 65°C overnight to reverse crosslinks.
950 The DNA was then purified with the Qiaquick PCR purification kit (Qiagen), and eluted
951 with 40 ul H2O. The immunoprecipitated DNA was either checked by qPCR or
952 subjected to high-throughput sequencing library preparation. The protocol for library
953 preparation for SET-9/26 ChIP–Seq is NEBNext® Ultra™ II DNA Library Prep Kit for
954 Illumina® (NEB).
955 ChIP experiments for H3K4me3 and H3K9me3 were performed as described (Pu et al.
956 2015). For worm collection, 1000-2000 F1 *set-9 set-26* double mutant worms were
957 collected from progenies of balanced heterozygote *set-9(rw5) set-26(tm2467)* /nT1. F3
958 *set-9 set-26* double mutant worms were collected from progenies of F2 *set-9 set-26*
959 double mutant worms. L4 worm pellets were ground with a mortar and pestle and cross-
960 linked with 1% formaldehyde in PBS for 10 min at room temperature. Worm fragments
961 were collected by spinning at 3000g for 5 min and resuspended in FA buffer followed by
962 sonication with Bioruptor. Chromatin extract was incubated with antibody overnight at
963 4°C. Precipitated DNA (10–15 ng) from each sample was used for Illumina sequencing
964 library preparation. DNA from ChIP was first end-repaired to generate a blunt end

965 followed by adding single adenine base for adaptor ligation. The ligation product with
966 adaptor was size-selected and amplified by PCR with primers targeting the adaptor. Up
967 to 12 samples were multiplexed in one lane for single-end 50-nt Illumina HiSeq
968 sequencing.
969 All ChIP-seq experiments were repeated at least two times.
970
971 **ChIP-seq data analysis**
972 The data analysis pipeline was performed as described (Pu et al. 2015). Low quality
973 reads were removed using the FASTX Toolkit. The sequencing reads from two
974 independent experiments were combined and then aligned to the WS250 *C. elegans*
975 genome using bowtie2. PCR duplicates were removed and bam files were generated
976 using SAMtools. The bam files were then used for calling peaks by MACS2 (combined
977 broad and narrow peaks). A GLM model was then applied to compute the counts of all
978 the peaks to identify significant ones using two independent replicates. H3 ChIP data
979 were used as a control for H3K4me3 ChIP and genomic DNA input was used as a
980 control for SET-9 & SET-26 ChIP. ChIP signals (z-score) were normalized and
981 calculated using bamCoverage software.
982 For analyses using genes, each peak was associated with its closest gene. Overlapping
983 peaks were determined by 1bp overlap between two peaks using bedtools. For oriented
984 meta plots, 3000bp upstream and downstream of the summit were included and 50bp
985 windows were used for normalized counts in each window. The summits determined by
986 MACS2 were assigned to their closest genes. If a gene is on the "-" strain, the
987 normalized counts for -3000bp to 3000bp of that summit were counted in a reverse

988 direction. For example, if a peak, which was assigned to a gene in the "-" strain, has a
989 summit of X, the extended region for this summit in 5' to 3' direction is X+3000bp to X-
990 3000bp; if a peak, which has assigned to a gene in the "+" strain, has a summit of Y, the
991 extended region for this summit in 5' to 3' direction is Y-3000bp to Y+3000bp. The 95%
992 confidence interval was calculated using bootstrap method. Briefly, 10% of the total
993 summits were randomly selected and the mean was calculated. This random selection
994 was repeated1000 times and the 95% confidence interval was calculated based on the
995 estimate that these 1000 mean number follow normal distribution (Hesterberg et al.
996 2005). Fishers' exact test was used when comparing two lists of genes or peaks.
997 H3K9ac ChIP-seq data was downloaded from: http://data.modencode.org/cgi-
998 bin/findFiles.cgi?download=3578
999

1000 **RNA isolation and library preparation for RNA-seq**

1001 RNA isolation was performed as described (Li et al. 2008). For worm collection, 100-
1002 200 F1 *set-9 set-26* double mutant worms were collected from progenies of balanced
1003 heterozygote *set-9(rw5) set-26(tm2467)* /nT1. F3 *set-9 set-26* double mutant worms
1004 were collected from progenies of F2 *set-9 set-26* double mutant worms. Synchronized
1005 mid/late L4 staged worms that grown at 20°C were homogenized in 1 ml Tri-reagent for
1006 30 min at room temperature. 0.1mL of BCP was added to the sample and mixed well.
1007 The sample was then spun at 12,000 g 15 min at 4°C and the aqueous phase was
1008 transferred to a new tube. 0.5ml Isopropanol was added to the sample, incubated at
1009 room temperature for 10 min and spun at 12,000g 10 min. The RNA pellet was washed
1010 twice with 75% EtOH and dissolved in water. The RNA sample was then was then

1011 purified to remove DNA using RNeasy Mini Kit (Qiagen). The protocol for library
1012 preparation was using Ovation Human FFPE RNA-Seq Library Systems (NuGEN).
1013

1014 **RNA-seq data analysis**

1015 The data analysis pipeline was performed as described (Pu et al. 2015). Low quality
1016 reads were removed using the FASTX Toolkit. Illumina primers (adaptors) were then
1017 removed using cutadapt. And tRNA and rRNA reads were removed using Bowtie and
1018 the remaining reads were aligned to WS250 *C. elegans* genome using TopHat2 with no
1019 novel junctions. Mapped reads were then input into Cufflinks to calculate raw counts for
1020 each gene, which were then used for differential expression analysis by edgeR. Genes
1021 with less than 20 reads mapped to them in all samples were removed and the remaining
1022 genes were used as input to test for differential expression. PCA analysis was
1023 performed using the built-in function in edgeR. 5% false discovery rate (FDR) was used
1024 to determine differential expression.
1025

1026 **Heatmap**

1027 Heatmaps were generated using CISTROME (Liu et al. 2011). H3K4me3 and H3K9me3
1028 ChIP-seq results from wild-type and the *set-9 set-26* double mutant were used to
1029 generate the maximum signal ranked heatmaps.
1030

1031 **RNAi screen**

1032 RNA constructs were obtained from the Ahringher libarary. HT115 bacteria containing
1033 RNAi constructs were grown at 37°C and seeded on nematode growth medium (NGM)

1034 plates containing carbenicillin and tetracycline and dry overnight. dsRNA expression
1035 was induced by adding IPTG to a final concentration 0.4 mM. Heterozygous adult *set-9*
1036 *set-26*/+ worms were put on plates for 1~2 hours to lay eggs and F1 homozygous *set-9*
1037 *set-26* worm was picked onto new plates with RNAi bacteria. Brood size of 3-4 RNAi
1038 treated worms were scored.
1039

1040 **Gene ontology analysis**

1041 Gene ontology (GO) analysis was carried out using the DAVID 6.8 Bioinformatics
1042 Database (http://david.abcc.ncifcrf.gov) (Huang et al. 2009).
1043

1044 **Competing interests**

1045 The authors declare that no competing interests exist.
1046

1047 **Acknowledgments**

1048 Some strains were provided by the CGC, which is funded by NIH Office of Research
1049 Infrastructure Programs (P40 OD010440). +/nT1[qIs51] was a gift from Dr. Jun Liu's lab
1050 (Cornell University). We thank Lin Wang (Cornell University) for help with generating
1051 *set-9(rw5)* strain, members of the Lee laboratory (Cornell University) and Charles
1052 Danko (Cornell University) for insightful discussions and manuscript reading. This work
1053 was supported by R01 grant AG024425 from the NIA to S.S.L.
1054

1055 **Reference**

1056 Ahmed S, Hodgkin J. 2000. MRT-2 checkpoint protein is required for germline

1057 immortality and telomere replication in C. elegans. *Nature* **403**: 159–164.
1058 Ali M, Rincon-Arano H, Zhao W, Rothbart SB, Tong Q, Parkhurst SM, Strahl BD, Deng
1059 L-W, Groudine M, Kutateladze TG. 2013. Molecular basis for chromatin binding and
1060 regulation of MLL5. *Proc Natl Acad Sci U S A* **110**: 11296–11301.
1061 Alvares SM, Mayberry GA, Joyner EY, Lakowski B, Ahmed S. 2014. H3K4 demethylase
1062 activities repress proliferative and postmitotic aging. *Aging Cell* **13**: 245–253.
1063 Bardet AF, He Q, Zeitlinger J, Stark A. 2011. A computational pipeline for comparative
1064 ChIP-seq analyses. *Nat Protoc* **7**: 45–61.
1065 Deng L-W, Chiu I, Strominger JL. 2004. MLL 5 protein forms intranuclear foci, and
1066 overexpression inhibits cell cycle progression. *Proc Natl Acad Sci U S A* **101**: 757–
1067 762.
1068 Dillon SC, Zhang X, Trievel RC, Cheng X. 2005. The SET-domain protein superfamily:
1069 protein lysine methyltransferases. *Genome Biol* **6**: 227.
1070 Ewald CY, Landis JN, Porter Abate J, Murphy CT, Blackwell TK. 2015. Dauer-
1071 independent insulin/IGF-1-signalling implicates collagen remodelling in longevity.
1072 *Nature* **519**: 97–101.
1073 Friedland AE, Tzur YB, Esvelt KM, Colaiacovo MP, Church GM, Calarco JA. 2013.
1074 Heritable genome editing in C. elegans via a CRISPR-Cas9 system. *Nat Methods*
1075 **10**: 741–743.
1076 Gallo M, Coutinho FJ, Vanner RJ, Gayden T, Mack SC, Murison A, Remke M, Li R,
1077 Takayama N, Desai K, et al. 2015. MLL5 Orchestrates a Cancer Self-Renewal
1078 State by Repressing the Histone Variant H3.3 and Globally Reorganizing
1079 Chromatin. *Cancer Cell* **28**: 715–729.

1080 Greer EL, Beese-Sims SE, Brookes E, Spadafora R, Zhu Y, Rothbart SB, Aristizabal-
1081 Corrales D, Chen S, Badeaux AI, Jin Q, et al. 2014. A histone methylation network
1082 regulates transgenerational epigenetic memory in C. elegans. *Cell Rep* **7**: 113–126.
1083 Greer EL, Maures TJ, Hauswirth AG, Green EM, Leeman DS, Maro GS, Han S, Banko
1084 MR, Gozani O, Brunet A. 2010. Members of the H3K4 trimethylation complex
1085 regulate lifespan in a germline-dependent manner in C. elegans. *Nature* **466**: 383–
1086 387.
1087 Greer EL, Shi Y. 2012. Histone methylation: a dynamic mark in health, disease and
1088 inheritance. *Nat Rev Genet* **13**: 343–357.
1089 Han S, Brunet A. 2012. Histone methylation makes its mark on longevity. *Trends Cell*
1090 *Biol* **22**: 42–49.
1091 Hesterberg T, Moore DS, Monaghan S, Clipson A, Epstein R. 2005. Bootstrap methods
1092 and permutation tests. *Introd to Pract Stat* **5**: 1–70.
1093 Heuser M, Yap DB, Leung M, de Algara TR, Tafech A, McKinney S, Dixon J, Thresher
1094 R, Colledge B, Carlton M, et al. 2009. Loss of MLL5 results in pleiotropic
1095 hematopoietic defects, reduced neutrophil immune function, and extreme sensitivity
1096 to DNA demethylation. *Blood* **113**: 1432–1443.
1097 Huang DW, Sherman BT, Lempicki RA. 2009. Systematic and integrative analysis of
1098 large gene lists using DAVID bioinformatics resources. *Nat Protoc* **4**: 44–57.
1099 Katz DJ, Edwards TM, Reinke V, Kelly WG. 2009. A C. elegans LSD1 demethylase
1100 contributes to germline immortality by reprogramming epigenetic memory. *Cell* **137**:
1101 308–320.
1102 Kerr SC, Ruppersburg CC, Francis JW, Katz DJ. 2014. SPR-5 and MET-2 function

1103 cooperatively to reestablish an epigenetic ground state during passage through the
1104 germ line. *Proc Natl Acad Sci U S A* **111**: 9509–9514.
1105 Li J, Ebata A, Dong Y, Rizki G, Iwata T, Lee SS. 2008. Caenorhabditis elegans HCF-1
1106 functions in longevity maintenance as a DAF-16 regulator. *PLoS Biol* **6**: e233.
1107 Li T, Kelly WG. 2011. A role for Set1/MLL-related components in epigenetic regulation
1108 of the Caenorhabditis elegans germ line. *PLoS Genet* **7**: e1001349.
1109 Liu T, Ortiz JA, Taing L, Meyer CA, Lee B, Zhang Y, Shin H, Wong SS, Ma J, Lei Y, et
1110 al. 2011. Cistrome: an integrative platform for transcriptional regulation studies.
1111 *Genome Biol* **12**: R83.
1112 Madan V, Madan B, Brykczynska U, Zilbermann F, Hogeveen K, Dohner K, Dohner H,
1113 Weber O, Blum C, Rodewald H-R, et al. 2009. Impaired function of primitive
1114 hematopoietic cells in mice lacking the Mixed-Lineage-Leukemia homolog MLL5.
1115 *Blood* **113**: 1444–1454.
1116 Ni Z, Ebata A, Alipanahiramandi E, Lee SS. 2012. Two SET domain containing genes
1117 link epigenetic changes and aging in Caenorhabditis elegans. *Aging Cell* **11**: 315–
1118 325.
1119 Nottke AC, Beese-Sims SE, Pantalena LF, Reinke V, Shi Y, Colaiacovo MP. 2011.
1120 SPR-5 is a histone H3K4 demethylase with a role in meiotic double-strand break
1121 repair. *Proc Natl Acad Sci U S A* **108**: 12805–12810.
1122 Osipovich AB, Gangula R, Vianna PG, Magnuson MA. 2016. Setd5 is essential for
1123 mammalian development and the co-transcriptional regulation of histone
1124 acetylation. *Development* **143**: 4595–4607.
1125 Paix A, Wang Y, Smith HE, Lee C-YS, Calidas D, Lu T, Smith J, Schmidt H, Krause MW,

1126 Seydoux G. 2014. Scalable and versatile genome editing using linear DNAs with
1127 microhomology to Cas9 Sites in Caenorhabditis elegans. *Genetics* **198**: 1347–1356.
1128 Pu M, Ni Z, Wang M, Wang X, Wood JG, Helfand SL, Yu H, Lee SS. 2015.
1129 Trimethylation of Lys36 on H3 restricts gene expression change during aging and
1130 impacts life span. *Genes Dev* **29**: 718–731.
1131 Reinke V, Gil IS, Ward S, Kazmer K. 2004. Genome-wide germline-enriched and sex-
1132 biased expression profiles in Caenorhabditis elegans. *Development* **131**: 311–323.
1133 Rincon-Arano H, Halow J, Delrow JJ, Parkhurst SM, Groudine M. 2012. UpSET recruits
1134 HDAC complexes and restricts chromatin accessibility and acetylation at promoter
1135 regions. *Cell* **151**: 1214–1228.
1136 Robert VJ, Mercier MG, Bedet C, Janczarski S, Merlet J, Garvis S, Ciosk R, Palladino F.
1137 2014. The SET-2/SET1 histone H3K4 methyltransferase maintains pluripotency in
1138 the Caenorhabditis elegans germline. *Cell Rep* **9**: 443–450.
1139 Robinson MD, McCarthy DJ, Smyth GK. 2010. edgeR: a Bioconductor package for
1140 differential expression analysis of digital gene expression data. *Bioinformatics* **26**:
1141 139–140.
1142 Santos F, Dean W. 2004. Epigenetic reprogramming during early development in
1143 mammals. *Reproduction* **127**: 643–651.
1144 Sebastian S, Sreenivas P, Sambasivan R, Cheedipudi S, Kandalla P, Pavlath GK,
1145 Dhawan J. 2009. MLL5, a trithorax homolog, indirectly regulates H3K4 methylation,
1146 represses cyclin A2 expression, and promotes myogenic differentiation. *Proc Natl*
1147 *Acad Sci U S A* **106**: 4719–4724.
1148 Shi X, Hong T, Walter KL, Ewalt M, Michishita E, Hung T, Carney D, Pena P, Lan F,

1149 Kaadige MR, et al. 2006. ING2 PHD domain links histone H3 lysine 4 methylation
1150 to active gene repression. *Nature* **442**: 96–99.
1151 Shi X, Kachirskaia I, Walter KL, Kuo J-HA, Lake A, Davrazou F, Chan SM, Martin DGE,
1152 Fingerman IM, Briggs SD, et al. 2007. Proteome-wide analysis in Saccharomyces
1153 cerevisiae identifies several PHD fingers as novel direct and selective binding
1154 modules of histone H3 methylated at either lysine 4 or lysine 36. *J Biol Chem* **282**:
1155 2450–2455.
1156 Sijen T, Fleenor J, Simmer F, Thijssen KL, Parrish S, Timmons L, Plasterk RH, Fire A.
1157 2001. On the role of RNA amplification in dsRNA-triggered gene silencing. *Cell*
1158 **107**: 465–476.
1159 Sims RJ 3rd, Millhouse S, Chen C-F, Lewis BA, Erdjument-Bromage H, Tempst P,
1160 Manley JL, Reinberg D. 2007. Recognition of trimethylated histone H3 lysine 4
1161 facilitates the recruitment of transcription postinitiation factors and pre-mRNA
1162 splicing. *Mol Cell* **28**: 665–676.
1163 Tasdogan A, Kumar S, Allies G, Bausinger J, Beckel F, Hofemeister H, Mulaw M,
1164 Madan V, Scharfetter-Kochanek K, Feuring-Buske M, et al. 2016. DNA Damage-
1165 Induced HSPC Malfunction Depends on ROS Accumulation Downstream of IFN-1
1166 Signaling and Bid Mobilization. *Cell Stem Cell* **19**: 752–767.
1167 Towbin BD, Gonzalez-Aguilera C, Sack R, Gaidatzis D, Kalck V, Meister P, Askjaer P,
1168 Gasser SM. 2012. Step-wise methylation of histone H3K9 positions
1169 heterochromatin at the nuclear periphery. *Cell* **150**: 934–947.
1170 Tsai W-W, Wang Z, Yiu TT, Akdemir KC, Xia W, Winter S, Tsai C-Y, Shi X, Schwarzer
1171 D, Plunkett W, et al. 2010. TRIM24 links a non-canonical histone signature to

1172 breast cancer. *Nature* **468**: 927–932.
1173 Xiao Y, Bedet C, Robert VJP, Simonet T, Dunkelbarger S, Rakotomalala C, Soete G,
1174 Korswagen HC, Strome S, Palladino F. 2011. Caenorhabditis elegans chromatin-
1175 associated proteins SET-2 and ASH-2 are differentially required for histone H3 Lys
1176 4 methylation in embryos and adult germ cells. *Proc Natl Acad Sci U S A* **108**:
1177 8305–8310.
1178 Yang J-S, Nam H-J, Seo M, Han SK, Choi Y, Nam HG, Lee S-J, Kim S. 2011. OASIS:
1179 online application for the survival analysis of lifespan assays performed in aging
1180 research. *PLoS One* **6**: e23525.
1181 Zhang X, Novera W, Zhang Y, Deng L-W. 2017. MLL5 (KMT2E): structure, function,
1182 and clinical relevance. *Cell Mol Life Sci*.
1183 Zhang Y, Wong J, Klinger M, Tran MT, Shannon KM, Killeen N. 2009. MLL5 contributes
1184 to hematopoietic stem cell fitness and homeostasis. *Blood* **113**: 1455–1463.
1185 Zhong M, Niu W, Lu ZJ, Sarov M, Murray JI, Janette J, Raha D, Sheaffer KL, Lam HYK,
1186 Preston E, et al. 2010. Genome-wide identification of binding sites defines distinct
1187 functions for Caenorhabditis elegans PHA-4/FOXA in development and
1188 environmental response. *PLoS Genet* **6**: e1000848.
1189
1190
1191 **Figure Legends**
1192 **Figure 1 *set-26* but not *set-9* is important for longevity.**
1193 (A) Schematic of the *set-9(rw5)* and *set-26(tm2467)* mutants. Red star indicates the
1194 position of the sgRNA (single guide RNA) targeting the *set-9* gene. Premature stop

1195 codons caused by deletions of 38 nucleotides in the *set-9* gene and 1,090 nucleotides
1196 in the *set-26* gene are depicted as red hexagons. Loss of *set-26* gene but not *set-9*
1197 gene extended lifespan (B), and increased resistance to heat stress (C). Survival curves
1198 for N2, *set-26(tm2467), set-9(rw5),* and *set-9(rw5) set-26(tm2467)* strains from
1199 representative experiments are shown. Quantitative data for all replicates are shown in
1200 Supplement 1 Table S1.
1201
1202 **Figure 2 *set-9* and *set-26* act redundantly to maintain fertility.**
1203 (A) The *set-9(rw5) set26(tm2467)* double mutant worms derived from heterozygous
1204 parents (F1) displayed a mild fertility defect. The double mutant worms displayed a
1205 much more severe fertility defect at later generations (F2-F6). Average brood size of N2,
1206 *set-26(tm2467), set-9(rw5),* and *set-9(rw5) set-26(tm2467)* strains at the indicated
1207 generation were shown (*p<0.05, ***p<0.001). The error bars represent standard errors.
1208 n=9~10 for N2, *set-9* mutant, *set-26* mutant, and F1 *set-9 set-26* double mutant worms;
1209 n=~50 for F2-F6 *set-9 set-26* double mutants. (B) The *set-9(rw5) set26(tm2467)* double
1210 mutant exhibited a mortal germline phenotype. At each generation, 6 L1s for N2, *set-*
1211 *26(tm2467), set-9(rw5)* and *set-9(rw5) set-26(tm2467)* strains were transferred to a new
1212 plate. Plates were scored as not fertile when no progeny were found. % of fertile lines
1213 indicated percentage of plates that were fertile. n=6 for N2, *set-9* and *set-26* mutants;
1214 n=25 for *set-9 set-26* double mutants. (C) Maternal contribution of *set-9* & *set-26*
1215 appeared important for alleviating the fertility defect in the double mutant. Average
1216 brood size of the *set-9(rw5) set26(tm2467)* double mutants derived from four different
1217 crosses were shown (***p<0.001, n.s. no significant). n=11~12 for assessing the brood

1218 size of the *set-9(rw5) set26(tm2467)* homozygous progeny from heterozygous male(P0)
1219 X heterozygous hermaphrodite(P0) and homozygous male(F1) X heterozygous
1220 hermaphrodite(P0); n=30~34 for progeny from homozygous male (F1) X heterozygous
1221 hermaphrodite(P0) and heterozygous male(P0) X homozygous hermaphrodite(F1). (D)
1222 The *set-9(rw5) set26(tm2467)* double mutant worms that remained fertile nevertheless
1223 exhibited reduced number of mitotic germ cells. Whole worms or dissected gonads of
1224 fertile *set-9(rw5) set26(tm2467)* mutants were stained by DAPI and the mitotic cells
1225 were counted. D2 adults were scored. n=18~27, ***p<0.001. Analyses of sterile *set-*
1226 *9(rw5) set26(tm2467)* double mutant worms are shown in Figure 2-figure supplement 1.
1227 Quantitative data are shown in Supplement 1 Table S2.
1228
1229 **Figure 2-figure supplement 1 Fertility defects of the *set-9 set-26* double mutant.**
1230 (A) The *set-9(rw5) set-26(tm2467)* double mutant exhibited variable percentage of
1231 sterility at the different generations. N=155-517. (B) Representative DAPI staining
1232 images showing the germline of three different sterile F3-F4 *set-9(rw5) set-26(tm2467)*
1233 double mutant worms. The germline of these sterile worms showed variable phenotypes,
1234 including no differentiated germ cells, no oocytes, or no sperms. D1-D2 adults were
1235 scored.
1236
1237 **Figure 3 SET-26 is broadly expressed and SET-9 is only detectable in the**
1238 **germline.**
1239 (A, B) Fluorescent micrographs of worms carrying *gfp* knock-in at the C-terminus of *set-*
1240 *9* or *set-26* gene (*set-9::gfp* and *set-26::gfp).* GFP-fused SET-26 was detected in all

1241 cells and GFP-fused SET-9 was only detected in the germline. Star indicates head,
1242 arrow indicates germline in the images. The signal outside of the germline detected in
1243 the *set-9::gfp* strain represented autofluorescence (marked by hashtag), which
1244 appeared yellow under the microscope. (C, D) Germline-specific knockdown of *set-9* &
1245 *set-26* was not sufficient to extend lifespan. RNAi Knockdown of *set-9 & set-26* or *wdr-*
1246 *5.1* extended lifespan in N2 worms (C). RNAi knockdown of *wdr-5.1*, but not *set-9 & set-*
1247 *26*, extended lifespan in the *rrf-1(pk1417)* mutant worms. Quantitative data are shown in
1248 Supplement 1 Table S3.
1249
1250 **Figure 3-figure supplement 1 GFP-tagged SET-9 & SET-26 are largely functional.**
1251 (A-B) Worms carrying a *gfp* knock-in at the C-terminus of *set-26* exhibited mild lifespan
1252 extension and heat resistance phenotypes, but the phenotypes were much weaker than
1253 those of the loss-of-function *set-26(tm2467)* mutant. (C) Worms carrying *gfp* knock-ins
1254 at the C-termini of *set-9* and *set-26* genes exhibited a mild fertility defect, which was
1255 significantly different from the severe fertility defect observed in the *set-9(rw5) set-*
1256 *26(tm2467)* double mutant (*$p<0.05$, ***$p<0.001$). n=8-10 for *set-9::gfp set-26::gfp* and
1257 N2; n=28 for F3 *set-9(rw5) set-26(tm2467).* Quantitative data are shown in Supplement
1258 1 Table S4. (D) SET-26::GFP expression upon RNAi knockdown of *set-9 & set-26* and
1259 L4440. *set-26::gfp; rrf-1(pk1417)* and *set-26::gfp* strains are shown. Arrow heads
1260 indicate germline, arrows indicate intestine nuclei in the images.
1261
1262 **Figure 3-figure supplement 2 GFP-tagged SET-9 is only detectable in the germline**

1263 Fluorescent micrographs of worms carrying *gfp* knock-in at the C-terminus of *set-9* gene
1264 (*set-9::gfp)* is shown. “GFP” indicates signals under GFP channel and
1265 “Autofluorescence” indicates signals under YFP channel. Top panel shows L4 stage
1266 worm whereas bottom panel shows L2/L3 stage.
1267
1268 **Figure 4 DAF-16-dependent somatic SET-26 regulated genes are enriched for**
1269 **lifespan determinant genes**
1270 (A) Venn diagrams show the overlap between up-regulated genes in *glp-1(e2141); set-*
1271 *26(tm2467)* (comparing with *glp-1(e2141)*) and down-regulated genes in *daf-*
1272 *16(mgDf47); glp-1(e2141); set-26(tm2467)* (comparing with *glp-1(e2141); set-*
1273 *26(tm2467)*); and the overlap between down-regulated genes in *glp-1(e2141); set-*
1274 *26(tm2467)* (comparing with *glp-1(e2141)*) and up-regulated genes in *daf-16(mgDf47);*
1275 *glp-1(e2141); set-26(tm2467)* (comparing with *glp-1(e2141); set-26(tm2467)*). (B) GO
1276 term analysis of DAF-16-dependent somatic SET-26 regulated genes. Gene lists can be
1277 found in Supplement 2.
1278
1279 **Figure 4-figure supplement 1 Transcriptional profile of *glp-1(e2141); set-***
1280 ***26(tm2467)* mutant.**
1281 (A) GO term analysis of genes with expression change in *glp-1(e2141); set-26(tm2467)*
1282 (comparing with *glp-1(e2141)*). (B) Venn diagram shows the overlap between *set-26*
1283 regulated genes in *glp-1(e2141); set-26(tm2467)* (comparing with *glp-1(e2141)*) and
1284 *set-26* regulated genes in *set-26(tm2467)* (comparing with N2). Gene lists can be found
1285 in Supplement 2.

1286

1287 **Figure 5 Transcriptional profiles of *set-9(rw5)*, *set-26(tm2467),* and F1 *set-9(rw5)***
1288 ***set-26(tm2467)* mutants.**

1289 (A) Venn diagrams show the overlap among *set-9(rw5)*, *set-26(tm2467)*, and *set-9(rw5)*
1290 *set-26(tm2467)* down-regulated (left) and up-regulated (right) gene sets. Hashtag
1291 indicates genes that only show expression change in the F1 *set-9(rw5) set-26(tm2467)*
1292 double mutant. GO term analysis of up-regulated (B) and down-regulated (C) genes that
1293 only show expression change in the F1 *set-9(rw5) set-26(tm2467)* double mutant. (D)
1294 Venn diagram shows the overlaps between genes that only show expression change in
1295 the F1 *set-9(rw5) set-26(tm2467)* double mutant identified in our RNA-seq data with the
1296 previously reported germline-specific gene lists (Reinke et al. 2004). Gene lists can be
1297 found in Supplement 2.

1298

1299 **Figure 5-figure supplement 1 Transcriptional profile comparison between F1 and**
1300 **F3 *set-9(rw5) set-26(tm2467) double mutants*.**

1301 (A) GO term analysis of down-regulated and up-regulated genes in F1 *set-9(rw5) set-*
1302 *26(tm2467)* double mutant. (B) GO term analysis of down-regulated and up-regulated
1303 genes in F3 *set-9(rw5) set-26(tm2467)* double mutant. (C) Venn diagrams show the
1304 overlaps between down-regulated and up-regulated genes in the F1 and F3 *set-9(rw5)*
1305 *set-26(tm2467)* double mutants. (D) Scatter plot of log2 fold change of all mRNAs in F3
1306 and F1 *set-9(rw5) set-26(tm2467)* double mutant. (E) Scatter plot of log2 fold change of
1307 genes in F3 and F1 *set-9(rw5) set-26(tm2467)* double mutants. Only genes that show

1308 significant expression change in *set-9(rw5) set-26(tm2467)* double mutants are shown.
1309 Gene lists can be found in Supplement 2.
1310
1311 **Figure 6 SET-9 & SET-26 bind to H3K4me3.**
1312 (A) PHD domain of SET-9 & SET-26 specifically pulled down H3 *in vitro*. Coomassie-
1313 blue stained gel showing pulldown results using GST–SET-9/26$_{PHD}$ and GST control.
1314 (B) Binding intensity of GST-SET-9/26$_{PHD}$ to the significant hits from histone peptide
1315 arrays. Quantitative data are shown in Supplement 1 Table S5. (C) Genome browser
1316 view showing ChIP z-scores (standardized log2 ratios of ChIP/Input or ChIP/H3ChIP
1317 signals) for SET-9/26, H3K4me3 and H3K9me3 at a representative region. (D) 75% of
1318 the SET-9 & SET-26 peaks overlapped with H3K4me3 peaks. (***$p<0.001$ indicates
1319 overlapping more than expected) (E) 49% of the H3K4me3 peaks overlapped with SET-
1320 9 & SET-26 peaks. (***$p<0.001$ indicates overlapping more than expected) (F) 8% of the
1321 SET-9/26 peaks overlapped with H3K9me3 peaks. (***$p<0.001$ indicates overlapping
1322 less than expected)
1323
1324 **Figure 6-figure supplement 1 SET-9 & SET-26 are not the major enzymes for**
1325 **H3K9me3 *in vivo.***
1326 (A) Clustal Omega alignment of the SET domains of SET-9 & SET-26 from *C. elegans*,
1327 SETD5, MLL5, SET7 and SUV91 from human, UpSET from *Drosophila melanogaster*
1328 and SET1 from *Saccharomyces*. Red boxes indicate the proposed key residues. The
1329 online tool used is: http://www.ebi.ac.uk/Tools/msa/clustalo/ . (B) Western blotting
1330 showing H3K9me3 levels in N2 and the *set-9(rw5) set-26(tm2467)* double mutant (left).

1331 Synchronized L4 worms for N2 and the *set-9(rw5) set-26(tm2467)* double mutant were
1332 used. Quantification of three independent Western experiments (right). (C)
1333 Representative genome browser views of H3K9me3 profiles in N2 (black) and the F3
1334 *set-9(rw5) set-26(tm2467)* double mutant (purple). z-scores for normalized H3K9me3
1335 and SET-9 & SET-26 ChIP signals in N2 and the *set-9(rw5) set-26(tm2467)* are shown.
1336 (D) Heatmaps showing the H3K9me3 profiles in wild-type and the F3 *set-9(rw5) set-*
1337 *26(tm2467)* double mutant for all H3K9me3 peaks.
1338
1339 **Figure 6-figure supplement 2 SET-9 & SET-26 bind to H3K4me3 *in vivo*.**
1340 A. Genome browser view showing ChIP z-scores (standardized log2 ratios of
1341 ChIP/Input or ChIP/H3ChIP signals) for SET-9, SET-26 and SET-9/26 at a
1342 representative region. (B) A large proportion of SET-9 peaks overlapped with SET-26
1343 peaks. (C) A large proportion of SET-26 peaks overlapped with SET-9 & SET-26 peaks.
1344
1345 **Figure 6-figure supplement 3 SET-9 & SET-26 bind to H3K4me3 *in vivo*.**
1346 (A) Metagene plots showing the average H3K4me3 z-score (standardized log2 ratios of
1347 H3K4me3ChIP/H3ChIP signals) for the H3K4me3 peaks bound (shown in blue) and not
1348 bound by SET-9 & SET-26 (shown in grey) in N2 worms. Regions 3000bp upstream
1349 and downstream of the peak summits are shown. The light blue and light grey indicate
1350 95% confidence intervals. (B) Metagene plots showed the average SET-9 & SET-26 z-
1351 score (standardized log2 ratios of SET-9 & SET-26 ChIP/input signals) for the
1352 H3K4me3 peaks bound (shown in blue) and not bound by SET-9 & SET-26 peaks
1353 (shown in grey). The light blue and light grey indicate 95% confidence intervals. (C)

1354 Scatter plot of H3K4me3 z-score and SET-9 & SET-26 z-score for H3K4me3 peak
1355 regions. (D) 28% of the SET-9 & SET-26 peaks overlapped with H3K9ac peaks.
1356 (***p<0.001 indicates overlapping more than expected) (E) Scatter plot of H3K4me3 z-
1357 score and H3K9ac z-score for all H3K4me3 peak regions. (F) Scatter plot of H3K4me3
1358 z-score and H3K9ac z-score for H3K4me3 peak regions bound by SET-9 & SET-26. (G)
1359 Scatter plot of H3K4me3 z-score and H3K9ac z-score for H3K4me3 peak regions not
1360 bound by SET-9 & SET-26.
1361
1362 **Figure 7 Binding of SET-9 & SET-26 regulate the RNA expression of specific**
1363 **target genes.**
1364 (A) Venn diagram showing comparisons of the genes with increased and decreased
1365 expression changes in the F1 *set-9(rw5) set-26(tm2467)* double mutant and the SET-9
1366 & SET-26 target genes. (B) GO term analyses of the up-regulated genes in the F1 *set-*
1367 *9(rw5) set-26(tm2467)* double mutant that were bound by SET-9 & SET-26. (C) GO
1368 term analyses of the down-regulated genes in the F1 *set-9(rw5) set-26(tm2467)* double
1369 mutant that were bound by SET-9 & SET-26. (D) Venn diagram showing comparisons
1370 of the up-regulated and down-regulated somatic SET-26 regulated genes and the SET-
1371 9 & SET-26 target genes. (E) GO term analyses of the up-regulated somatic SET-26
1372 regulated genes bound by SET-9 & SET-26. (F) GO term analyses of the down-
1373 regulated somatic SET-26 regulated genes bound by SET-9 & SET-26. Gene lists can
1374 be found in Supplement 2.
1375
1376 **Figure 7-figure supplement 1 SET-9 & SET-26 target genes.**

1377 (A) Venn diagrams showing comparisons of the genes with increased and decreased
1378 expression changes in the *set-9(rw5)* mutant. (B) GO term analyses of the up-regulated
1379 genes in *set-9(rw5)* bound by SET-9 & SET-26. (C) GO term analyses of the down-
1380 regulated genes in *set-9(rw5)* bound by SET-9 & SET-26. (D) Venn diagrams showing
1381 comparisons of the genes with increased and decreased expression changes in the *set-*
1382 *26(tm2467)* mutant. (E) GO term analyses of the up-regulated genes in *set-26(tm2467)*
1383 bound by SET-9 & SET-26. (F) GO term analyses of the down-regulated genes in *set-*
1384 *26(tm2467)* bound by SET-9 & SET-26. Gene lists can be found in Supplement 2.
1385
1386 **Figure 8 SET-9 & SET-26 restrict the spreading of H3K4me3.**
1387 (A) Western blotting of H3K4me3 levels in three independent replicates of wild type and
1388 F3 *set-9(rw5) set-26(tm2467)* double mutant (left). Synchronized L4 worms for N2 and
1389 the F3 *set-9(rw5) set-26(tm2467)* double mutant were used. Quantification of
1390 normalized H3K4me3 levels from three independent Western experiments (right).
1391 (*$p<0.05$) (B) Elevated H3K4me3 levels were observed in the dissected gonads of the
1392 F3 *set-9(rw5) set-26(tm2467)* double mutant. Synchronized D1-D2 adults for N2 and the
1393 F3 *set-9(rw5) set-26(tm2467)* double mutant were used. Representative
1394 immunostaining images are shown. Right panel shows quantification of images shown
1395 on left. (*$p<0.05$) (C) Metagene plots showing the average H3K4me3 z-score
1396 (standardized log2 ratios of ChIP/H3ChIP signals) for the peaks bound by SET-9 &
1397 SET-26 in N2 (black) and the F1 (blue) and F3 (purple) *set-9(rw5) set-26(tm2467)*
1398 double mutants. Regions 3000bp upstream and downstream of the peak summits are
1399 shown. The grey areas indicate 95% confidence intervals. (D) Metagene plots showing

1400 the average H3K4me3 z-score for the peaks not bound by SET-9 & SET-26 in N2
1401 (black) and the F1 (blue) and F3 (purple) *set-9(rw5) set-26(tm2467)* double mutant. The
1402 grey areas indicate 95% confidence intervals.
1403
1404 **Figure 8-figure supplement 1 SET-9 & SET-26 restrict the spreading of H3K4me3.**
1405 (A) H3K4me3 and H3K9me3 levels in N2, *set-9(rw5)* and *set-26(tm2467)* mutants.
1406 Synchronized L4 worms were used. Quantification showed results from three
1407 independent experiments. (B) Western blotting showing elevated H3K9ac levels in the
1408 *set-9(rw5) set-26(tm2467)* double mutant (left). Synchronized L4 worms for N2 and the
1409 *set-9(rw5) set-26(tm2467)* double mutant were used. Quantification of normalized
1410 H3K9ac levels from three independent Western experiments (right). (*$p<0.05$) (C)
1411 Representative genome browser views of H3K4me3 profiles in N2 (black) and the F1
1412 (blue) and F3 (purple) *set-9(rw5) set-26(tm2467)* double mutant surrounding SET-9 &
1413 SET-26 binding sites (red). z-scores for normalized H3K4me3 and SET-9 & SET-26
1414 ChIP signals in N2 and the F1 and F3 *set-9(rw5) set-26(tm2467)* are shown. (D)
1415 Heatmaps showing the H3K4me3 profiles in wild-type and the F1 and F3 *set-9(rw5) set-*
1416 *26(tm2467)* double mutant for H3K4me3 peaks bound and not bound by SET-9/26. (E)
1417 Metagene plots showing the average H3K4me3 z-score (standardized log2 ratios of
1418 ChIP/H3ChIP signals) in N2 (black) and the F1 (blue) and F3 (purple) *set-9(rw5) set-*
1419 *26(tm2467)* double mutants. Regions 3000bp upstream and downstream of the peak
1420 summits of SET-9 & SET-26 binding are shown. The light grey and light purple areas
1421 indicate 95% confidence intervals. (F) Metagene plots showing the average H3K4me3
1422 z-score (standardized log2 ratios of ChIP/H3ChIP signals) in *glp-1(e2141)* (black) and

1423 *glp-1(e2141); set-26(tm2467)* (orange) for H3K4me3 peaks bound by SET-9 & SET-26
1424 (left), not bound by SET-9 & SET-26 (middle) and SET-9 & SET-26 peaks overlapping
1425 H3K4me3 (right). The light grey and light purple areas indicate 95% confidence intervals.
1426 (G), (H) Venn diagrams showing genes with altered expression in the F1 and F3 *set-*
1427 *9(rw5) set-26(tm2467)* double mutant identified by RNA-seq and genes with altered
1428 H3K4me3 in the F1 and F3 *set-9(rw5) set-26(tm2467)* double mutant identified by ChIP-
1429 seq. (***p<0.001 indicate less than expected). Gene lists can be found in Supplement 2.
1430

1431 **Figure 8-figure supplement 2 Germline-specific genes show correlated changes**
1432 **in H3K4me3 and RNA expression.**
1433 (A) Venn diagram shows the overlaps between SET-9/26 target genes with expression
1434 change in F1 *set-9(rw5) set-26(tm2467)* and germline-specific genes. (B) Average
1435 H3K4me3 z-score in N2 (black) and the F1 (blue) and F3 (purple) *set-9(rw5) set-*
1436 *26(tm2467)* double mutants for the SET-9/26 germline target genes that showed
1437 elevated expression in F1 *set-9(rw5) set-26(tm2467)* (compared to N2). (C) Venn
1438 diagram shows the overlap between SET-9/26 germline target genes with increased
1439 RNA expression in F1 *set-9(rw5) set-26(tm2467)* double mutant and genes with
1440 expanded H3K4me3 marking in F1 *set-9(rw5) set-26(tm2467)* double mutant. Gene lists
1441 can be found in Supplement 2.
1442

1443 **Figure 9 SET-9 & SET-26 and SET-2 act synergistically to regulate fertility.**
1444 (A) Ratio of eggs laid by F1 *set-9(rw5) set-26(tm2467)* double mutant worms fed dsRNA
1445 of *C. elegans* potential histone modifiers (mainly methyltransferases and demethylases)

1446 or empty vector (L4440) for one generation. (B) Average brood size in N2, *set-2(ok952)*,
1447 F1 *set-9(rw5) set-26(tm2467)* double mutant and F1 *set-2(ok952)*; *set-9(rw5) set-*
1448 *26(tm2467)* triple mutant.
1449
1450 **Figure 10 SET-9 & SET-26 regulate H3K4me3 and target gene expression.**
1451 In the germline, loss of *set-9* & *set-26* results in the broadening of H3K4me3 domains
1452 surrounding most SET-9 & SET-26 binding regions and up-regulation of germline genes.
1453 In the soma, loss of *set-26* modulates lifespan by indirectly regulating DAF-16-
1454 dependent genes. We propose that SET-9 and SET-26 are critical for organizing local
1455 chromatin environment and regulating the expression of specific target genes, and
1456 these activities together contribute to their roles in germline development and longevity.
1457
1458 **Supplemental File 1**
1459 **Table S1**
1460 (A) Lifespan data for Figure 1B were shown. (B) Heat stress resistance data for Figure
1461 1C were shown.
1462
1463 **Table S2**
1464 (A) Brood size data for Figure 2A were shown. (B) Mortal germline assay data for Figure
1465 2B were show. (C) Maternal and paternal effect on brood size for Figure 2C were shown.
1466 (D) Mitotic germ cell number for Figure 2D were shown.
1467
1468 **Table S3**

1469 (A) Wild type lifespan data with RNAi treatment for Figure 3B were shown. (B) *rrf-*
1470 *1(pk1417)* mutant lifespan data with RNAi treatment for Figure 3C were shown.
1471
1472 **Table S4**
1473 (A) Lifespan data for Figure 3-figure supplement 1A were shown. (B) Heat stress
1474 resistance data for Figure 3-figure supplement 1B were shown. (C) Brood size data for
1475 Figure 3-figure supplement 1C were shown.
1476
1477 **Table S5**
1478 (A) Histone peptide array binding assay for Figure 6B were shown.
1479
1480 **Table S6**
1481 (A) qPCR RNA-seq validation for *set-26*(tm2467) compare with wild type data were
1482 shown. (B) qPCR RNA-seq validation for F3 *set-9(rw5) set-26*(tm2467) compare with
1483 wild type data were shown.
1484
1485 **Supplemental File 2**
1486 Gene lists for comparison indicated gene list comparisons were shown.

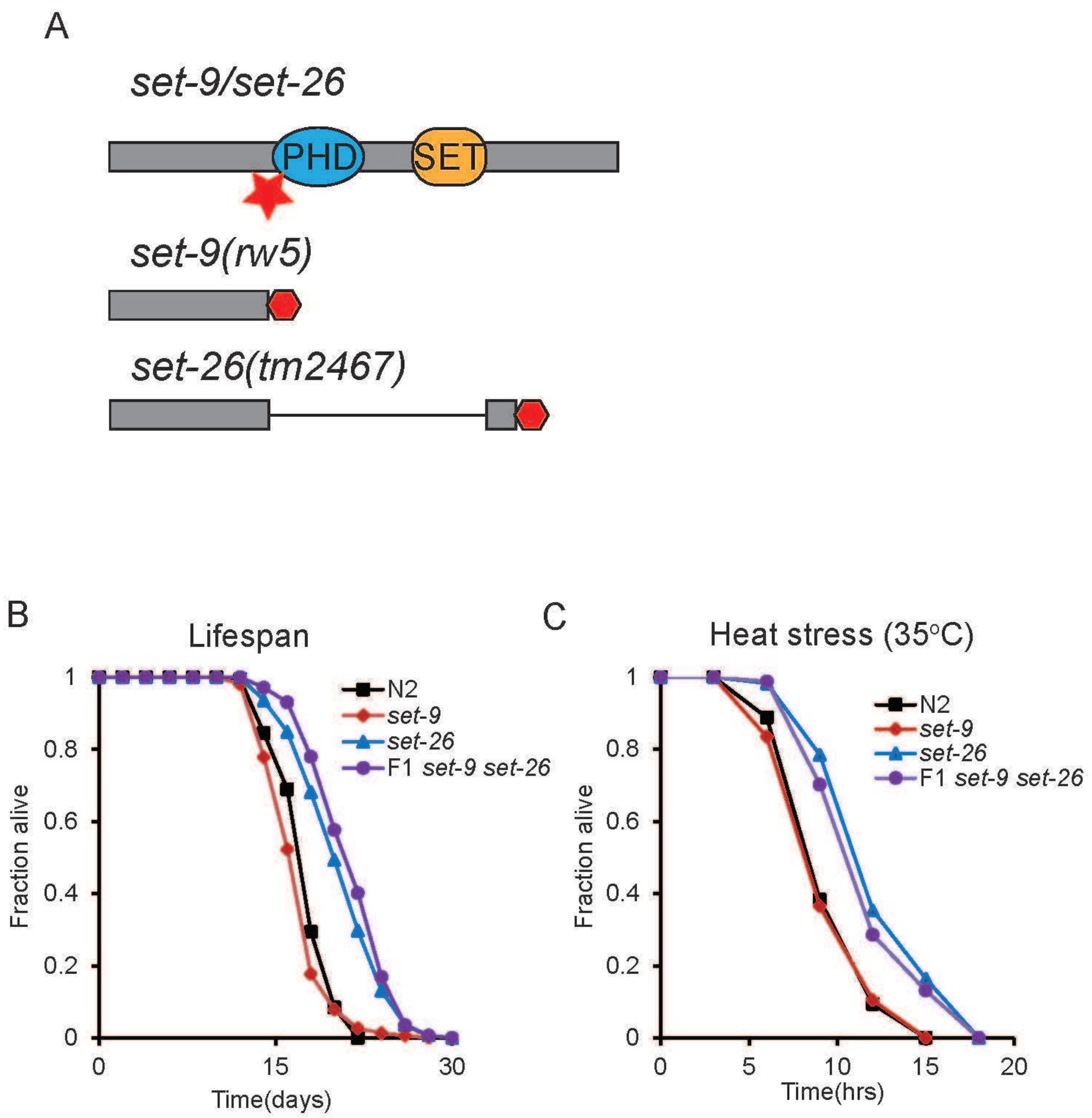
A
set-9/set-26
PHD
SET
set-9(rw5)
set-26(tm2467)
B
Lifespan
Fraction alive
Time(days)
N2
set-9
set-26
F1 set-9 set-26
C
Heat stress (35°C)
Fraction alive
Time(hrs)
N2
set-9
set-26
F1 set-9 set-26

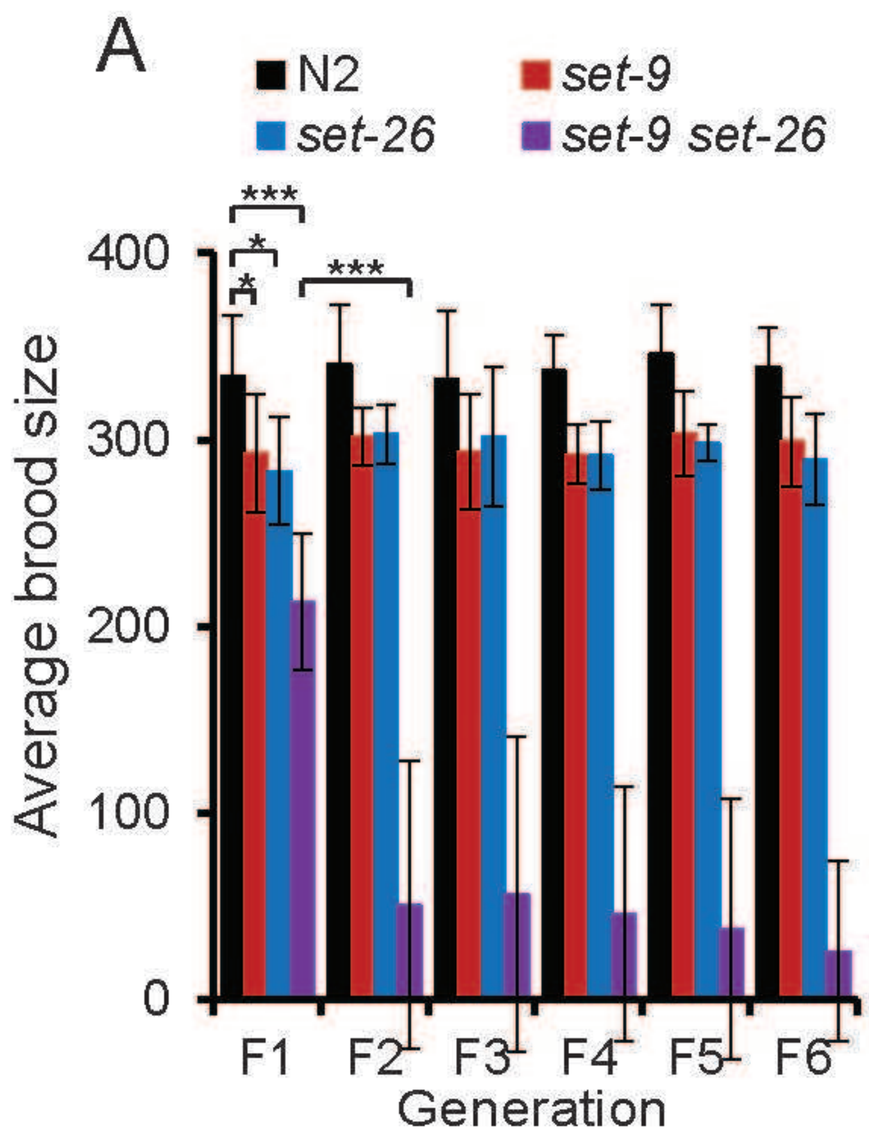
A
N2
set-9
set-26
set-9 set-26
***
*
*
***
400
300
200
100
0
Average brood size
F1
F2
F3
F4
F5
F6
Generation

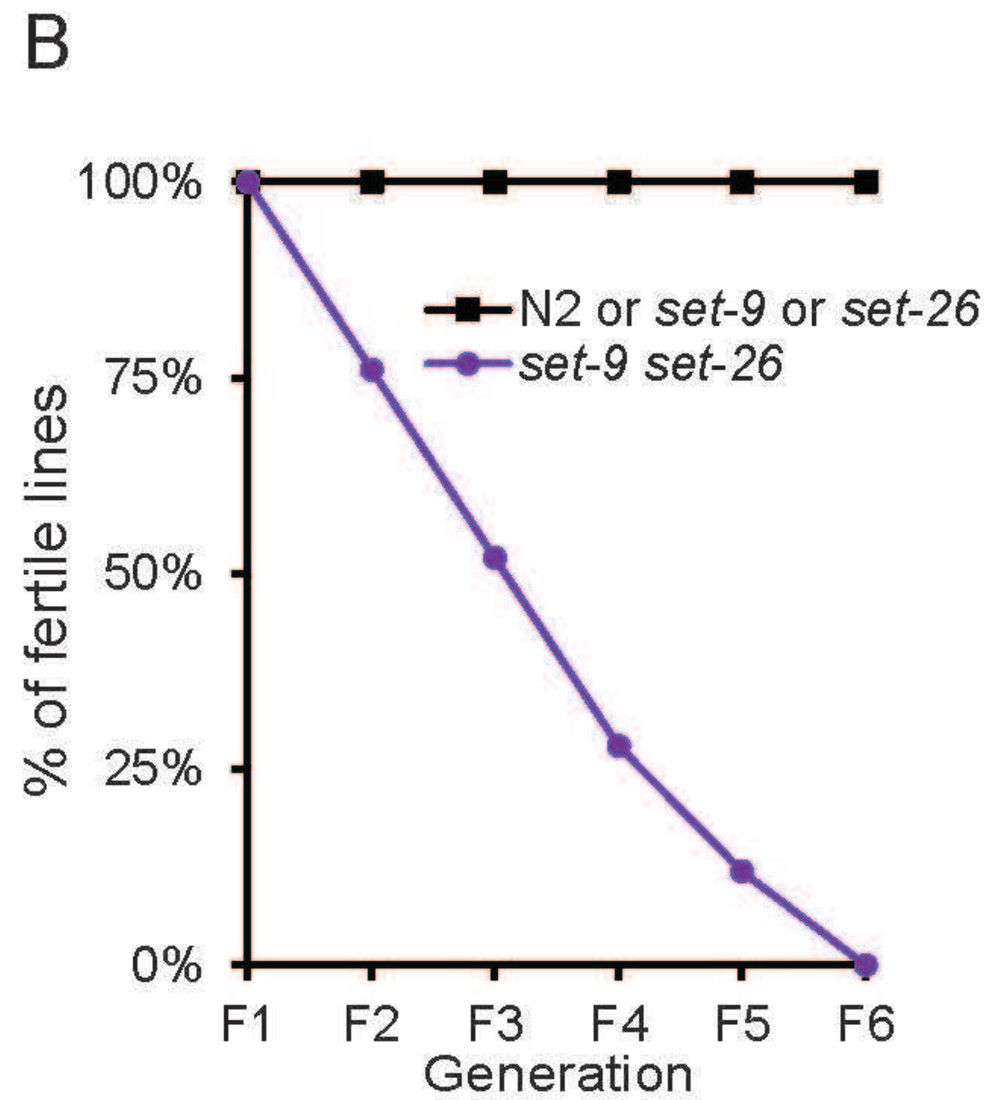
B
100%
75%
50%
25%
0%
% of fertile lines
N2 or set-9 or set-26
set-9 set-26
F1
F2
F3
F4
F5
F6
Generation

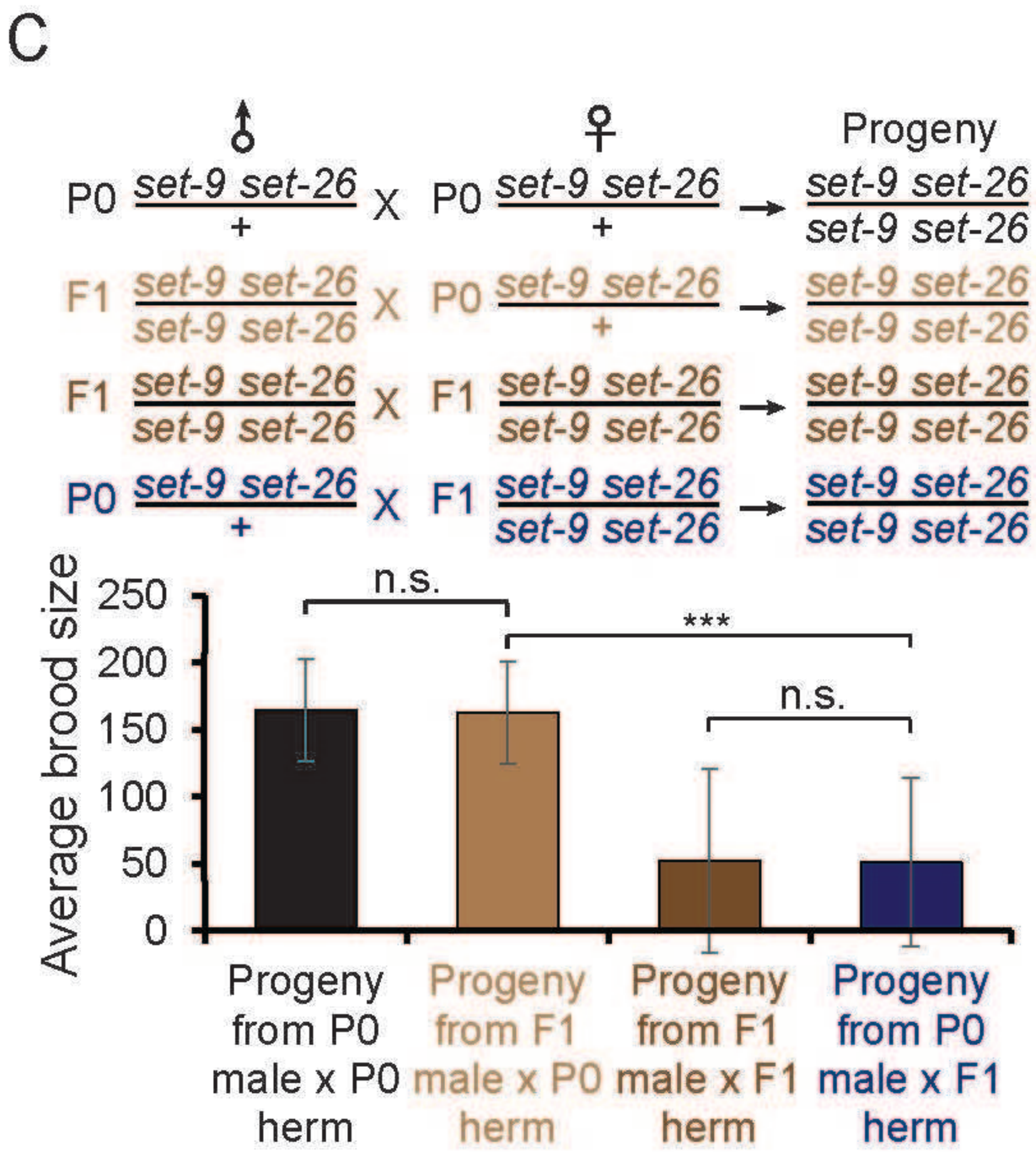
C
♂
♀
Progeny
P0 set-9 set-26 / + X P0 set-9 set-26 / + → set-9 set-26 / set-9 set-26
F1 set-9 set-26 / set-9 set-26 X P0 set-9 set-26 / + → set-9 set-26 / set-9 set-26
F1 set-9 set-26 / set-9 set-26 X F1 set-9 set-26 / set-9 set-26 → set-9 set-26 / set-9 set-26
P0 set-9 set-26 / + X F1 set-9 set-26 / set-9 set-26 → set-9 set-26 / set-9 set-26
Average brood size
250
200
150
100
50
0
n.s.
***
n.s.
Progeny from P0 male x P0 herm
Progeny from F1 male x P0 herm
Progeny from F1 male x F1 herm
Progeny from P0 male x F1 herm

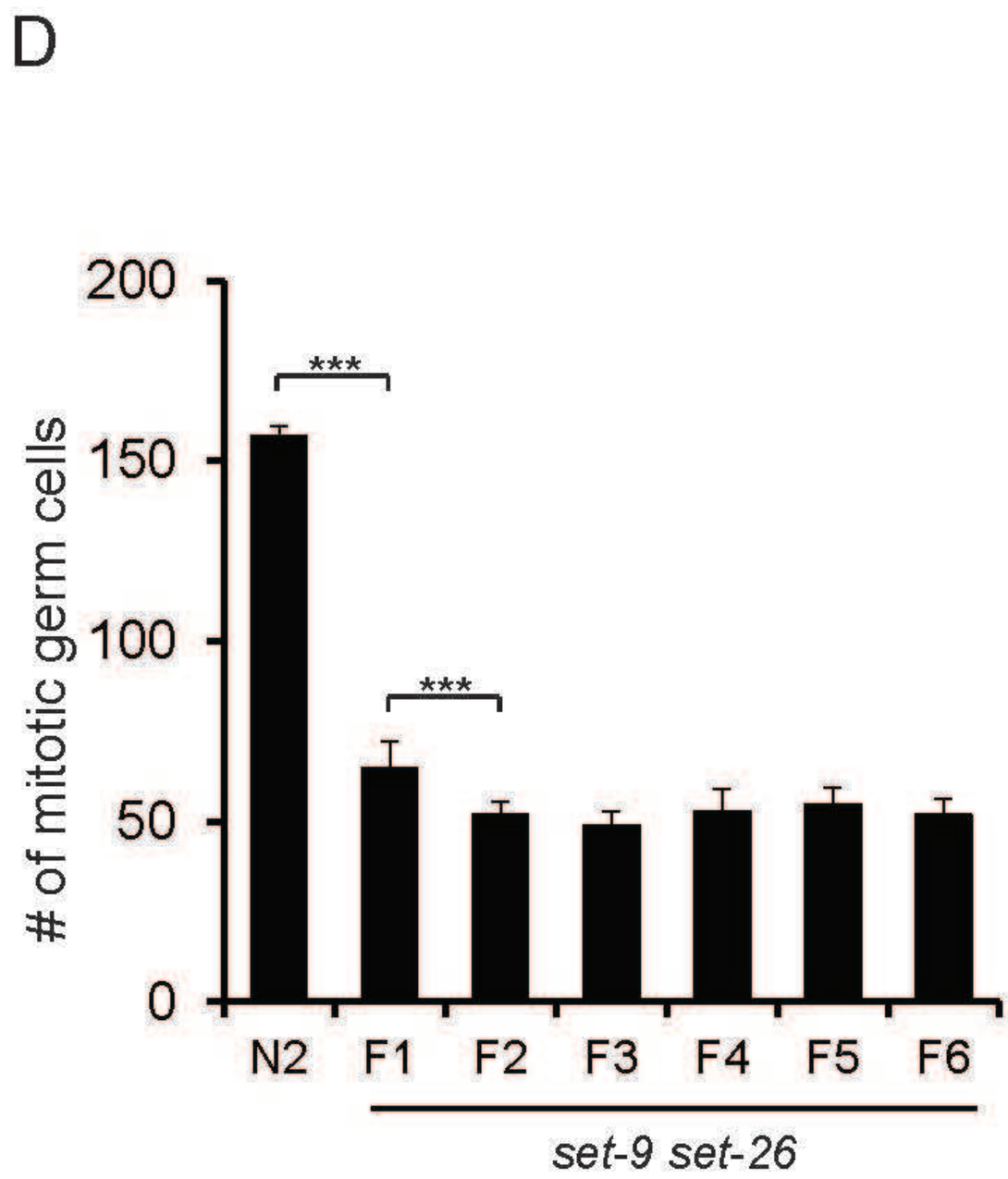
D
200
150
100
50
0
# of mitotic germ cells
***
***
N2
F1
F2
F3
F4
F5
F6
set-9 set-26

Wang_Figure 2-figure supplement 1

A

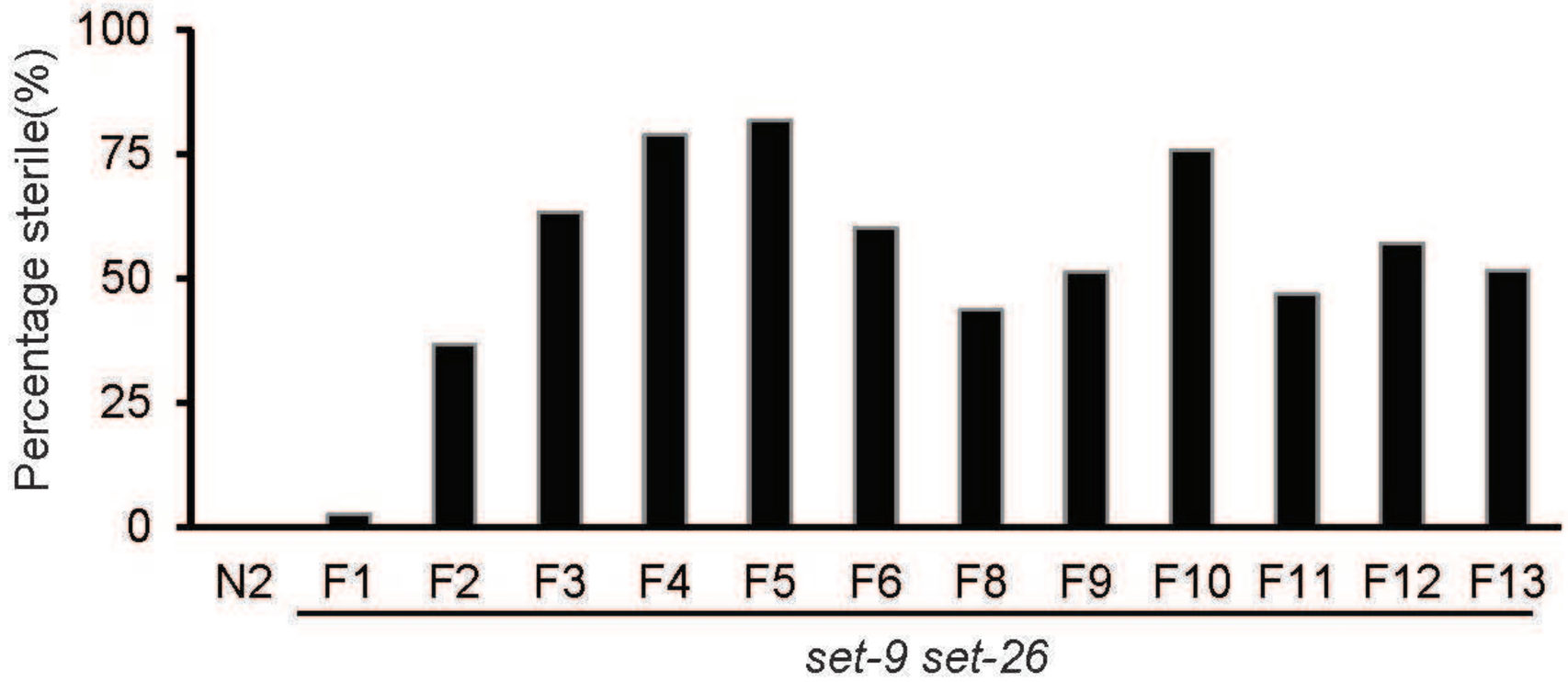

B

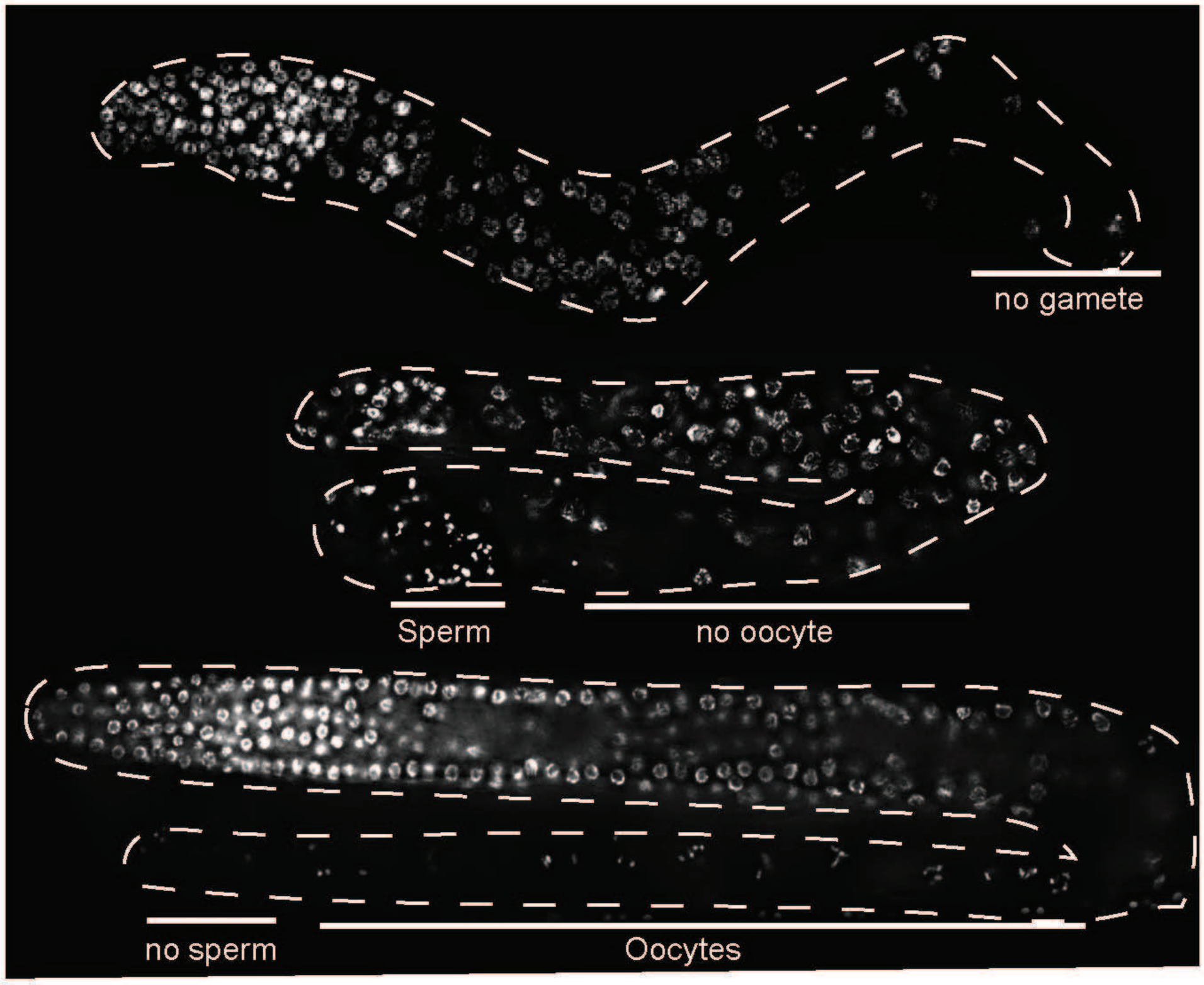

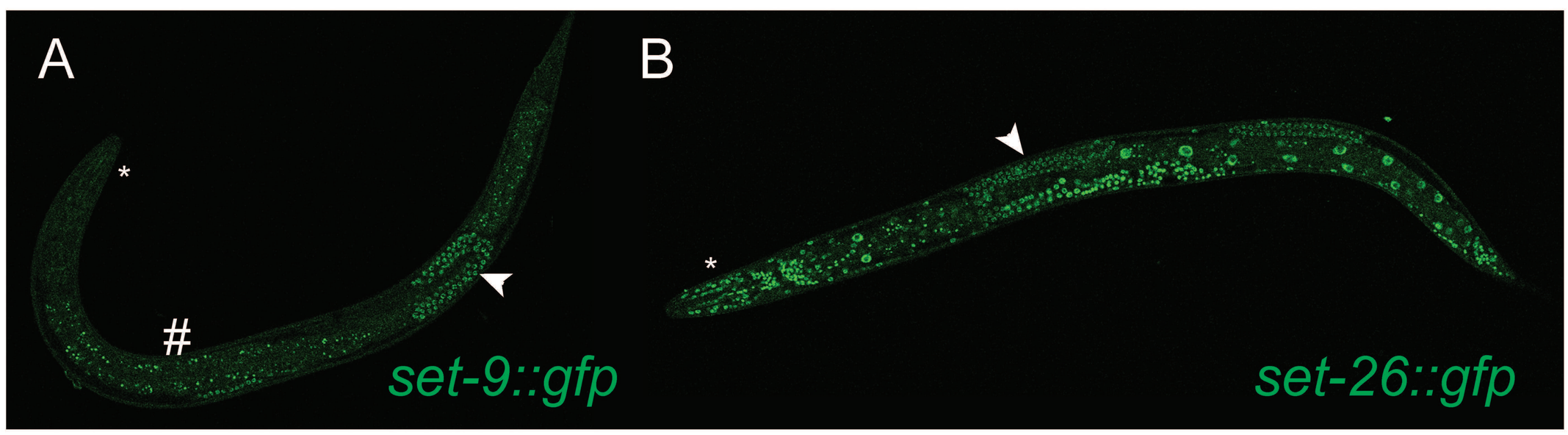
A
*
#
set-9::gfp
B
*
set-26::gfp

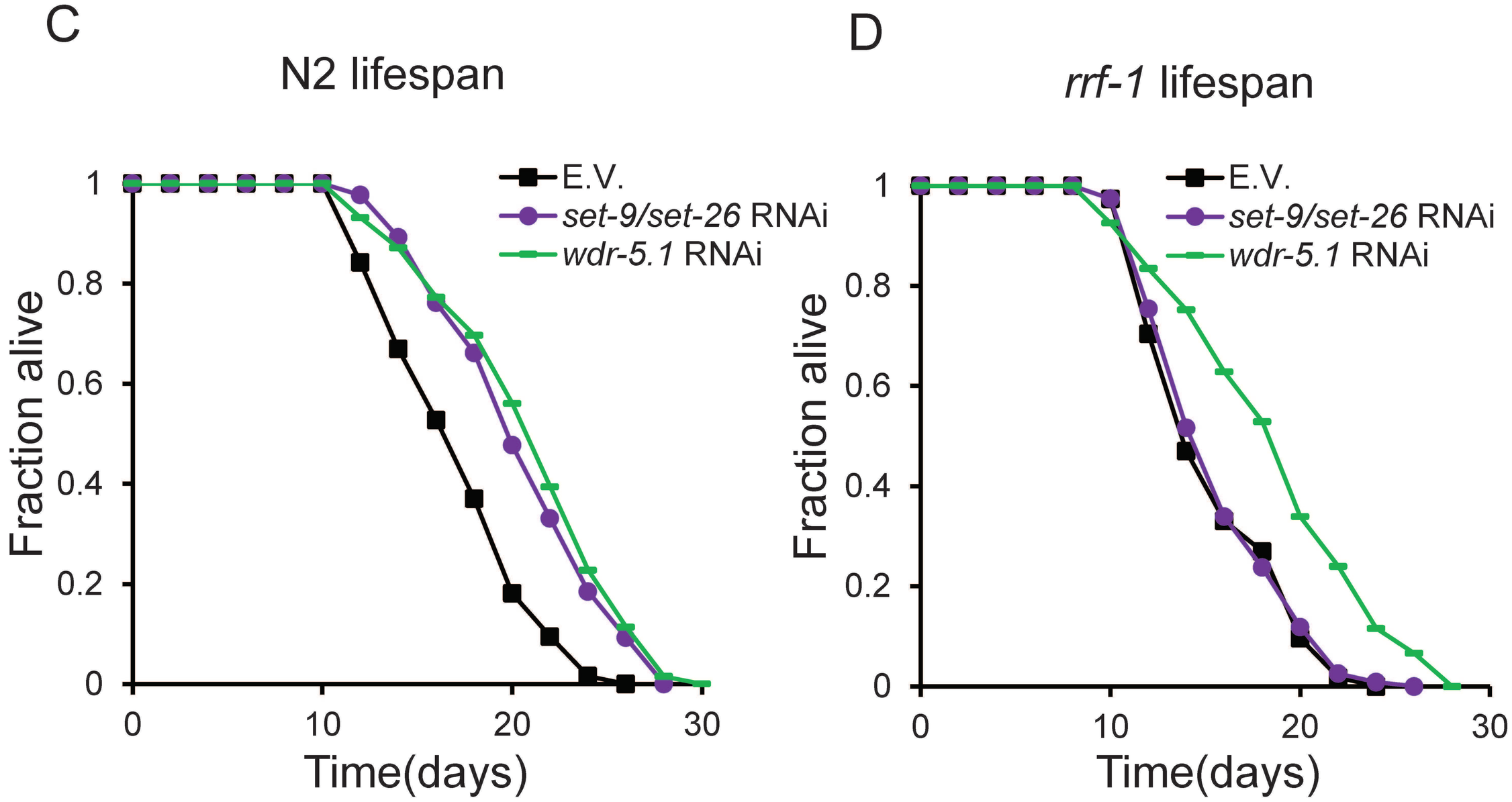
C
N2 lifespan
E.V.
set-9/set-26 RNAi
wdr-5.1 RNAi
Fraction alive
1
0.8
0.6
0.4
0.2
0
0
10
20
30
Time(days)
D
rrf-1 lifespan
E.V.
set-9/set-26 RNAi
wdr-5.1 RNAi
Fraction alive
1
0.8
0.6
0.4
0.2
0
0
10
20
30
Time(days)

Wang_Figure 3-figure supplement 1

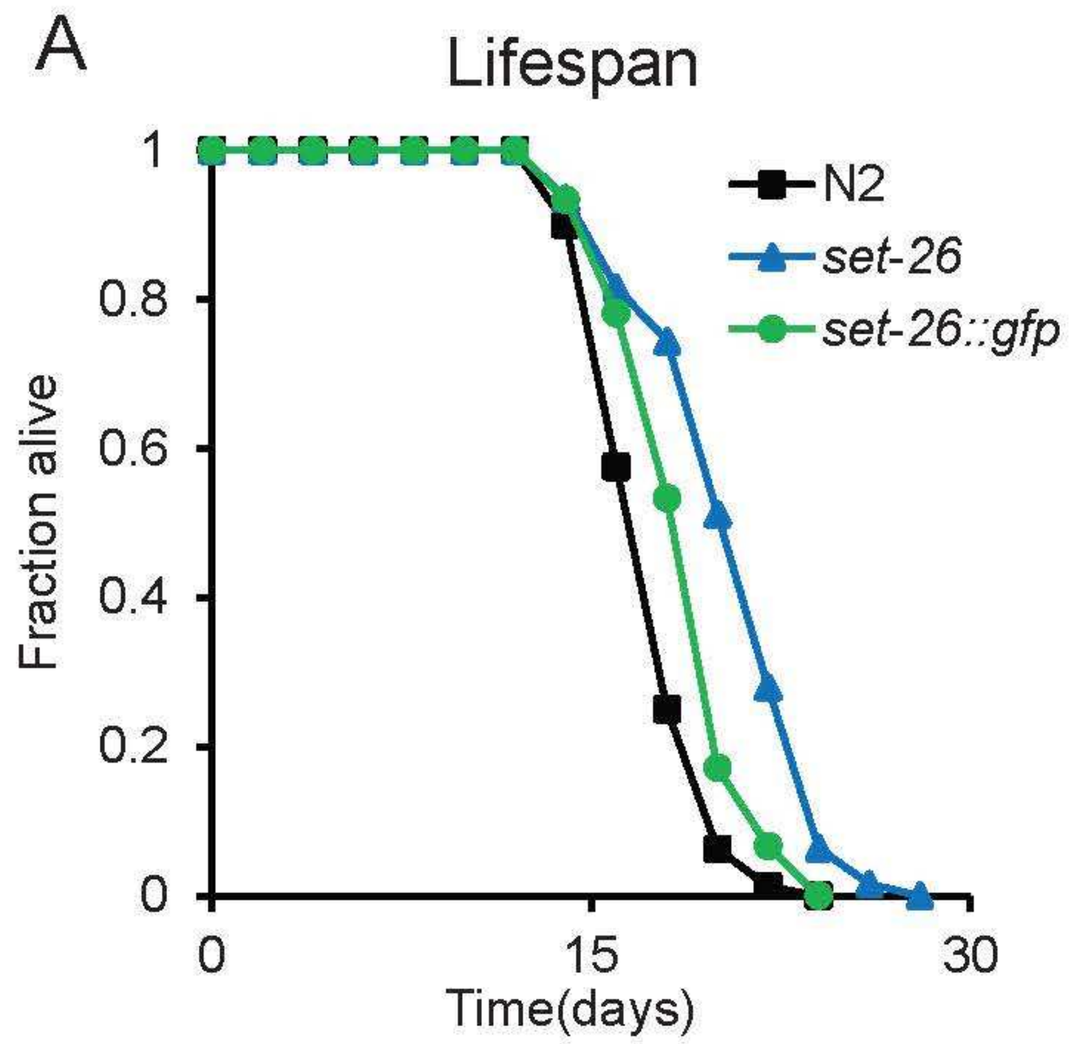

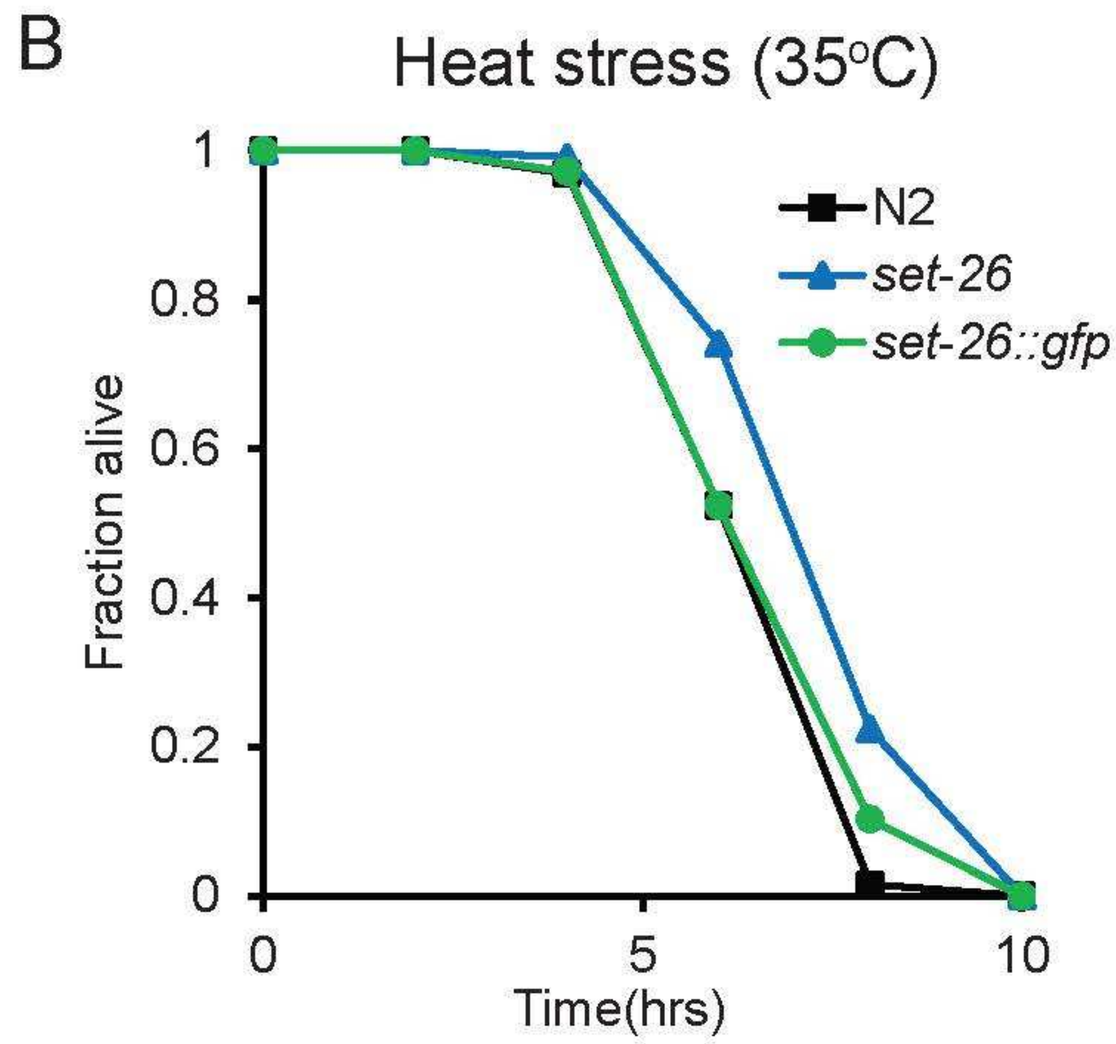

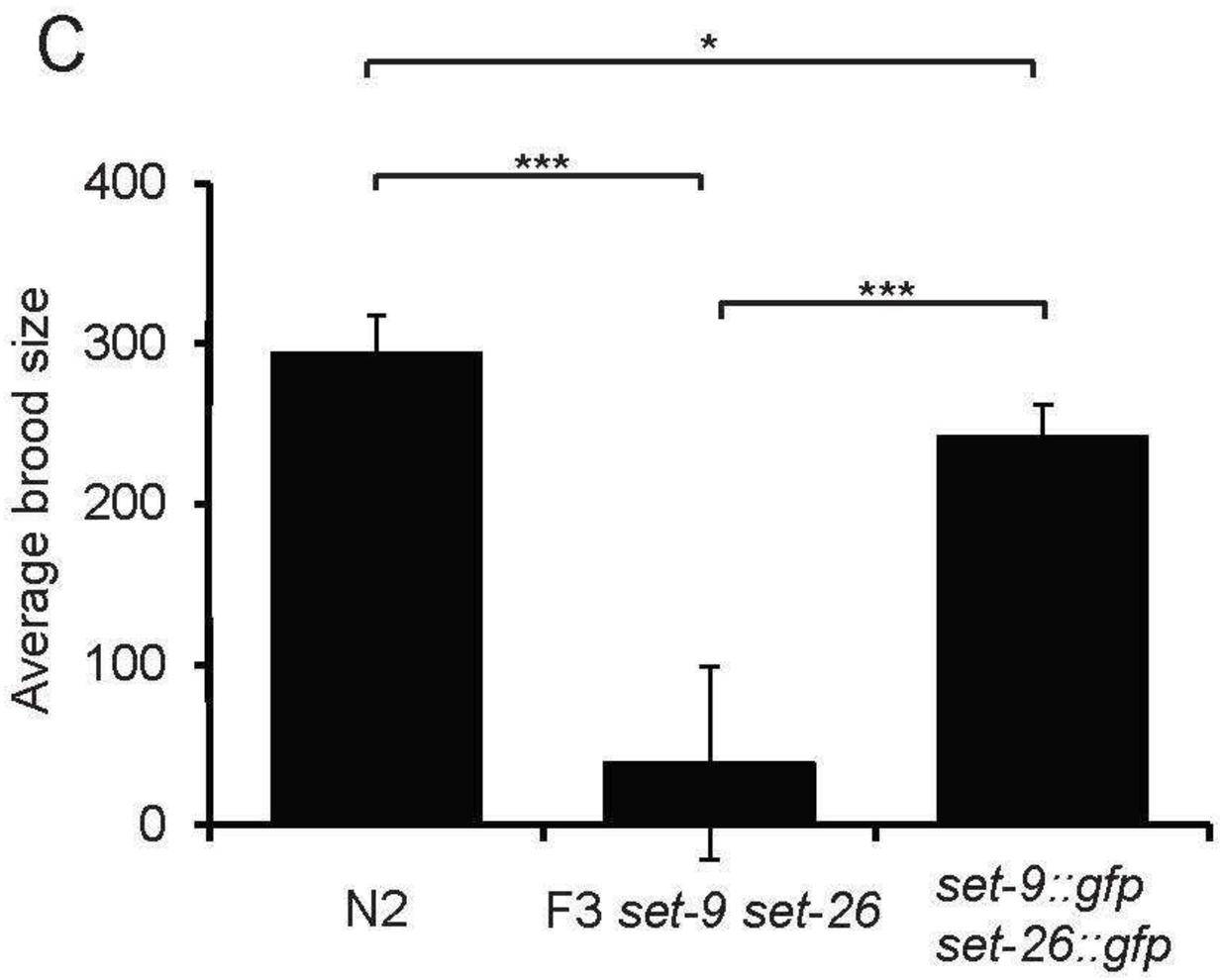

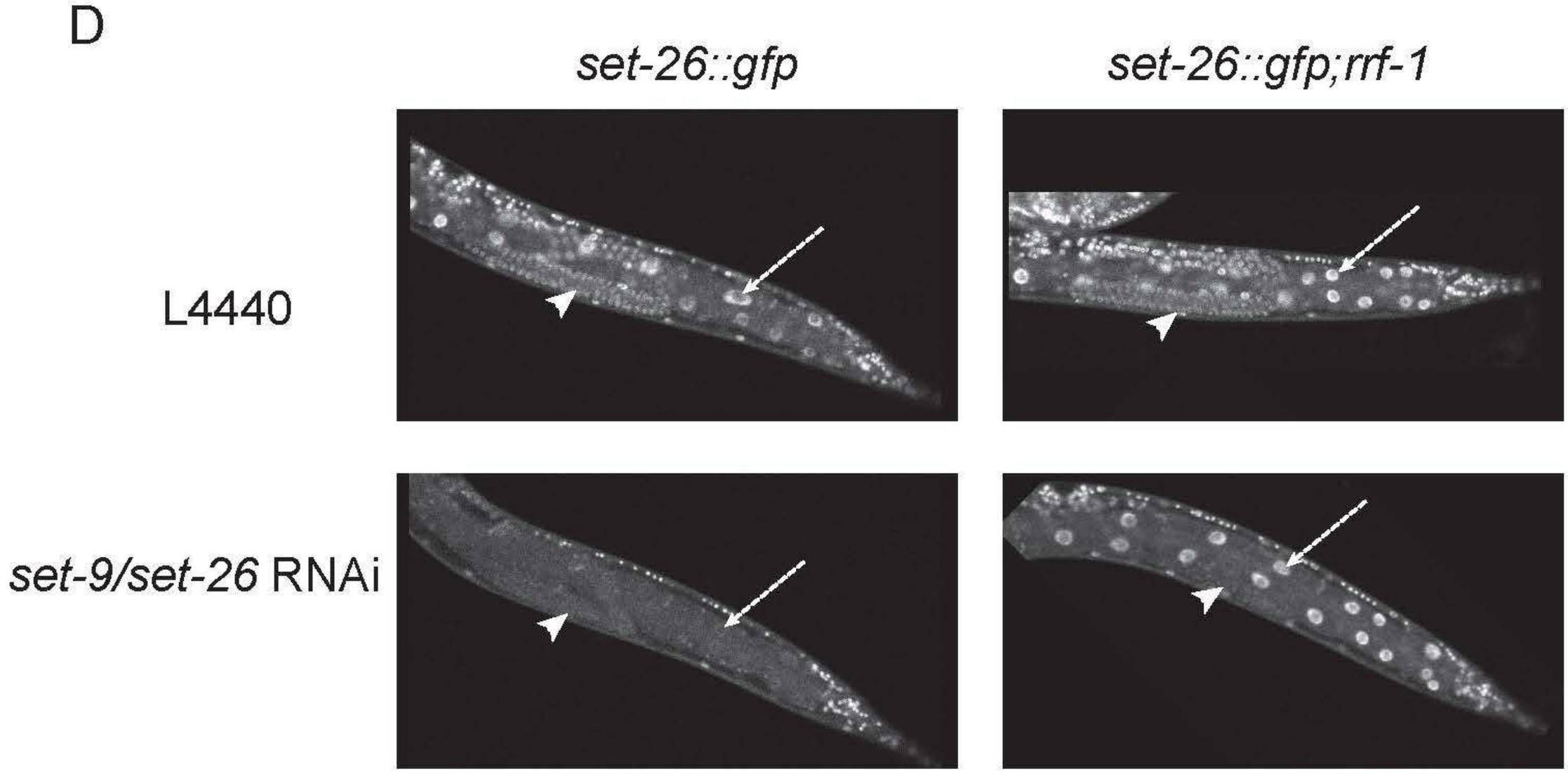

Wang_Figure 3-figure supplement 2

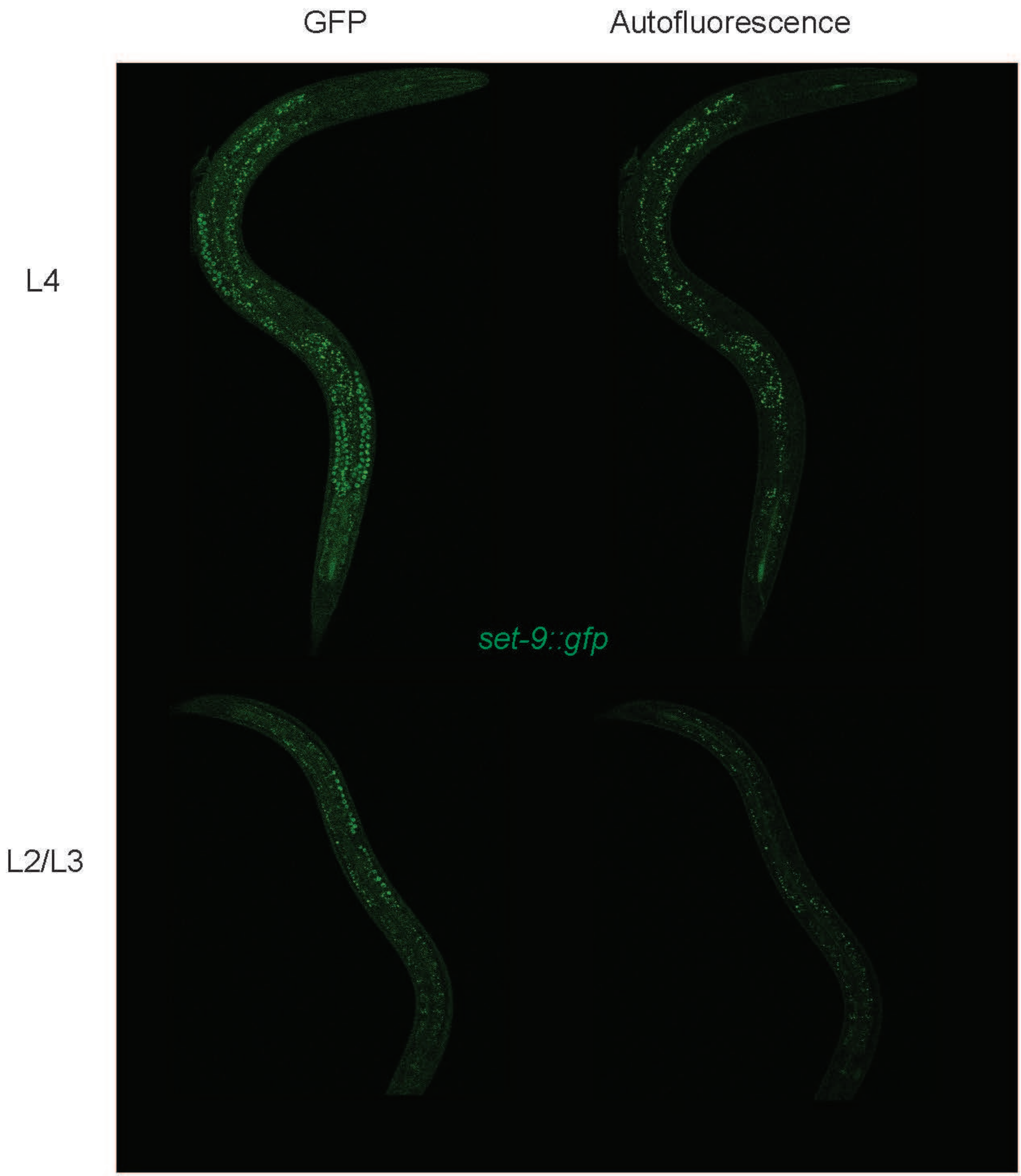

A

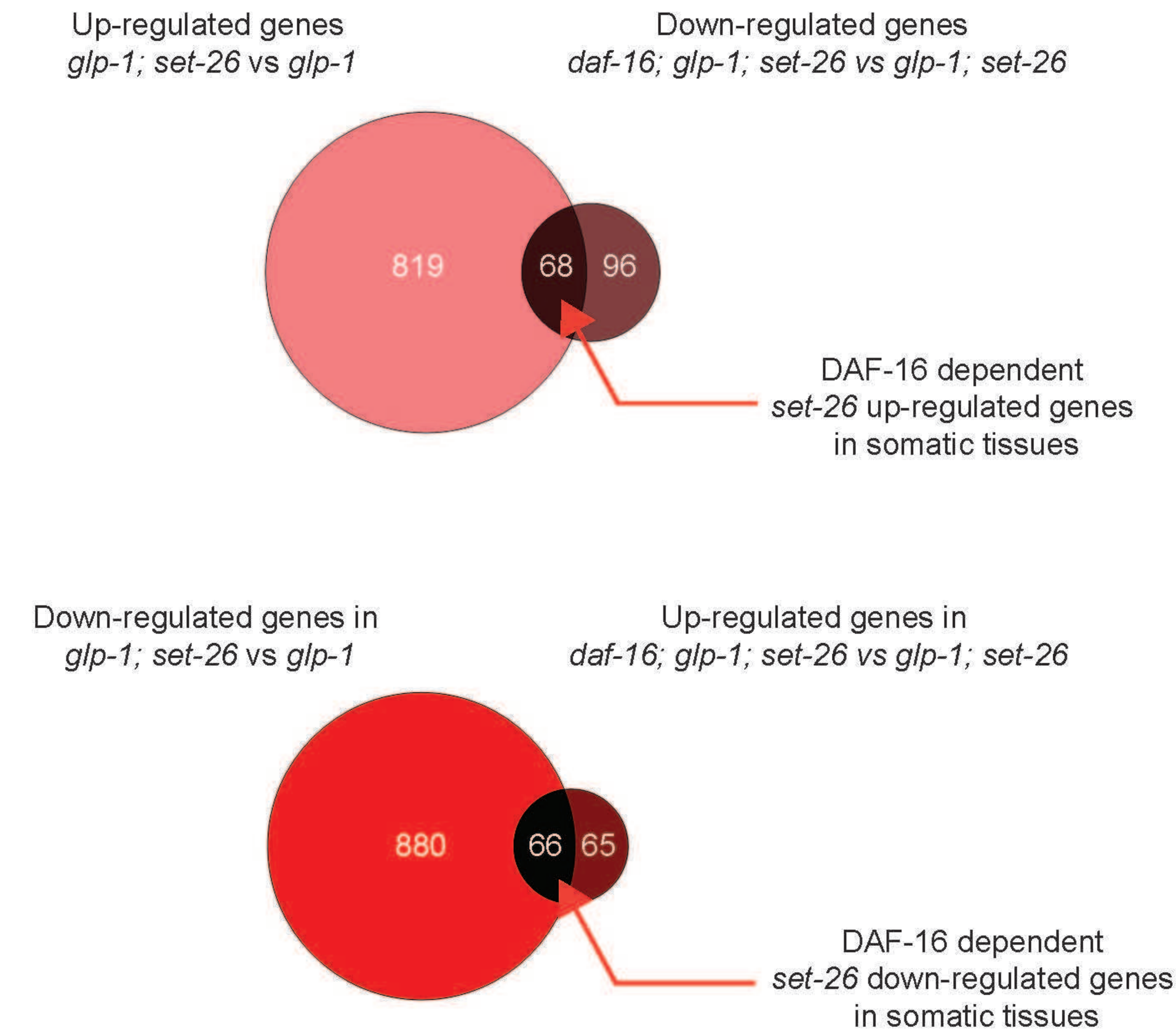
Up-regulated genes
glp-1; set-26 vs glp-1
Down-regulated genes
daf-16; glp-1; set-26 vs glp-1; set-26
819
68
96
DAF-16 dependent
set-26 up-regulated genes
in somatic tissues
Down-regulated genes in
glp-1; set-26 vs glp-1
Up-regulated genes in
daf-16; glp-1; set-26 vs glp-1; set-26
880
66
65
DAF-16 dependent
set-26 down-regulated genes
in somatic tissues

B

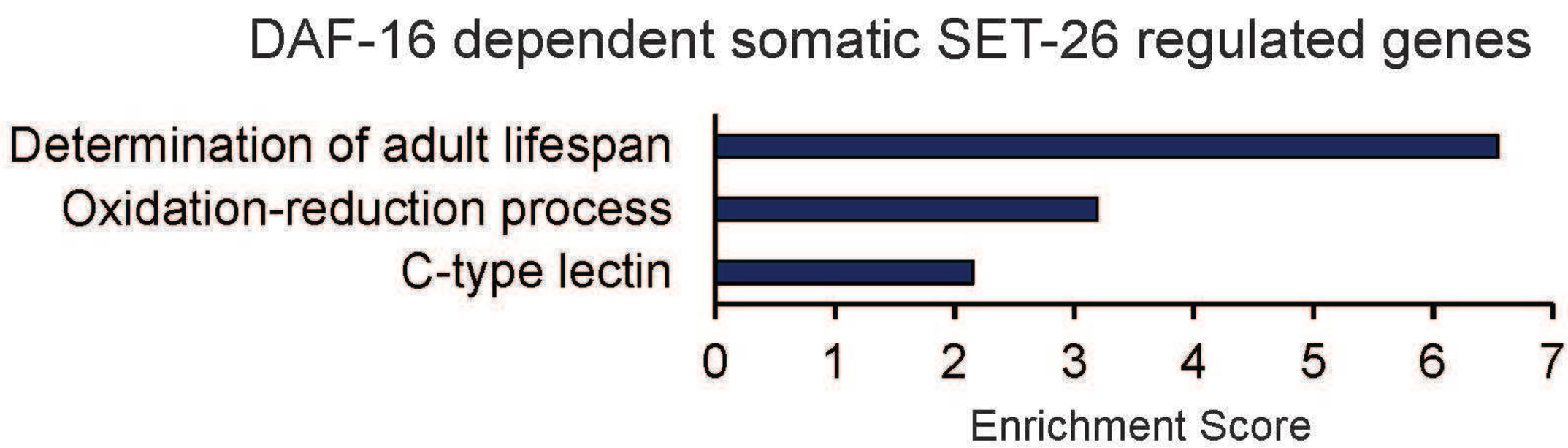
DAF-16 dependent somatic SET-26 regulated genes
Determination of adult lifespan
Oxidation-reduction process
C-type lectin
0
1
2
3
4
5
6
7
Enrichment Score

A

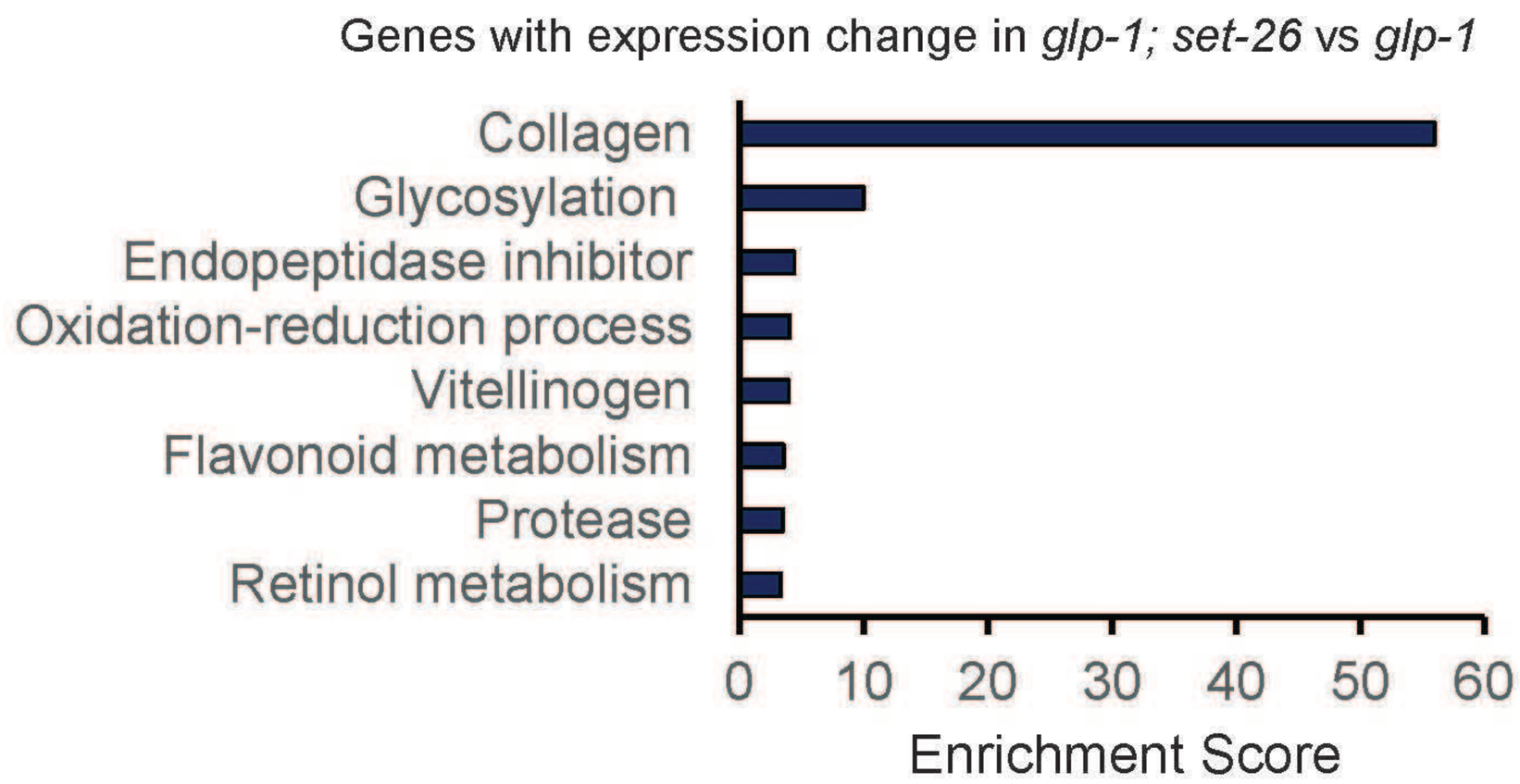
Genes with expression change in *glp-1; set-26* vs *glp-1*
Collagen
Glycosylation
Endopeptidase inhibitor
Oxidation-reduction process
Vitellinogen
Flavonoid metabolism
Protease
Retinol metabolism
0
10
20
30
40
50
60
Enrichment Score

B

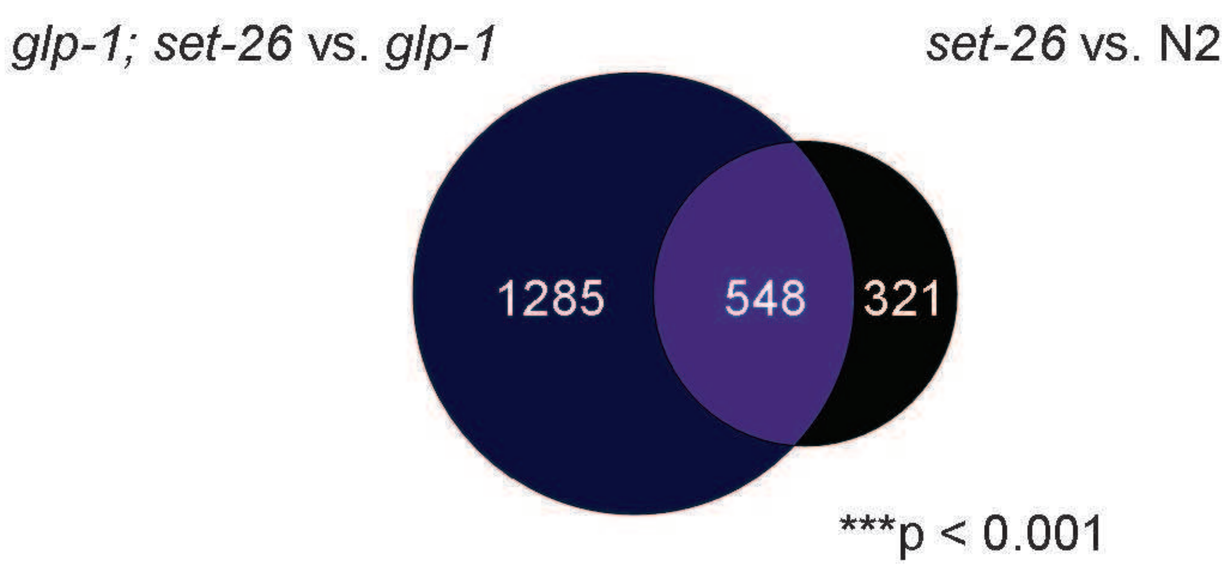
glp-1; set-26 vs. *glp-1*
set-26 vs. N2
1285
548
321
***p < 0.001

Wang_Figure 5

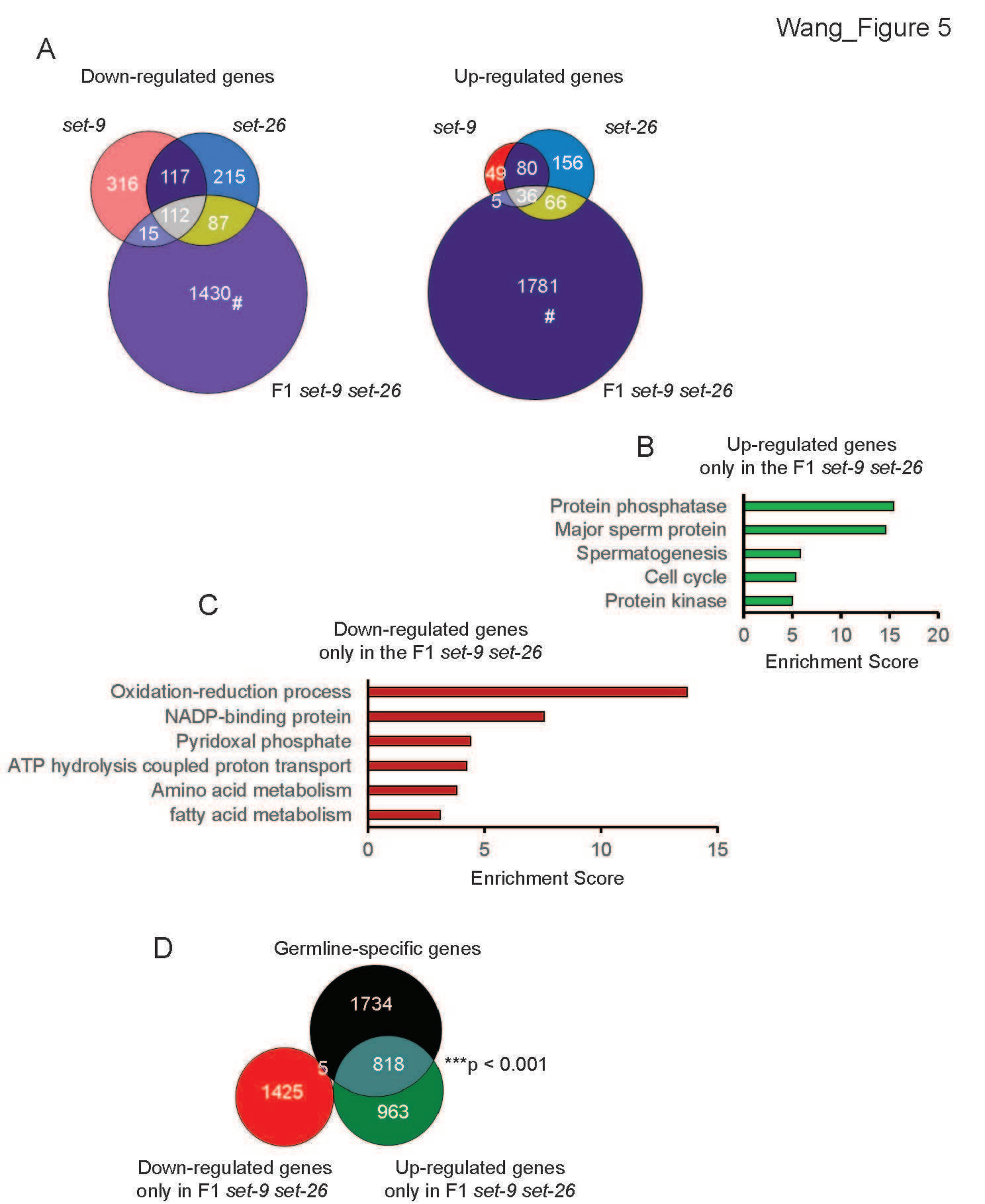

Wang_Figure 5-figure supplement 1

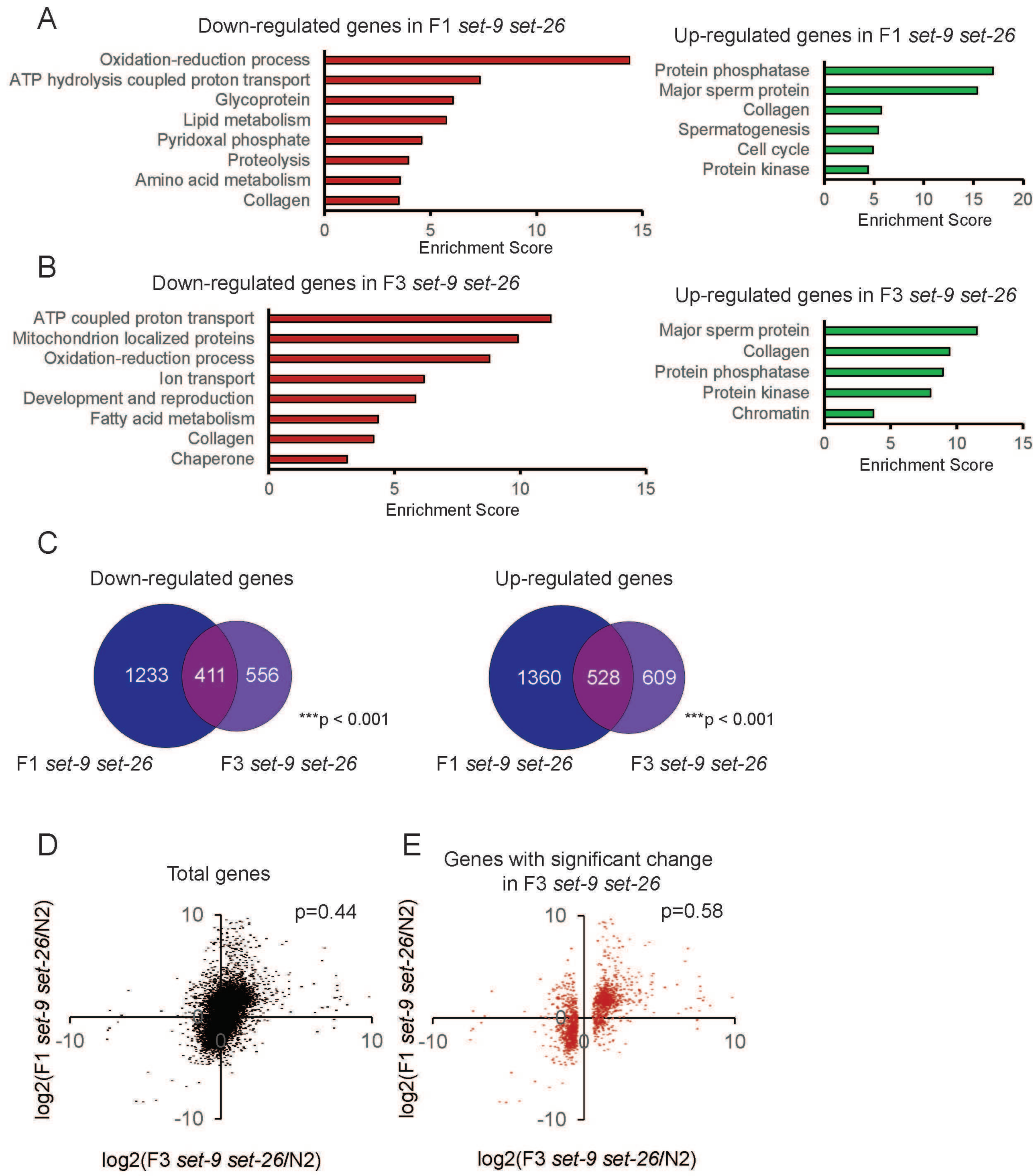

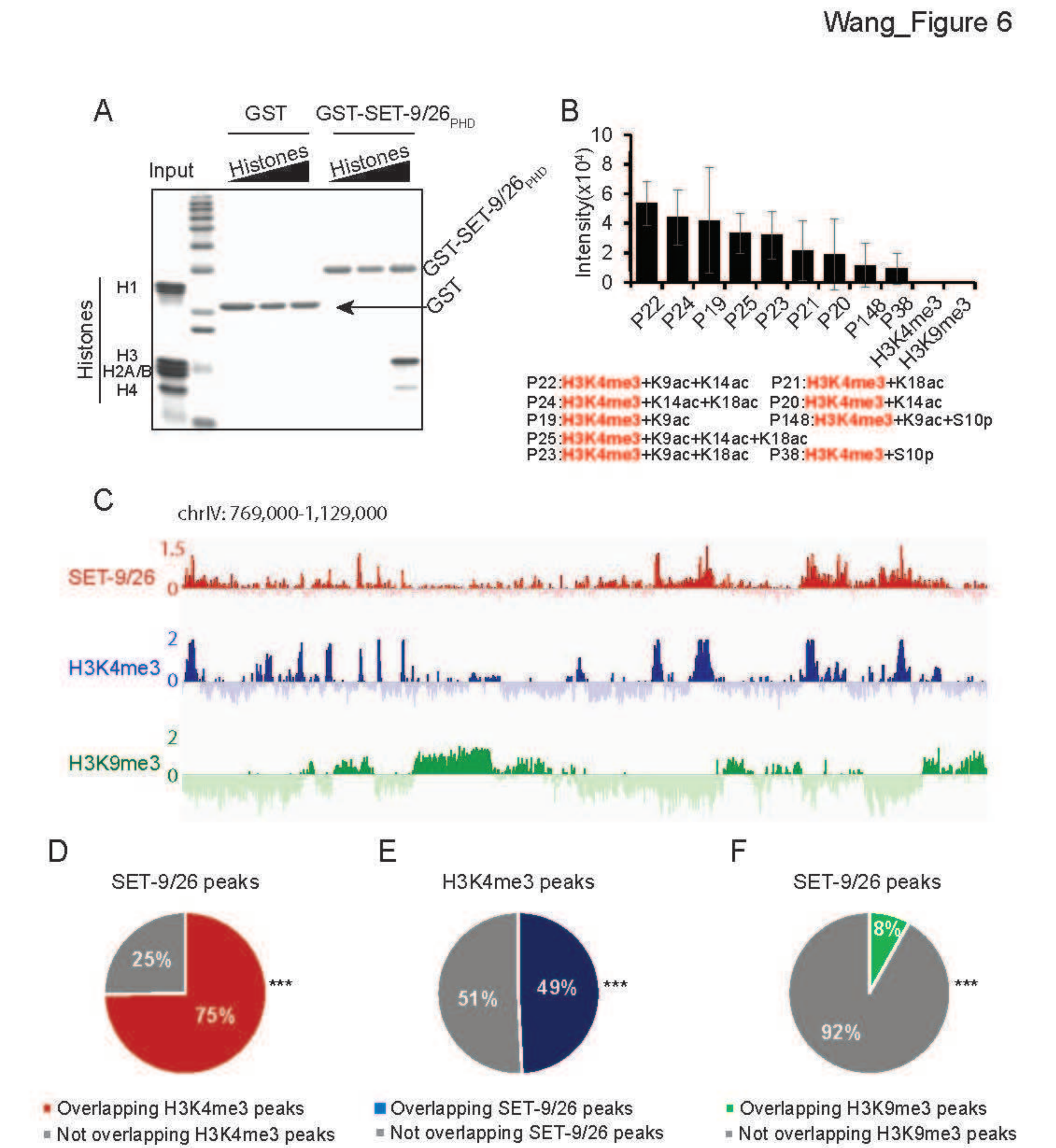
A
GST
GST-SET-9/26PHD
Input
Histones
Histones
GST-SET-9/26PHD
GST
Histones
H1
H3
H2A/B
H4
B
Intensity(x10⁴)
10
8
6
4
2
0
P22
P24
P19
P25
P23
P21
P20
P148
P38
H3K4me3
H3K9me3
P22:H3K4me3+K9ac+K14ac
P21:H3K4me3+K18ac
P24:H3K4me3+K14ac+K18ac
P20:H3K4me3+K14ac
P19:H3K4me3+K9ac
P148:H3K4me3+K9ac+S10p
P25:H3K4me3+K9ac+K14ac+K18ac
P23:H3K4me3+K9ac+K18ac
P38:H3K4me3+S10p
C
chrIV: 769,000-1,129,000
SET-9/26
1.5
0
H3K4me3
2
0
H3K9me3
2
0
D
SET-9/26 peaks
25%
75%
***
Overlapping H3K4me3 peaks
Not overlapping H3K4me3 peaks
E
H3K4me3 peaks
51%
49%
***
Overlapping SET-9/26 peaks
Not overlapping SET-9/26 peaks
F
SET-9/26 peaks
8%
92%
***
Overlapping H3K9me3 peaks
Not overlapping H3K9me3 peaks

A

cSET-9/26-SET
dUpSET-SET
hMLL5-SET
hSETD5-SET
hSET7-SET
scSET1-SET
hSUV91

B

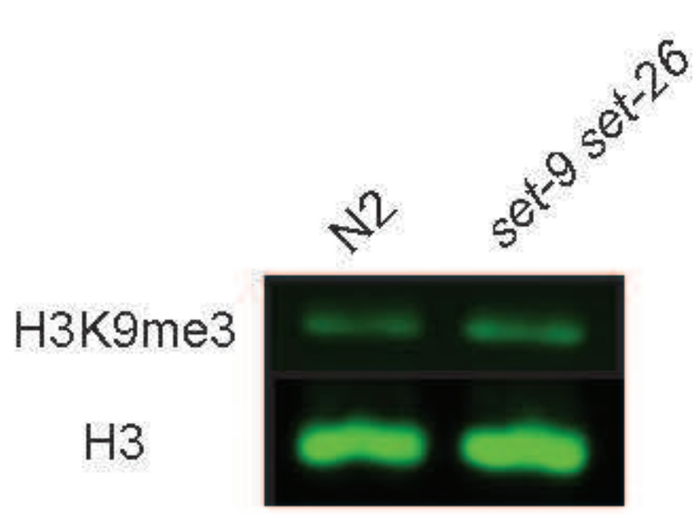
N2
set-9 set-26
H3K9me3
H3

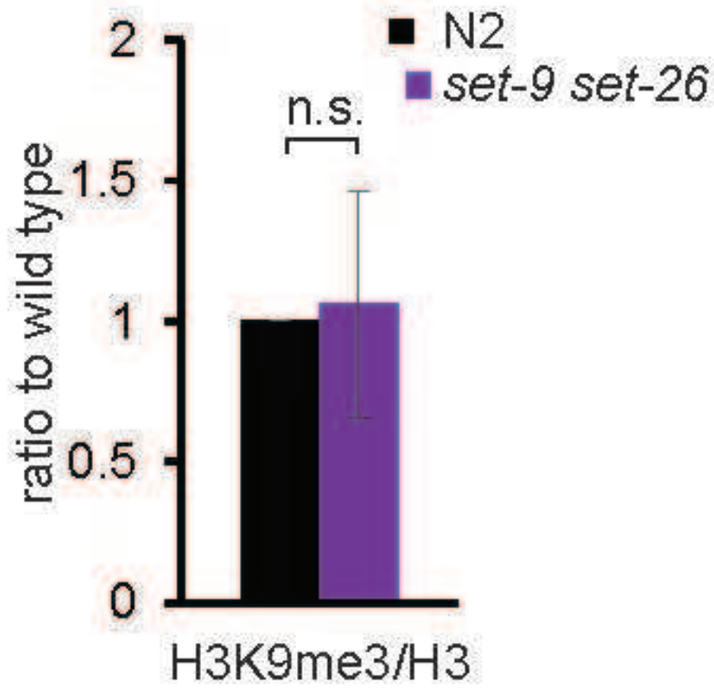
N2
set-9 set-26
n.s.
ratio to wild type
2
1.5
1
0.5
0
H3K9me3/H3

C

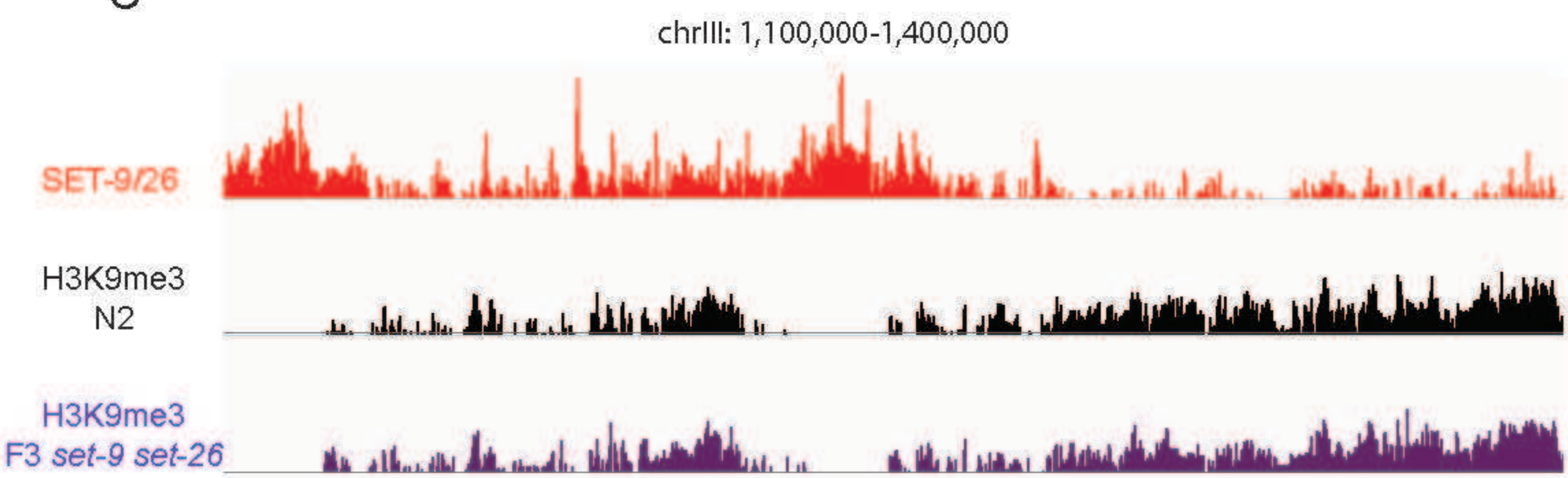
chrIII: 1,100,000-1,400,000
SET-9/26
H3K9me3
N2
H3K9me3
F3 set-9 set-26

D

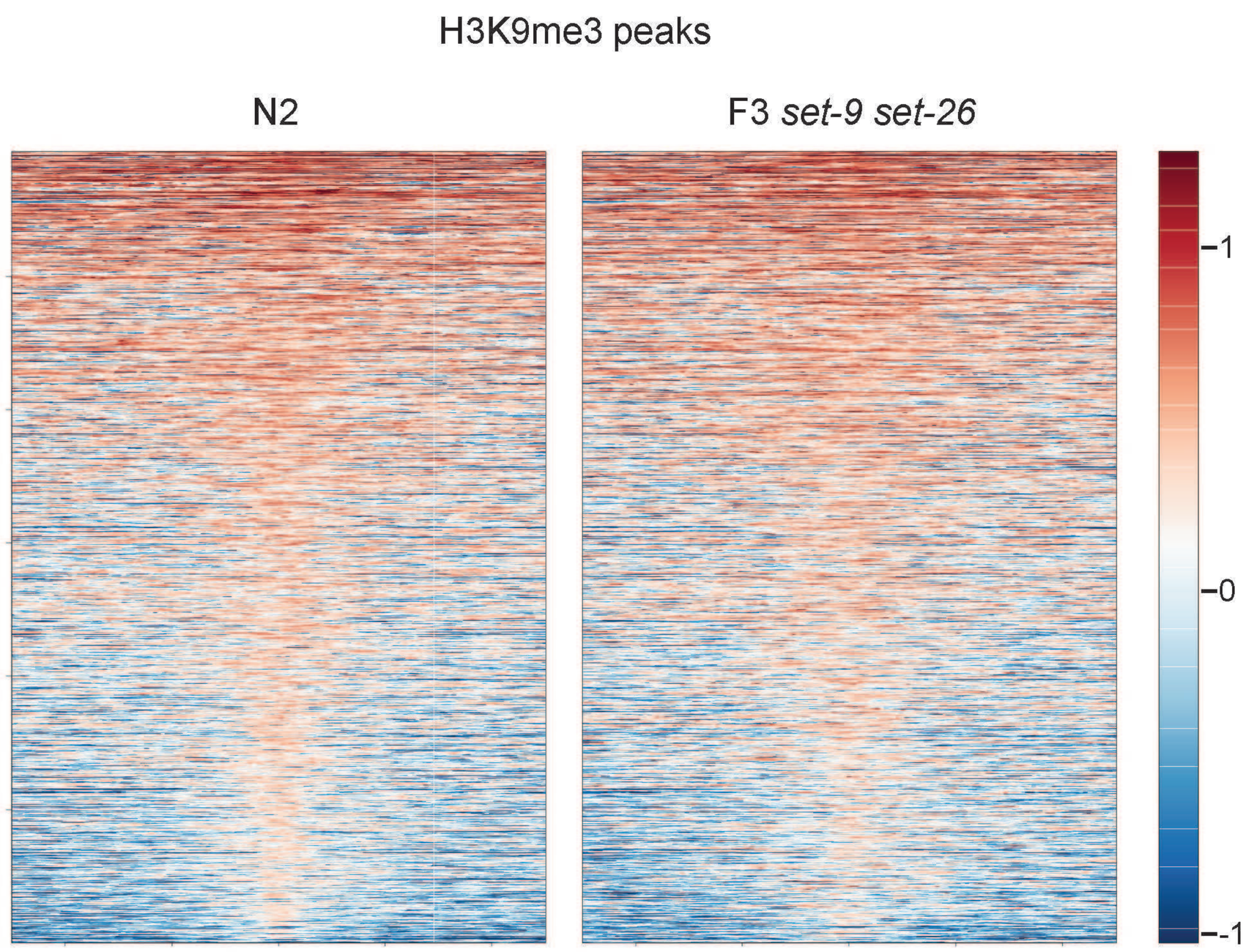

Wang_Figure 6-figure supplement 2

A

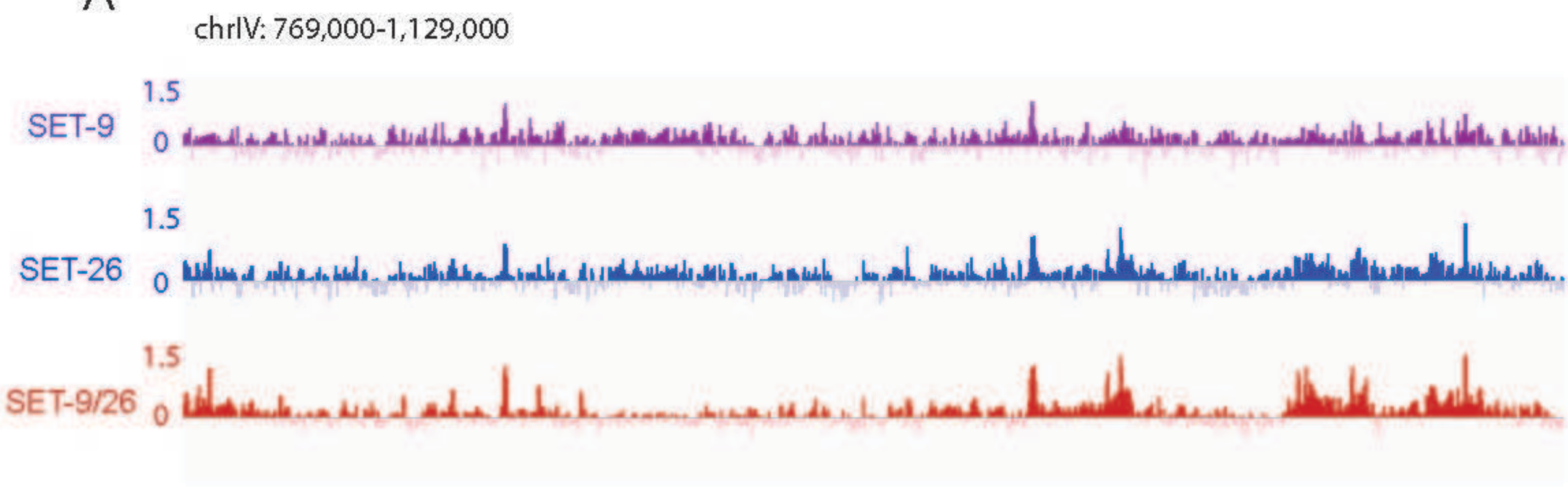

B

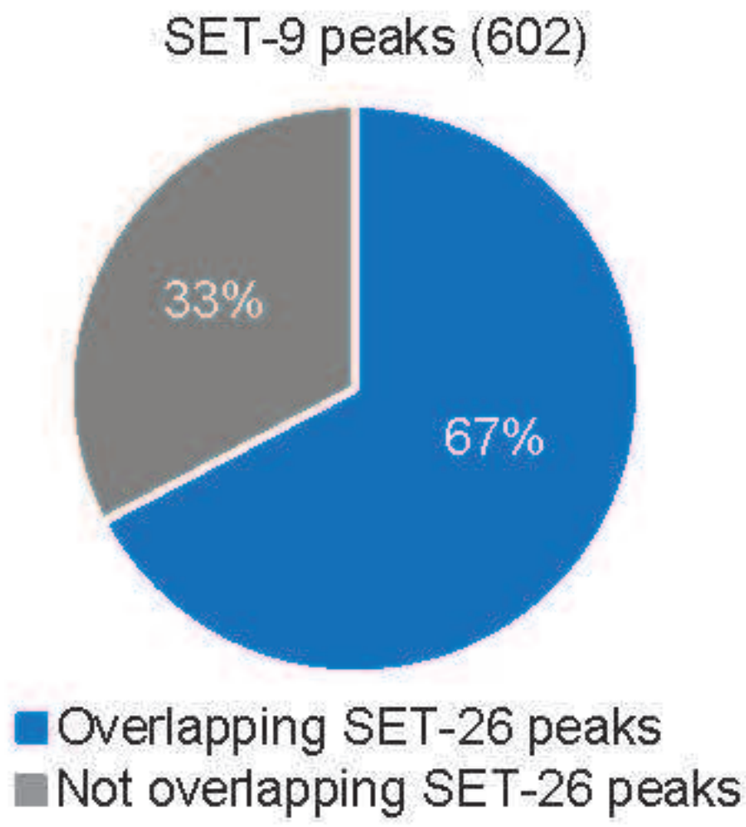

C

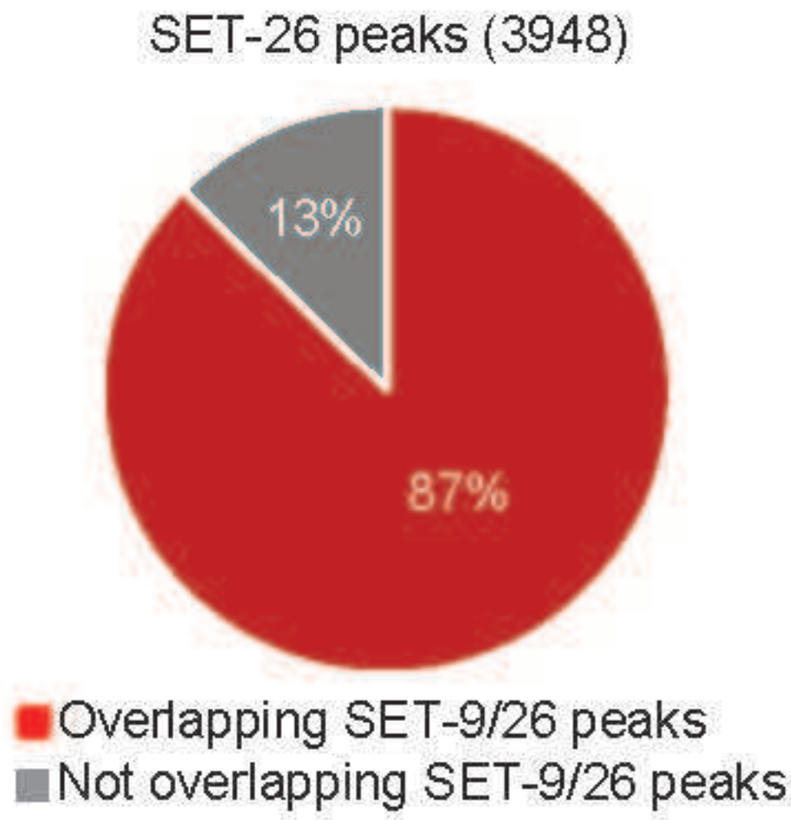

Wang_Figure 6-figure supplement 3

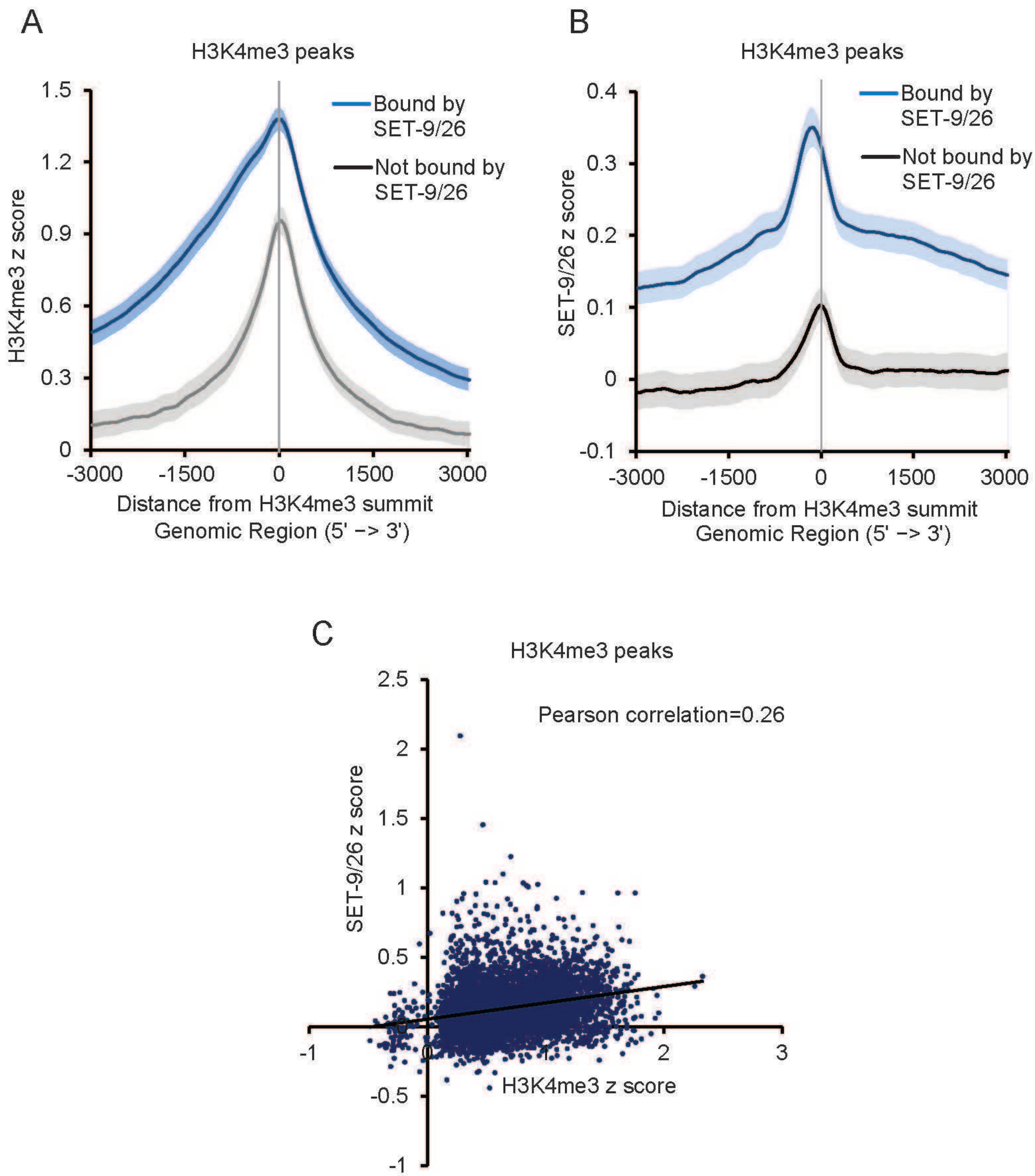

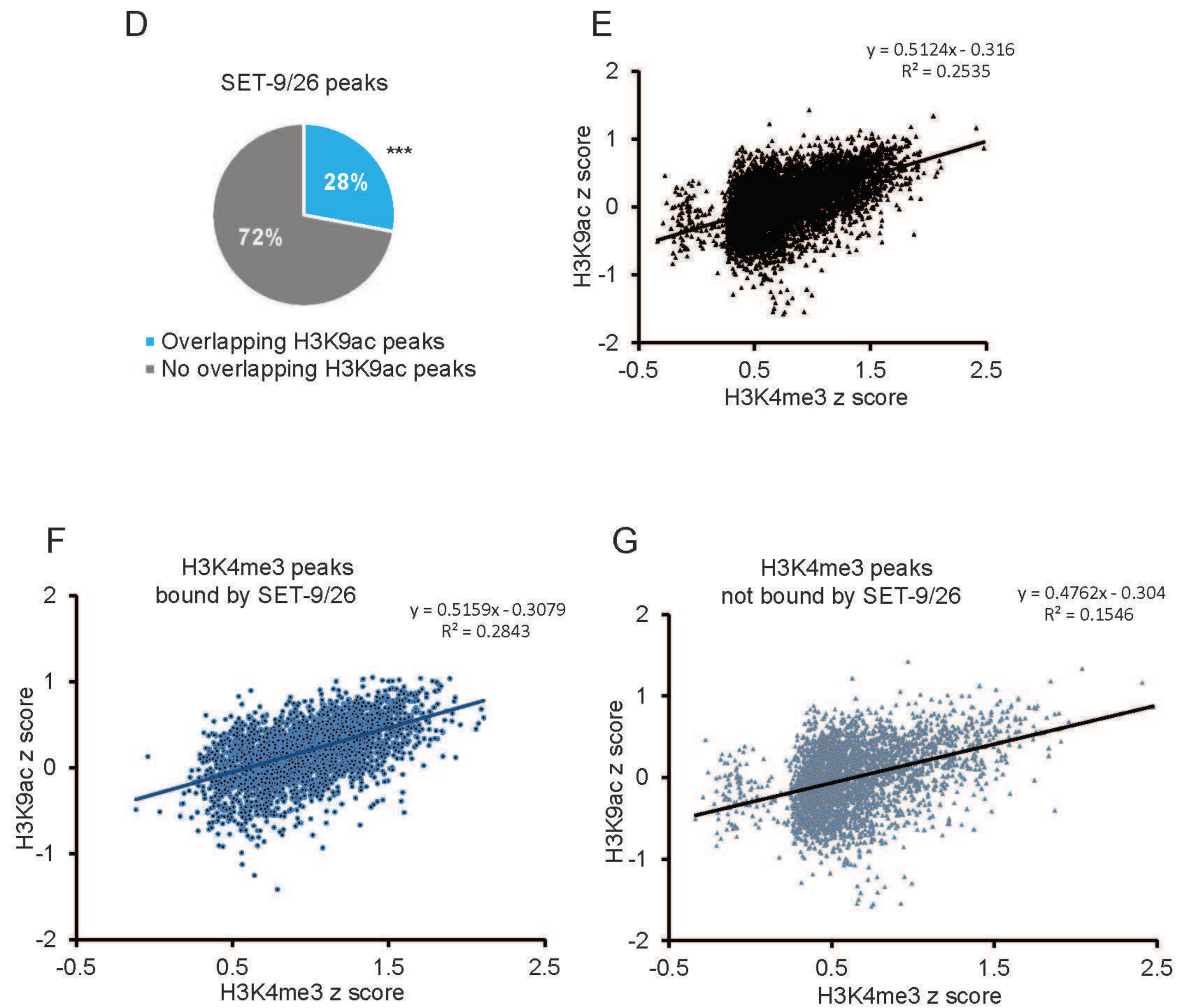
D
SET-9/26 peaks
28%
72%
***
Overlapping H3K9ac peaks
No overlapping H3K9ac peaks
E
y = 0.5124x - 0.316
R² = 0.2535
H3K9ac z score
H3K4me3 z score
F
H3K4me3 peaks
bound by SET-9/26
y = 0.5159x - 0.3079
R² = 0.2843
H3K9ac z score
H3K4me3 z score
G
H3K4me3 peaks
not bound by SET-9/26
y = 0.4762x - 0.304
R² = 0.1546
H3K9ac z score
H3K4me3 z score

Wang_Figure 7

A

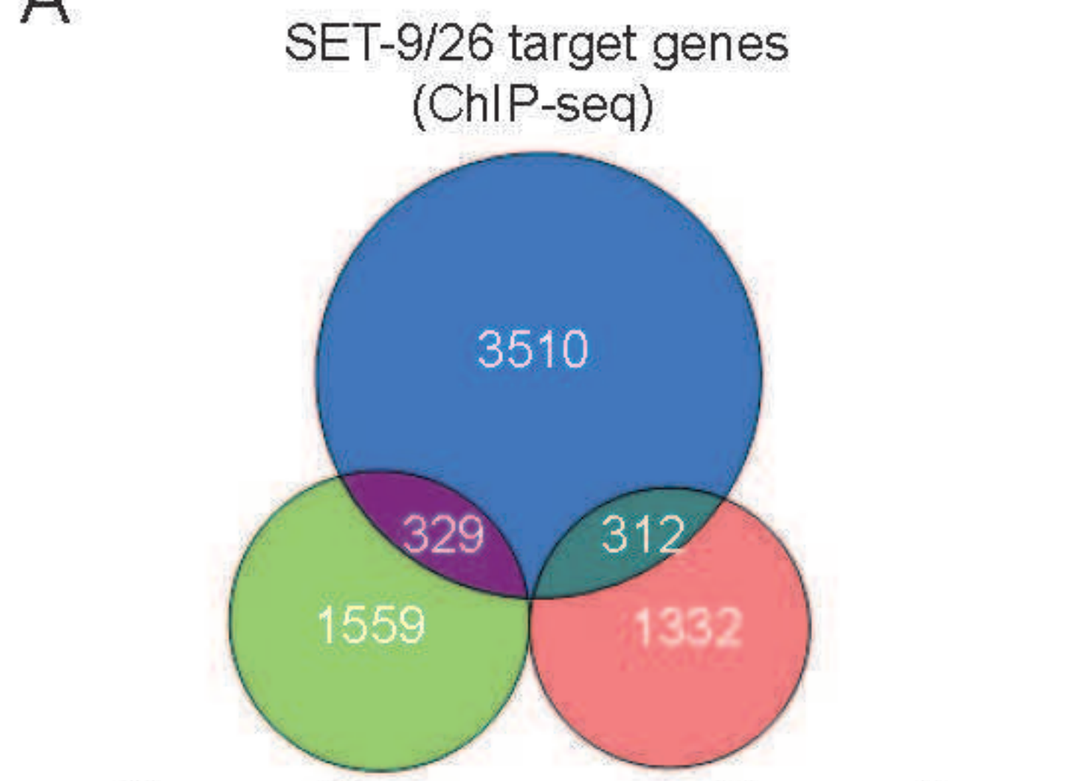

D

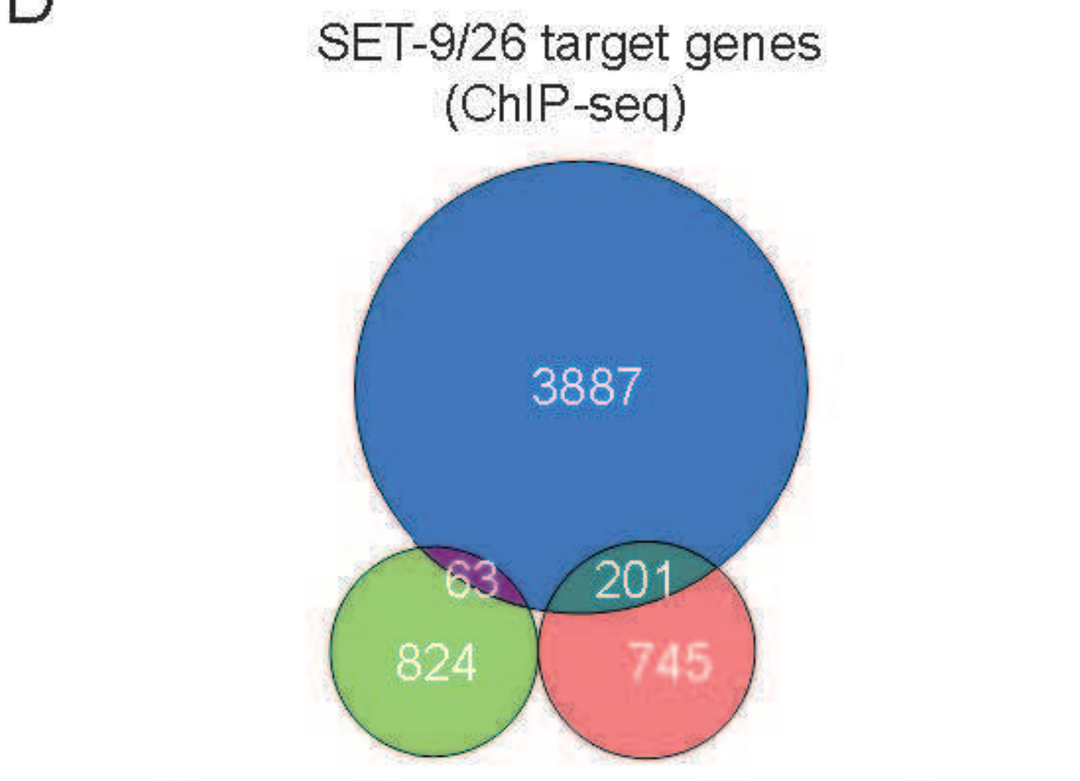

B

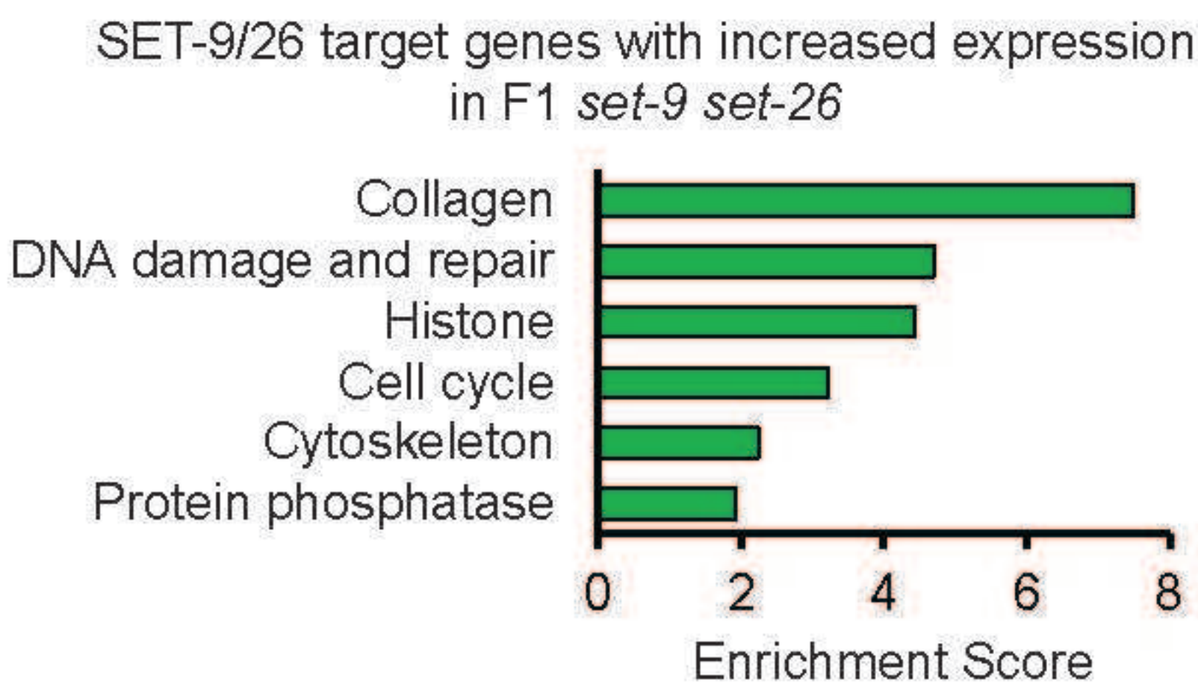

E

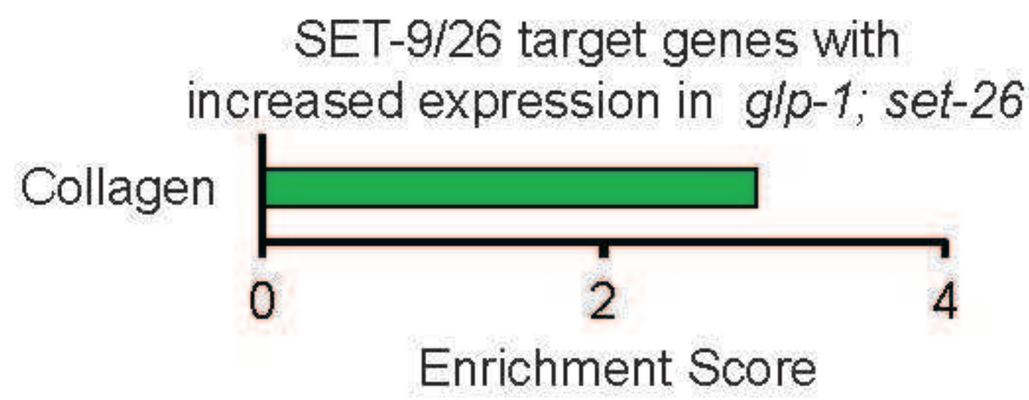

F

C

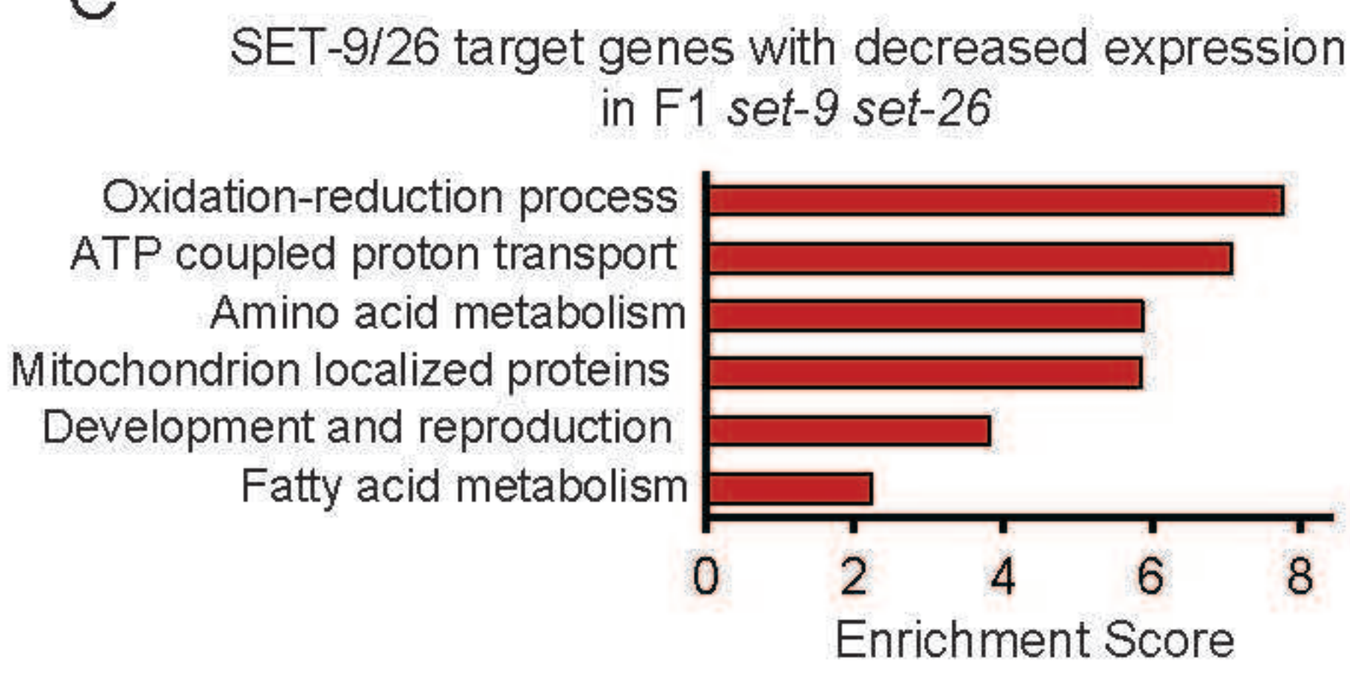

Wang_Figure 7-figure supplement 1

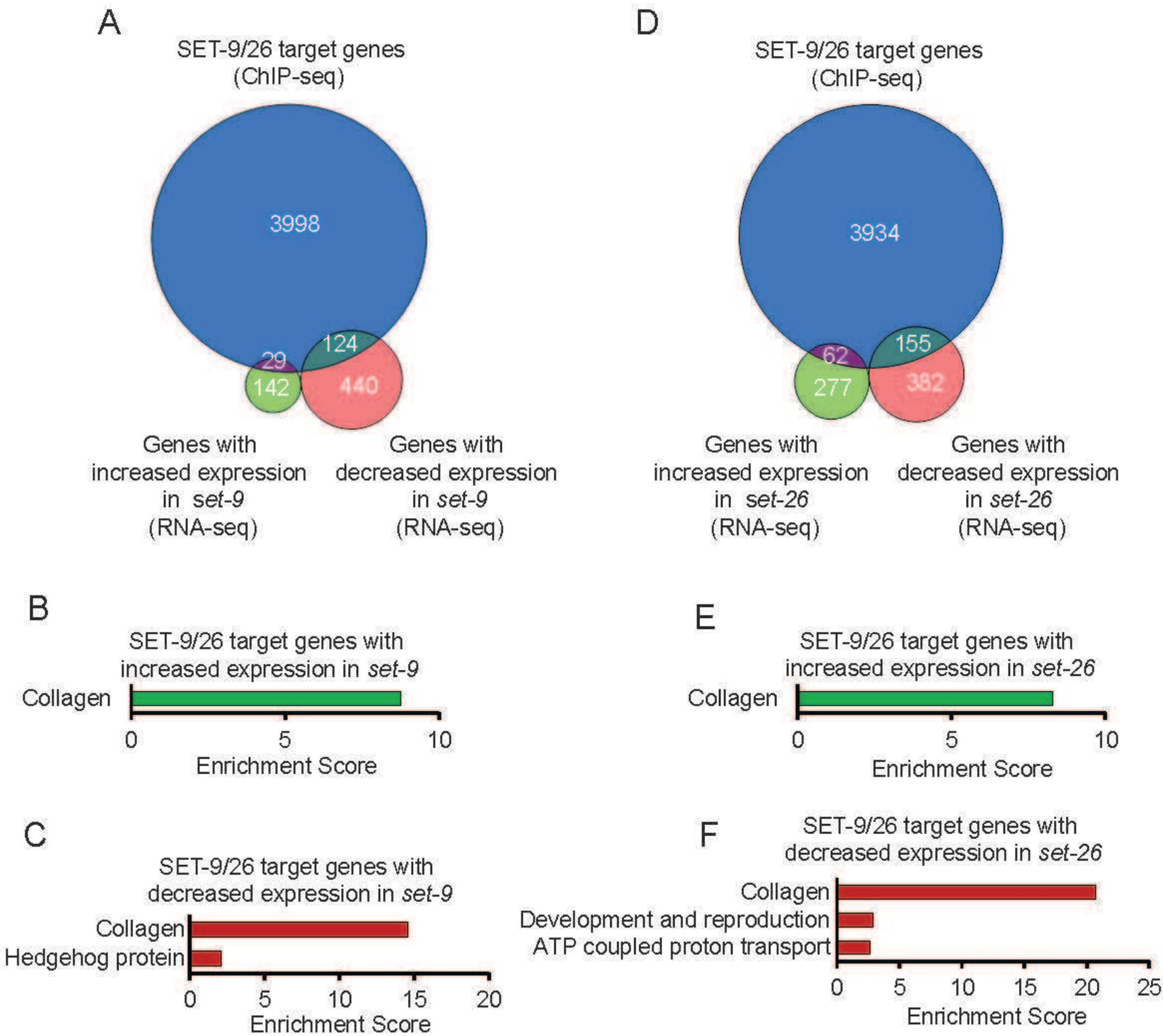

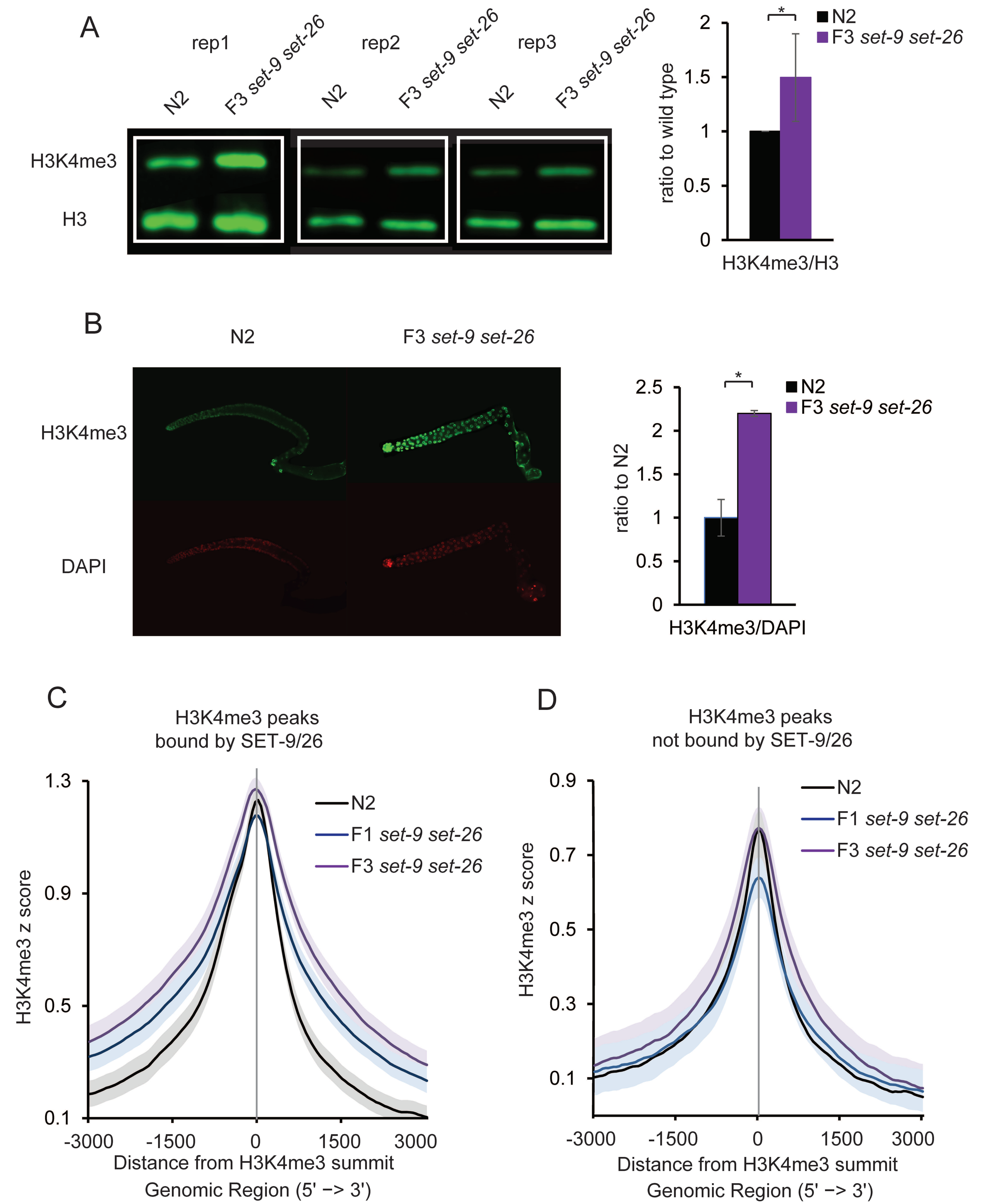
A
rep1
rep2
rep3
N2
F3 set-9 set-26
H3K4me3
H3
ratio to wild type
H3K4me3/H3
N2
F3 set-9 set-26
B
N2
F3 set-9 set-26
H3K4me3
DAPI
ratio to N2
H3K4me3/DAPI
C
H3K4me3 peaks
bound by SET-9/26
H3K4me3 z score
N2
F1 set-9 set-26
F3 set-9 set-26
Distance from H3K4me3 summit
Genomic Region (5' -> 3')
D
H3K4me3 peaks
not bound by SET-9/26
H3K4me3 z score
N2
F1 set-9 set-26
F3 set-9 set-26
Distance from H3K4me3 summit
Genomic Region (5' -> 3')

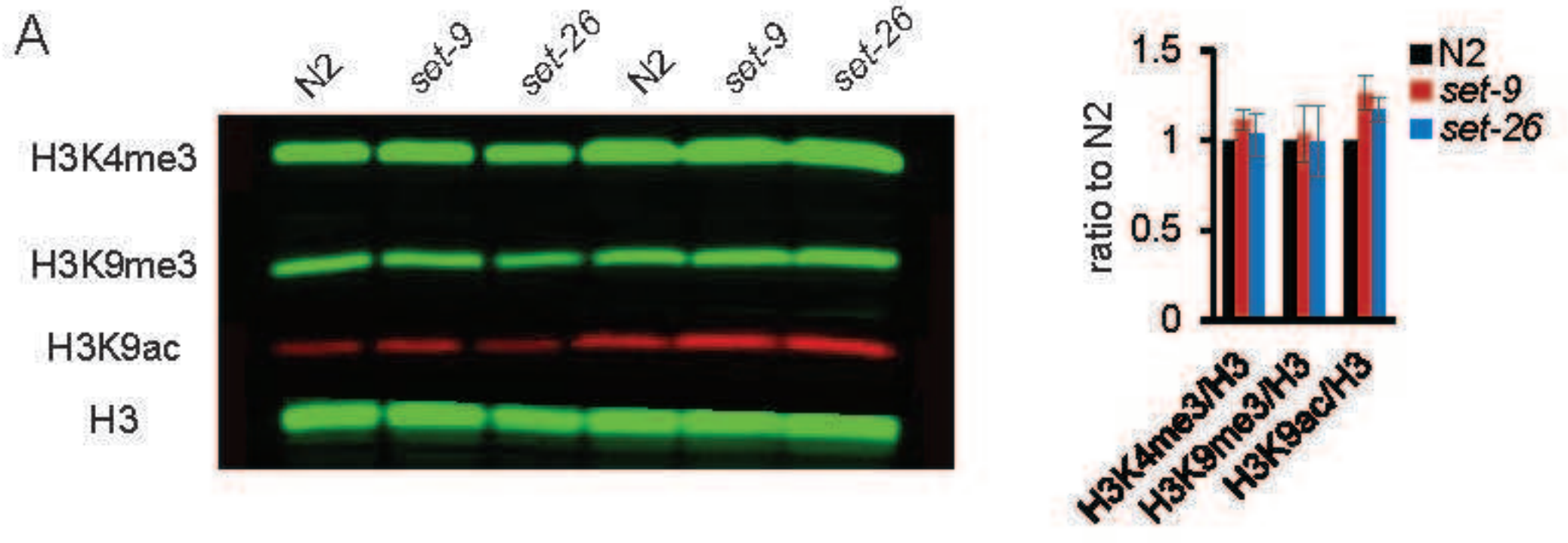
A
N2
set-9
set-26
N2
set-9
set-26
H3K4me3
H3K9me3
H3K9ac
H3
1.5
1
0.5
0
ratio to N2
N2
set-9
set-26
H3K4me3/H3
H3K9me3/H3
H3K9ac/H3

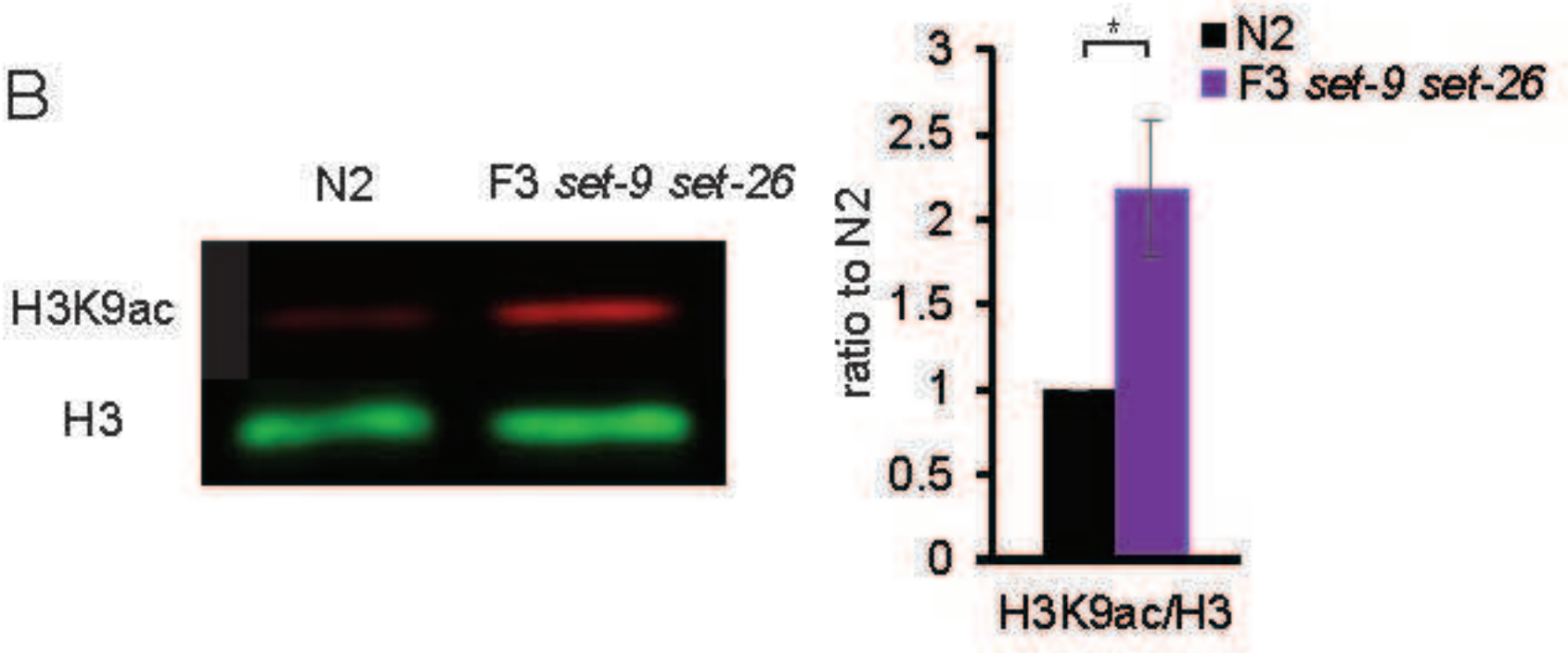
B
N2
F3 set-9 set-26
H3K9ac
H3
3
2.5
2
1.5
1
0.5
0
ratio to N2
*
N2
F3 set-9 set-26
H3K9ac/H3

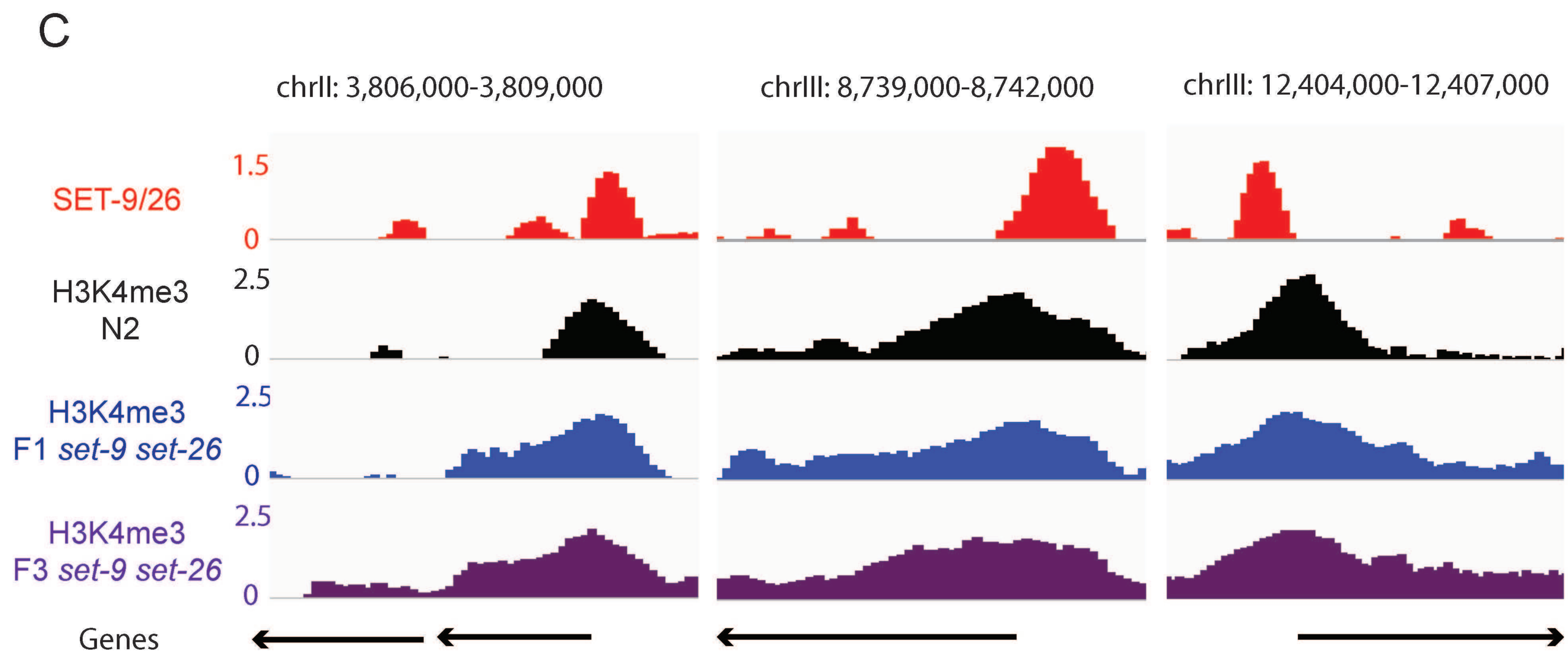
C
chrII: 3,806,000-3,809,000
chrIII: 8,739,000-8,742,000
chrIII: 12,404,000-12,407,000
SET-9/26
1.5
0
H3K4me3
N2
2.5
0
H3K4me3
F1 set-9 set-26
2.5
0
H3K4me3
F3 set-9 set-26
2.5
0
Genes

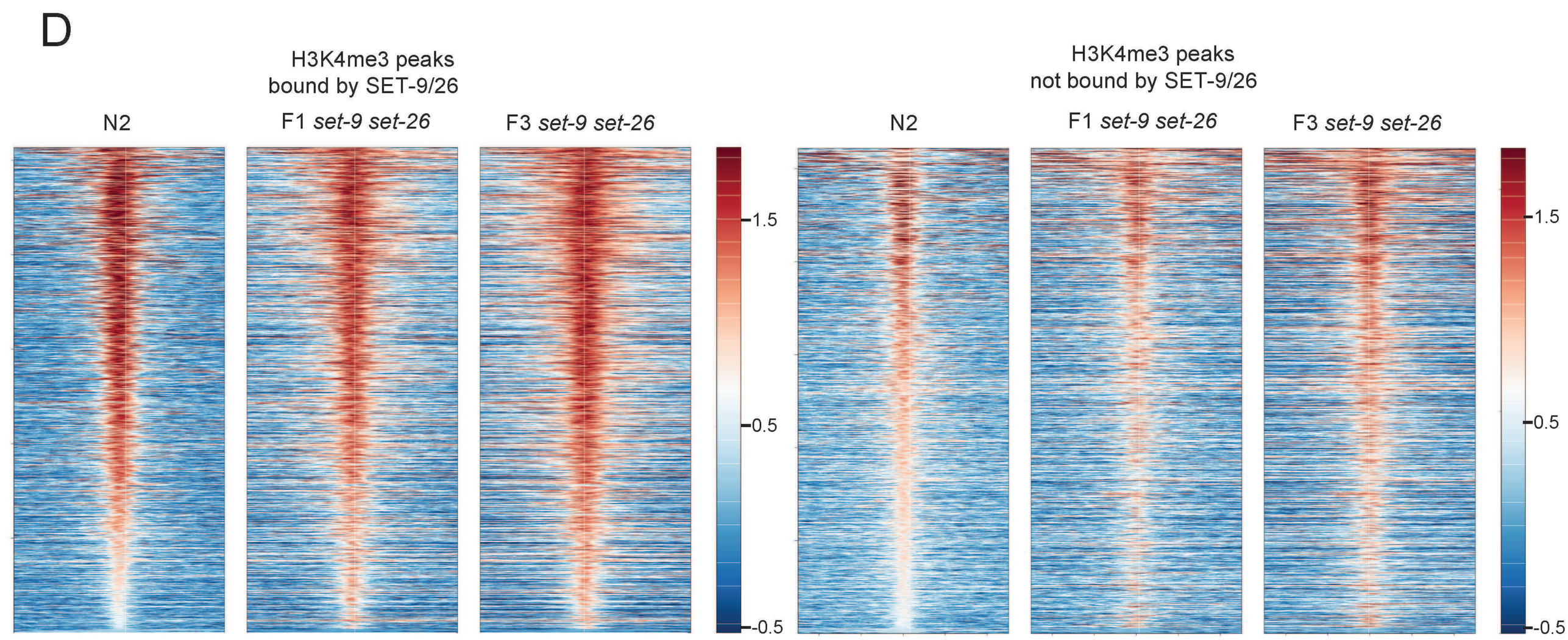
D
H3K4me3 peaks
bound by SET-9/26
N2
F1 set-9 set-26
F3 set-9 set-26
1.5
0.5
-0.5
H3K4me3 peaks
not bound by SET-9/26
N2
F1 set-9 set-26
F3 set-9 set-26
1.5
0.5
-0.5

Wang_Figure 8-figure supplement 1

E

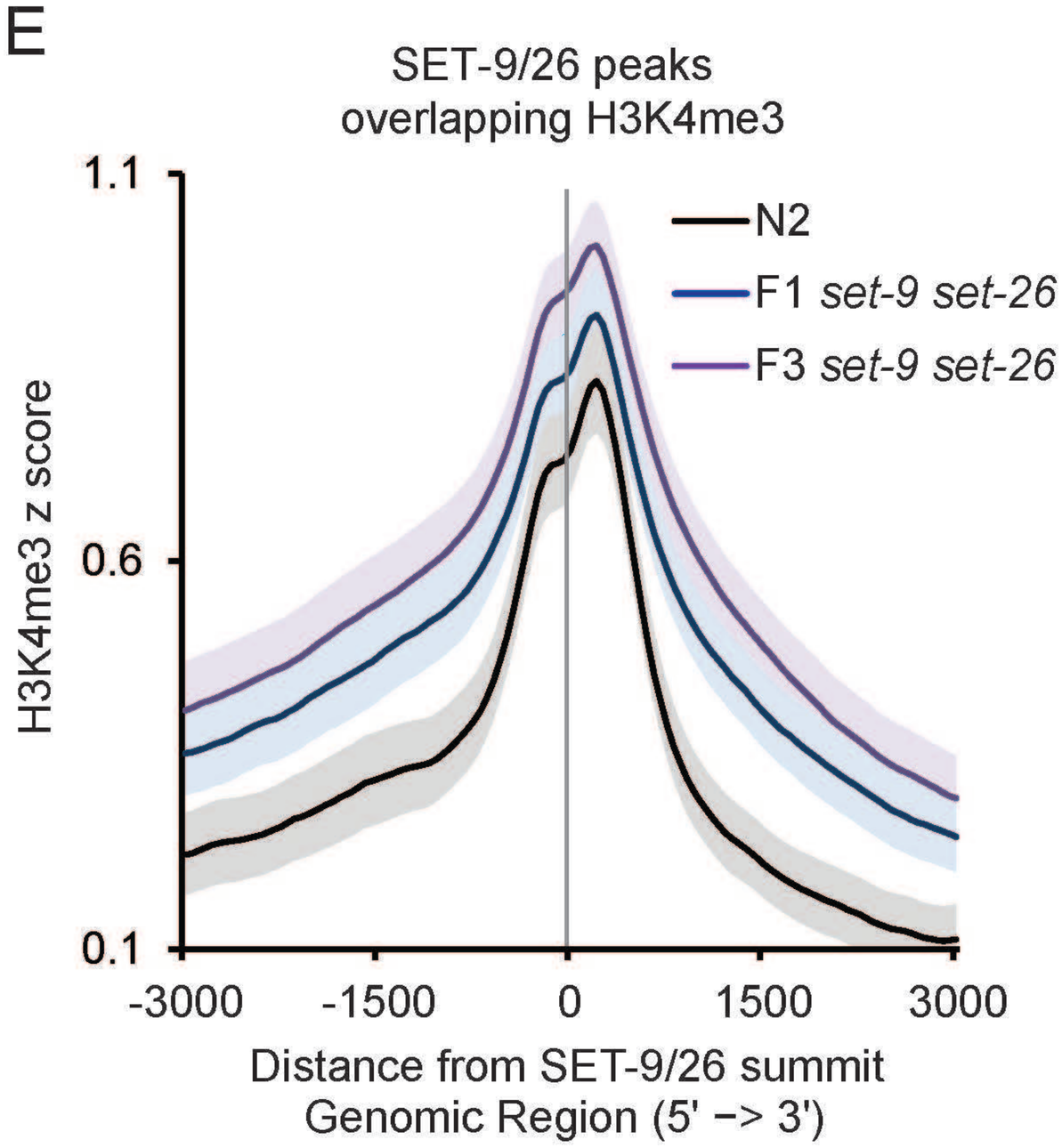

F

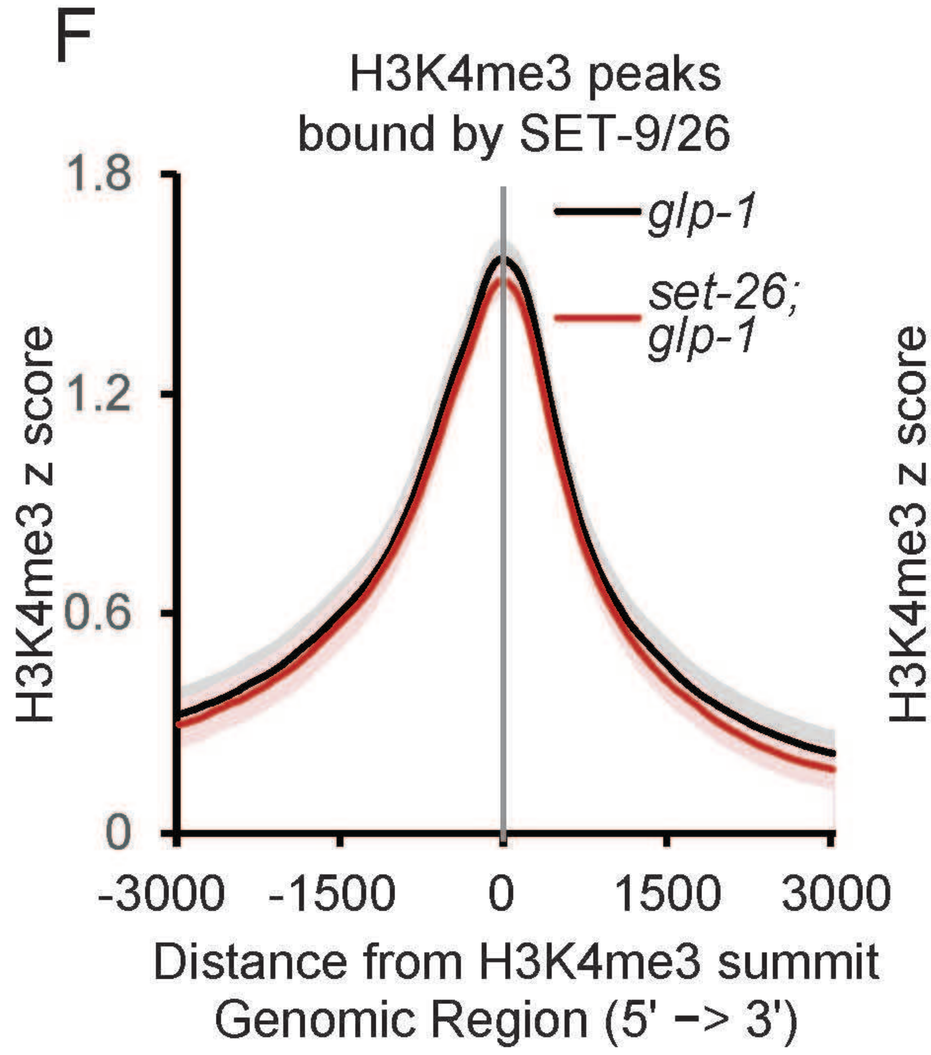

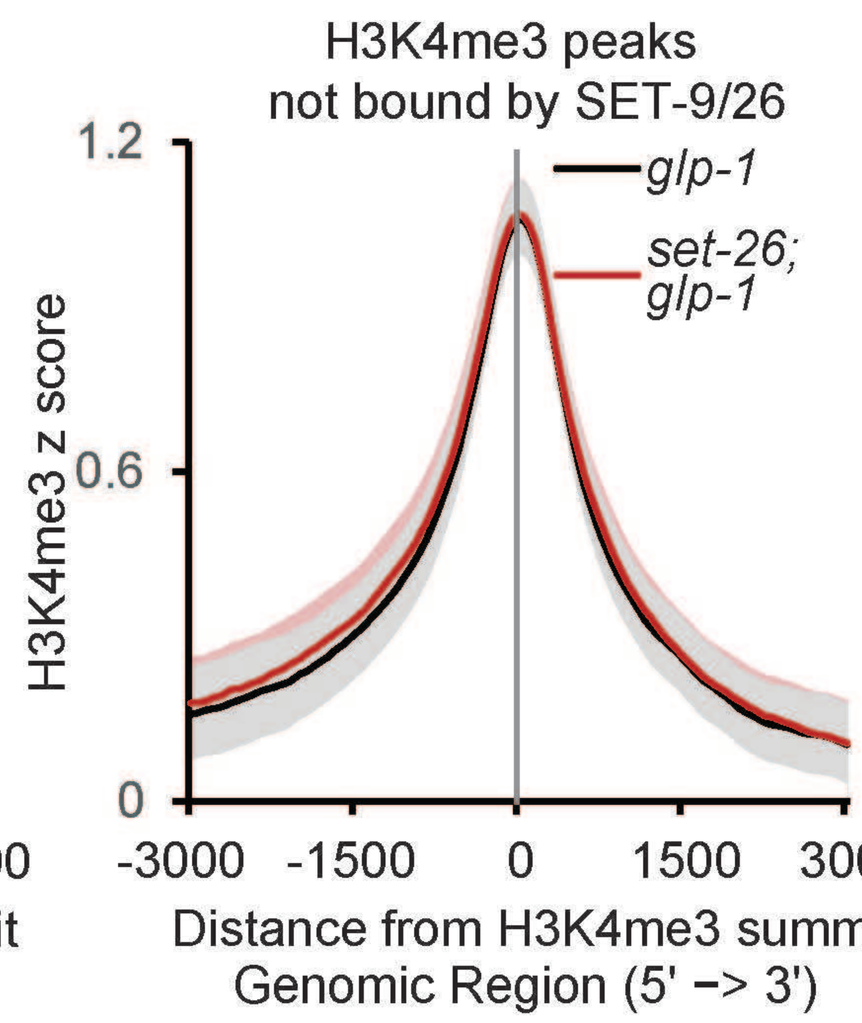

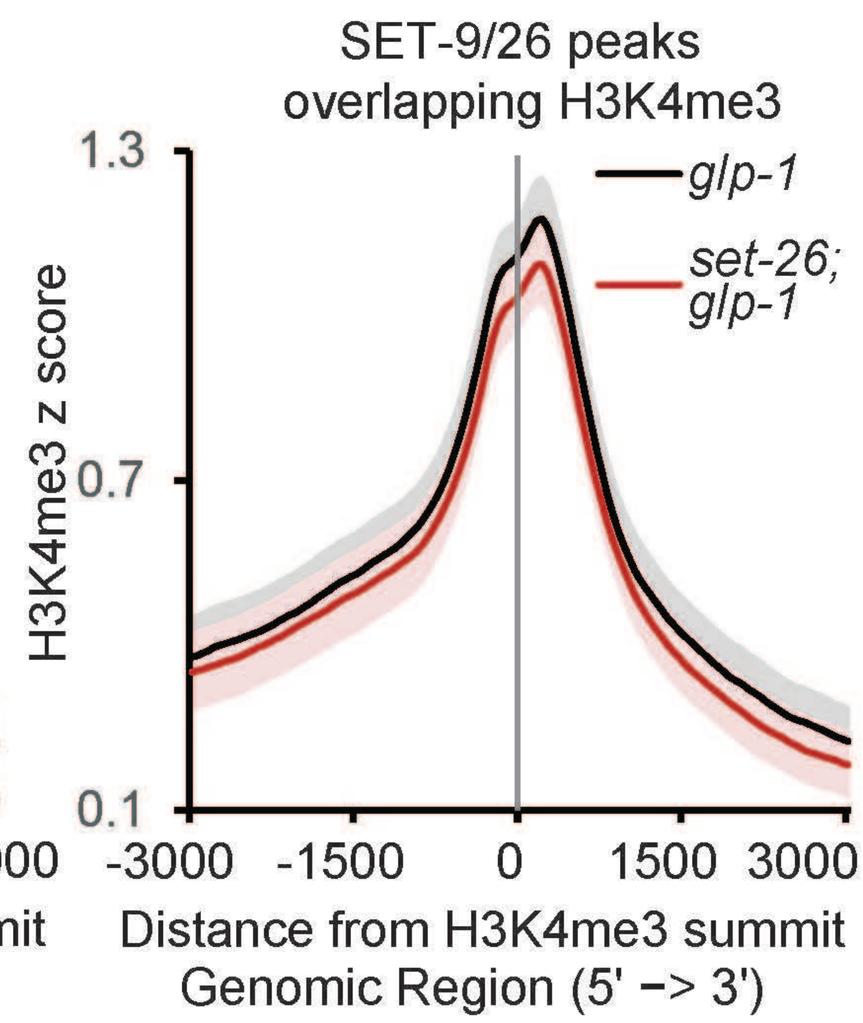

G

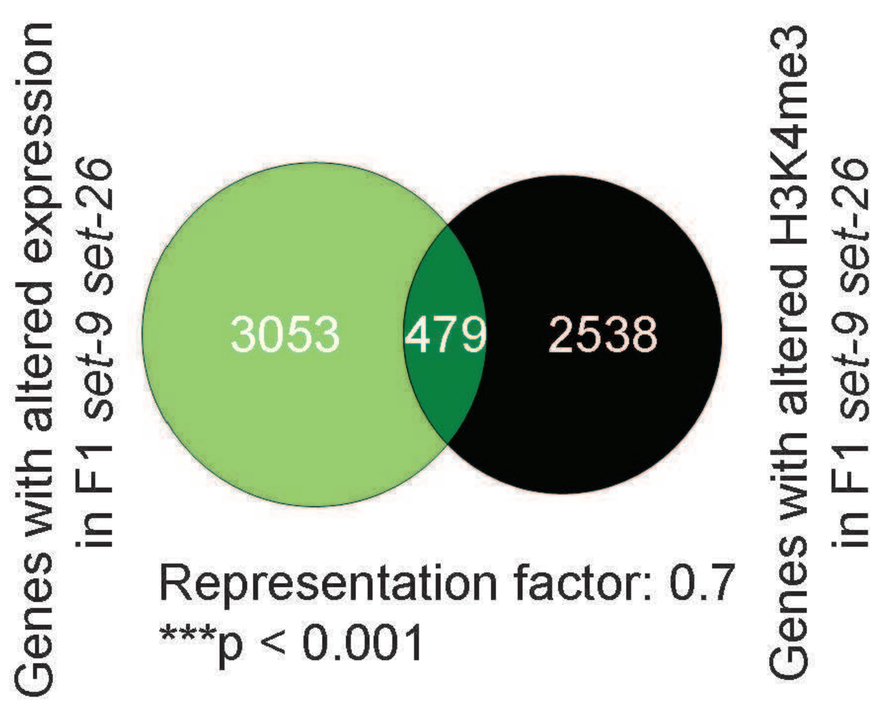

H

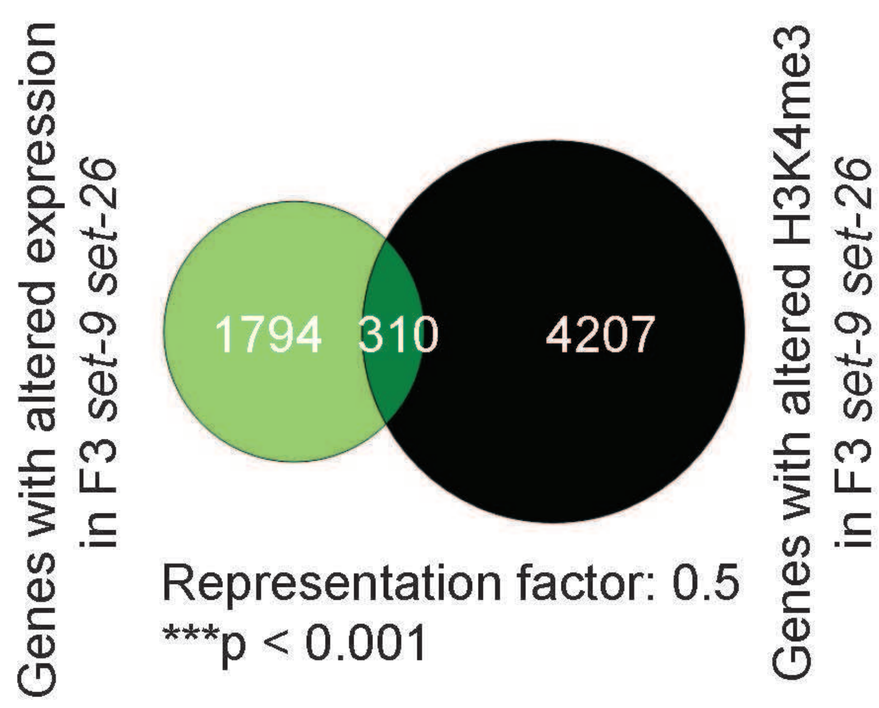

A

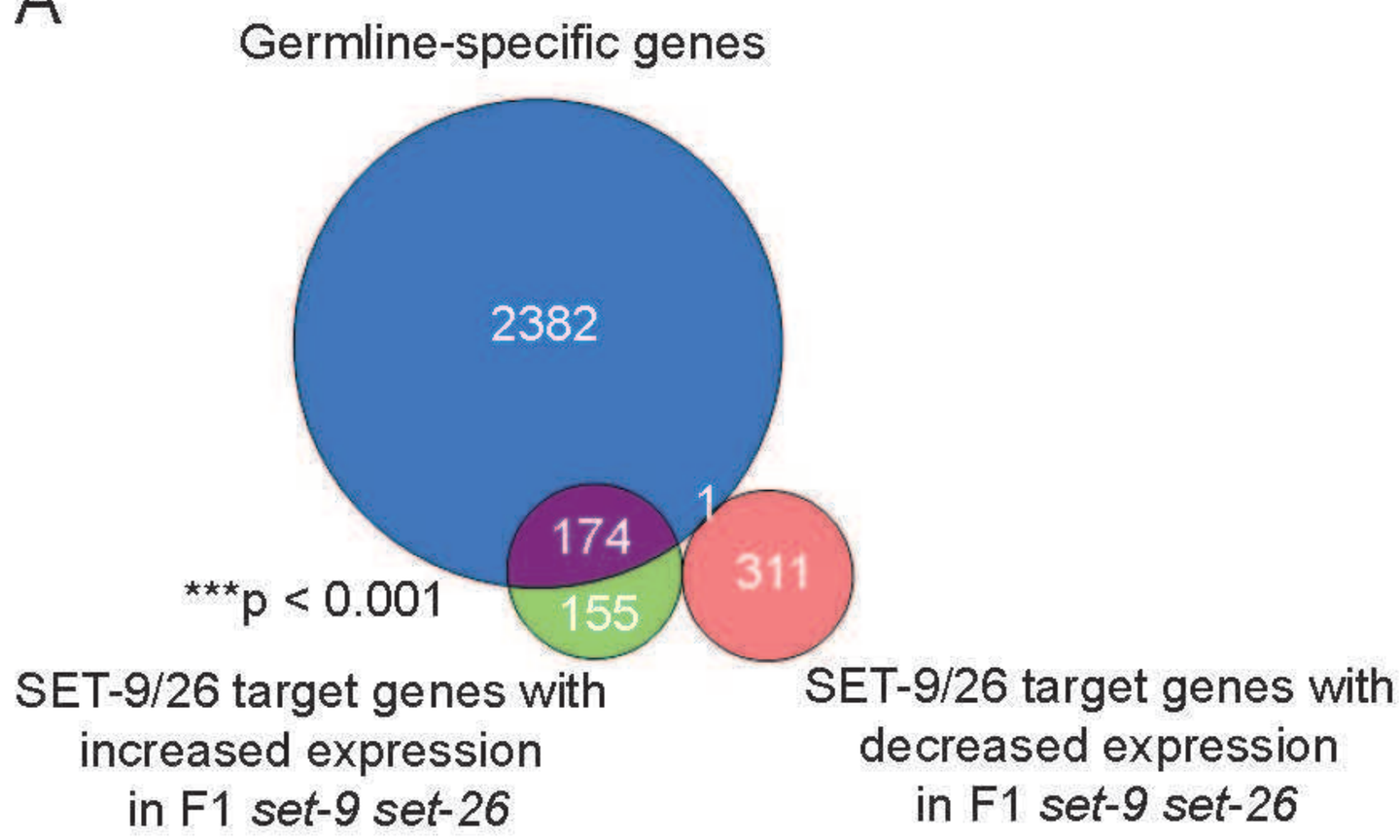
Germline-specific genes
2382
174
1
311
155
***p < 0.001
SET-9/26 target genes with increased expression in F1 *set-9 set-26*
SET-9/26 target genes with decreased expression in F1 *set-9 set-26*

B

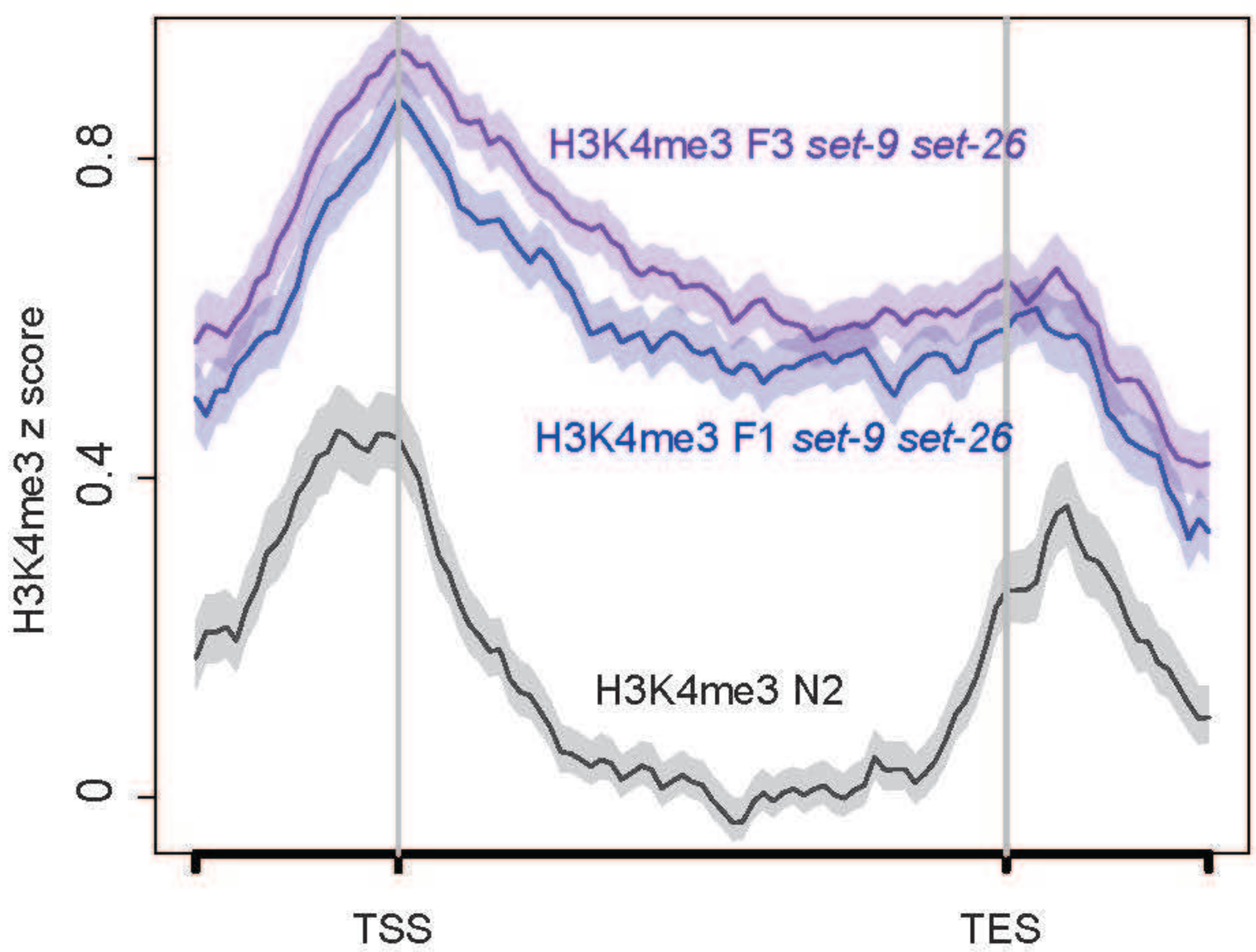
SET-9/26 germline target genes with increased expression in F1 *set-9 set-26*
H3K4me3 F3 *set-9 set-26*
H3K4me3 F1 *set-9 set-26*
H3K4me3 N2
H3K4me3 z score
0.8
0.4
0
TSS
TES

C

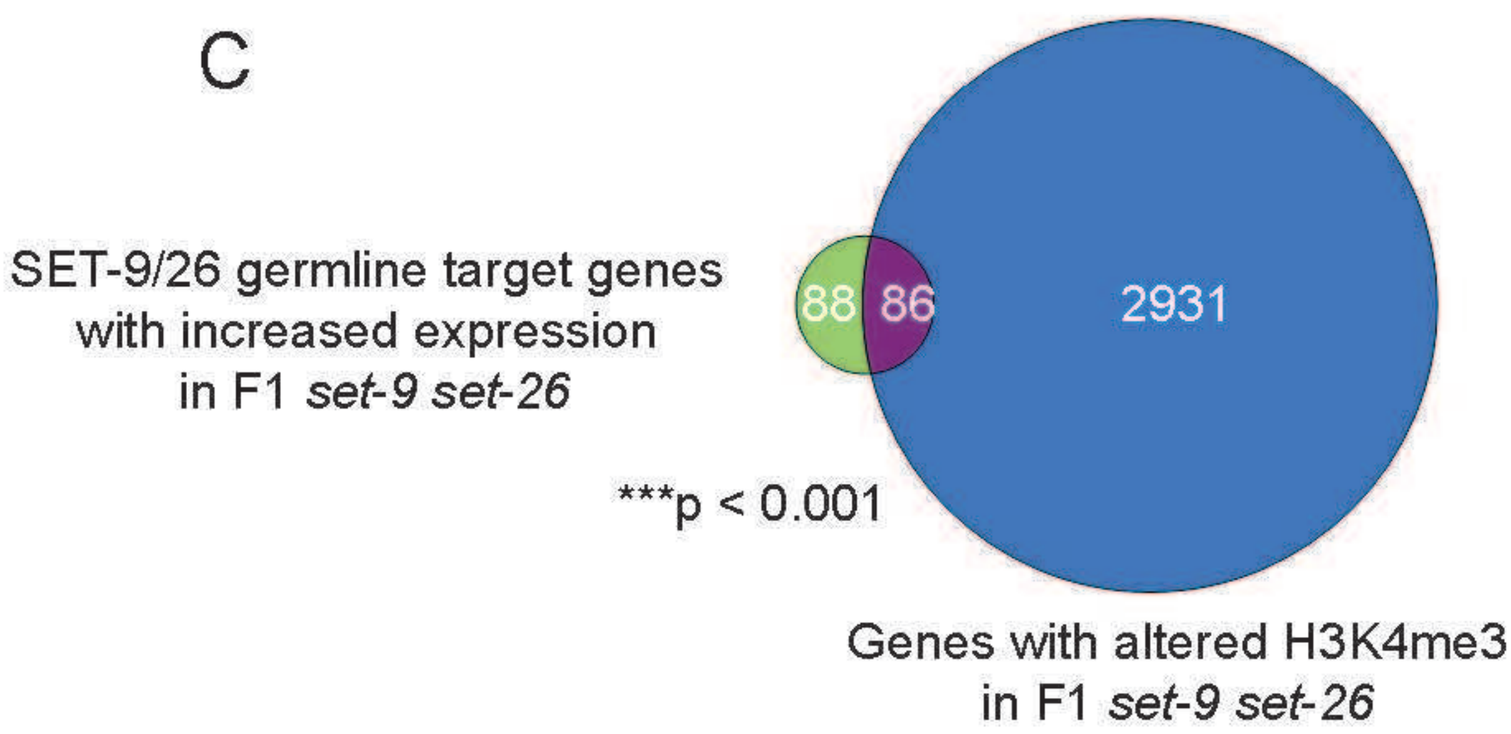
SET-9/26 germline target genes with increased expression in F1 *set-9 set-26*
88
86
2931
***p < 0.001
Genes with altered H3K4me3 in F1 *set-9 set-26*

Wang_Figure 9

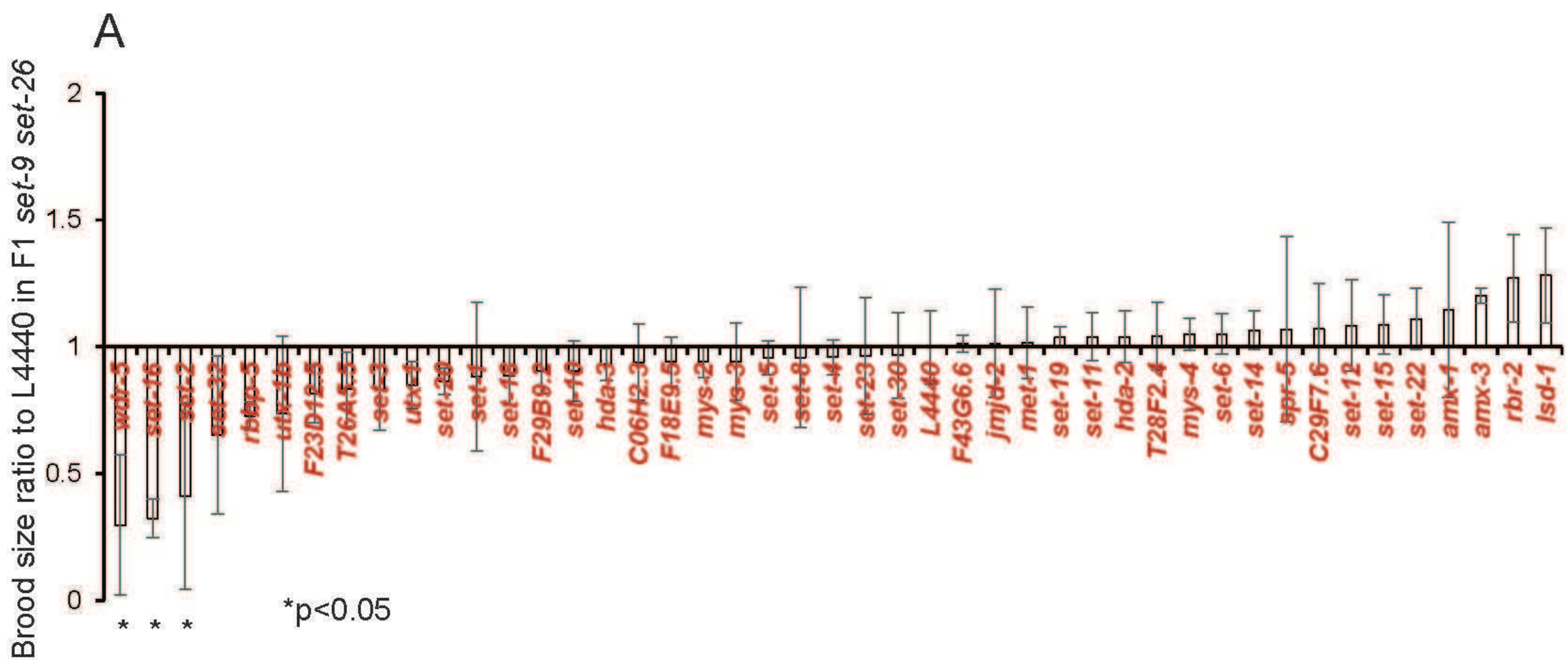

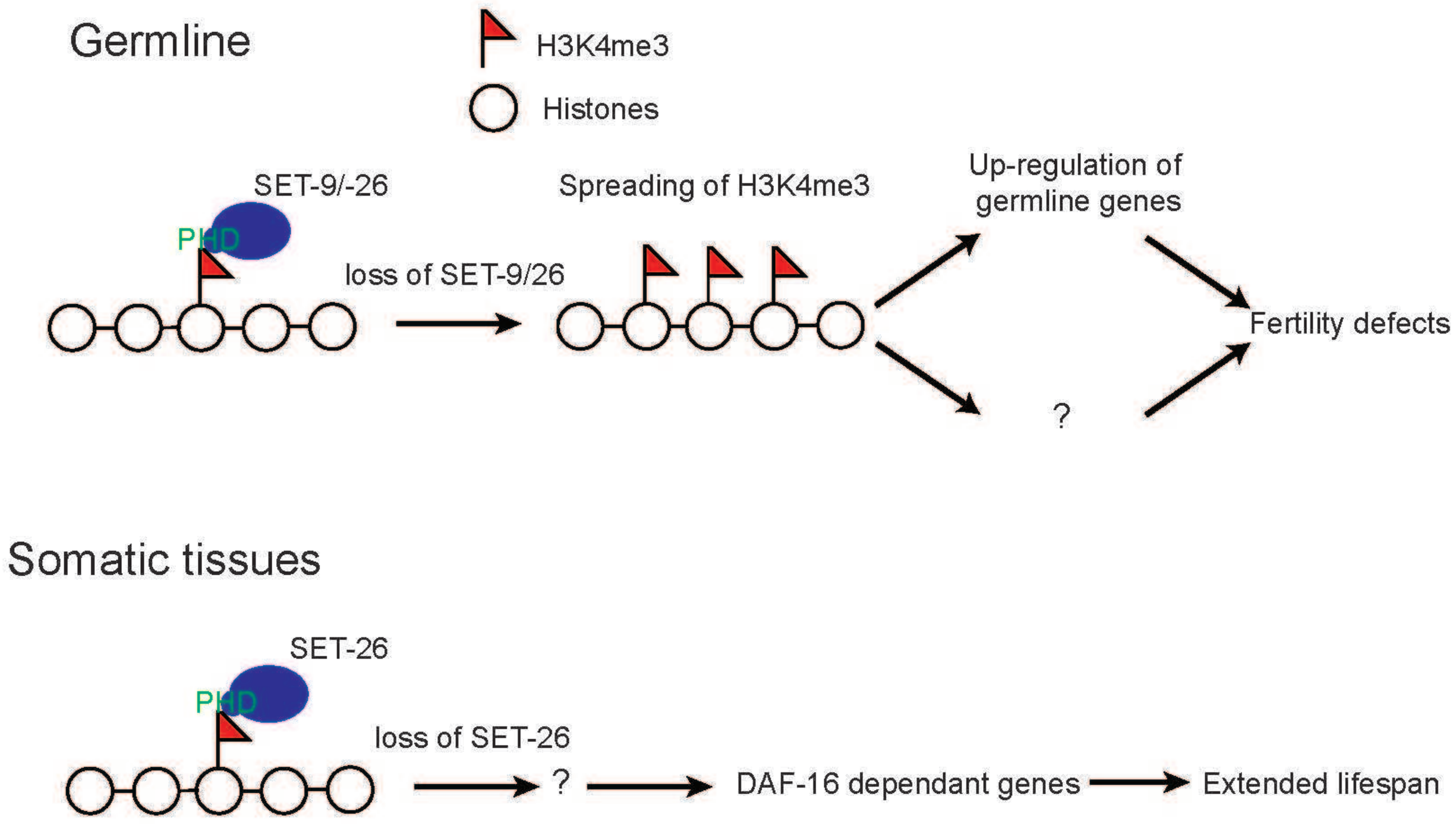
Germline
H3K4me3
Histones
SET-9/-26
PHD
loss of SET-9/26
Spreading of H3K4me3
Up-regulation of germline genes
?
Fertility defects
Somatic tissues
SET-26
PHD
loss of SET-26
?
DAF-16 dependant genes
Extended lifespan